# NAVAL POSTGRADUATE SCHOOL
## Monterey, California






# THESIS

**SPECTRAL AND POLARIMETRIC ANALYSIS OF HYPERSPECTRAL DATA COLLECTED BY AN ACOUSTO-OPTIC TUNABLE FILTER SYSTEM**

by

Melissa A. Sturgeon

September, 1993

Thesis Advisor: Philip A. Durkee





# REPORT DOCUMENTATION PAGE

Form Approved OMB No. 0704



| 1. AGENCY USE ONLY *(Leave blank)* | 2. REPORT DATE<br>23 SEP 93 | 3. REPORT TYPE AND DATES COVERED<br>Master's Thesis |
|---|---|---|

4. TITLE AND SUBTITLE : Spectral and Polarimetric Analysis of Hyperspectral Data Collected by an Acousto-optic Tunable Filter System

5. FUNDING NUMBERS

6. AUTHOR: Sturgeon, Melissa A.

7. PERFORMING ORGANIZATION NAME(S) AND ADDRESS(ES)
Naval Postgraduate School
Monterey CA 93943-5000

8. PERFORMING ORGANIZATION REPORT NUMBER

9. SPONSORING/MONITORING AGENCY NAME(S) AND ADDRESS(ES)
Director, Navy Space Systems Division (N63)
Space and Electronic Warfare Directorate
Chief of Naval Operations
Washington DC 20350-2000

Naval Space Command
Code N4/6T
Dahlgren VA
22448-5170

10. SPONSORING/MONITORING AGENCY REPORT NUMBER

11. SUPPLEMENTARY NOTES The views expressed in this thesis are those of the author and do not reflect the official policy or position of the Department of Defense or the U.S. Government.

12a. DISTRIBUTION/AVAILABILITY STATEMENT
Approved for public release; distribution is unlimited.

12b. DISTRIBUTION CODE
A

13. ABSTRACT *(maximum 200 words)*

Analysis of data collected during a ground-based experiment of an acousto-optic tunable filter (AOTF) hyperspectral imaging system illustrates the utility of this technology for military applications. The unique ability of an AOTF system to simultaneously acquire two orthogonally polarized images allows both spectral and polarimetric characterization of targets. The data images selected for analysis contain camouflaged military equipment deployed in a desert background. After geometric and atmospheric correction, spectral analysis is accomplished using two different methods. Comparing images created by the difference between polarizations for each band provides the basis for polarimetric analysis of the data. An algorithm developed to combine the information provided by spectral and polarimetric analysis shows how features within a scene can be distinguished from the background. Results show that AOTF hyperspectral technology has potential to enhance current military intelligence collection capabilities.

14. SUBJECT TERMS: Imaging spectroscopy, hyperspectral imagery, spectral and polarimetric characteristics, acousto-optic tunable filter design.

15. NUMBER OF PAGES
148

16. PRICE CODE

| 17. SECURITY CLASSIFICATION OF REPORT | 18. SECURITY CLASSIFICATION OF THIS PAGE | 19. SECURITY CLASSIFICATION OF ABSTRACT | 20. LIMITATION OF ABSTRACT |
|---|---|---|---|
| Unclassified | Unclassified | Unclassified | UL |

NSN 7540-01-280-5500

Standard Form 298 (Rev. 2-89)
Prescribed by ANSI Std. 239-18

**Approved for public release; distribution is unlimited.**

**SPECTRAL AND POLARIMETRIC ANALYSIS OF HYPERSPECTRAL DATA COLLECTED BY AN ACOUSTO-OPTIC TUNABLE FILTER SYSTEM**

**by**

**Melissa A. Sturgeon**
**Captain , United States Army**
**B.S., United States Military Academy, 1985**

**Submitted in partial fulfillment**
**of the requirements for the degree of**

**MASTER OF SCIENCE IN SYSTEMS TECHNOLOGY**
**(SPACE OPERATIONS)**

**from the**

**NAVAL POSTGRADUATE SCHOOL**
**September 1993**

Author: _____
Melissa A. Sturgeon

Approved by: _____
Philip A. Durkee, Thesis Advisor

_____
Richard C. Olsen, Second Reader

_____
Rudolf Panholzer, Chairman
Space Systems Academic Group

## ABSTRACT

Analysis of data collected during a ground-based experiment of an acousto-optic tunable filter (AOTF) hyperspectral imaging system illustrates the utility of this technology for military applications. The unique ability of an AOTF system to simultaneously acquire two orthogonally polarized images allows both spectral and polarimetric characterization of targets. The data images selected for analysis contain camouflaged military equipment deployed in a desert background. After geometric and atmospheric correction, spectral analysis is accomplished using two *different* methods. Comparing images created by the difference between polarizations for each band provides the basis for polarimetric analysis of the data. An algorithm developed to combine the information provided by spectral and polarimetric analysis shows how features within a scene can be distinguished from the background. Results show that AOTF hyperspectral technology has potential to enhance current military intelligence collection capabilities.

## TABLE OF CONTENTS

**ACKNOWLEDGMENTS**

Professor Chris Olsen deserves recognition for his generous donation of time and talent that made this thesis possible. He wrote all of the interactive computer programs that facilitated efficient and accurate data analysis. His expertise in the areas of data visualization and computer processing were invaluable in accomplishing the unique image processing and analysis required by this research.

Also worthy of note is the assistance in transferring and converting the experiment data files into an accessible format provided by Mr. Kurt Nielsen.

Lieutenant Sean Peters is due special thanks for his late night help in printing spectra graphs.

Expert advice and direction from Professor Phil Durkee was instrumental in completing this project. His insight, guidance and patience are greatly appreciated.

# I. INTRODUCTION

Exciting new developments in remote sensing techniques and systems can provide unprecedented information about the earth's surface. Currently, an approach called imaging spectroscopy is making valuable contributions to research in the fields of ecology, oceanography, geology and many others. Imaging spectroscopy, also known as hyperspectral imaging, is the collection of images in many contiguous spectral bands [Ref. 1:p. 1147]. This technology has outstanding potential for military applications. The interest by both the Army and Navy in utilizing imaging spectroscopy is evidenced by the ongoing research and development projects of each service. The Naval Research Laboratory (NRL) has a program called Hyperspectral Digital Imagery Collection Experiment (HYDICE) and the Army is developing an imaging spectrometer under the TERRA SCOUT II project. The purpose of this thesis is to analyze data collected during an experiment of the Army's prototype hyperspectral imaging system with the goal of determining the military utility of imaging spectroscopy.

## A. BACKGROUND

Hyperspectral imagery has tremendous potential to enhance military capabilities in a variety of areas by measuring the

spectral reflectance characteristics of selected targets. This unique technology could provide immense support to strategic intelligence requirements in the areas of threat definition, treaty monitoring, arms control, counternarcotics, and counterterrorism. On a tactical level, hyperspectral sensors could accomplish missions not possible with any other system, such as camouflage and concealment detection; nuclear biological and chemical detection; terrain and trafficability analysis; mapping; broad area search; mobile missile and weapons systems location; and identification friend or foe. Imaging spectroscopy could make significant contributions to military operations in many different scenarios. The capability exists for a hyperspectral sensor to operate in space, either on the space shuttle or as a light satellite; as an airborne system, on a reconnaissance airplane or an unmanned aerial vehicle (UAV); and as a ground-based long range surveillance system.

The organization in the Army tasked to develop intelligence systems that correct identified deficiencies in current systems is the Intelligence Center's Directorate of Combat Developments (DCD) at Fort Huachuca, Arizona. In an effort to provide tactical commanders with more timely imagery intelligence, DCD initiated a project called TERRRA SCOUT. The concept of TERRA SCOUT was to determine if a trained imagery analyst could identify and locate targets more quickly and accurately with high resolution optics from space, than

could be accomplished using existing systems and procedures. The normal imagery cycle begins with data collection at the sensor. The data is then transmitted to a ground station, processed, and analyzed. Finally, the image with its corresponding analysis is sent to the user. TERRA SCOUT was successful in that a payload specialist aboard the space shuttle was able to downlink accurate analyzed imagery more rapidly than the current procedures allow.

As an improvement to the original TERRA SCOUT project, DCD incorporated hyperspectral imaging technology into the concept of providing better imagery support to commanders. The follow-on project is called TERRA SCOUT II. The Army Space Technology Research Office (ASTRO) supplied initial funding for the effort and is the program sponsor. Jet Propulsion Laboratory (JPL) and Massachusetts Institute of Technology's Lincoln Laboratory (MIT/LL) are the contractors responsible for designing and building the system. Development of the TERRA SCOUT II system involves a phased approach, requiring proof of concept demonstrations to achieve rapid prototyping of the hyperspectral imaging system. A prototype of the sensor subsystem was delivered by JPL in March 1993 and used in a ground-based proof of concept experiment conducted in April 1993. The next step in the TERRA SCOUT II development process requires analysis of the data collected during this experiment to validate the sensor's capabilities and determine its utility for military applications.

## B. SENSOR

The sensor design selected for TERRA SCOUT II uses an acousto-optic tunable filter (AOTF). The operational technique of the AOTF is different than existing hyperspectral imaging systems. The AOTF sensor creates an image by measuring the energy intensity over an entire scene at one time for a particular wavelength. The other type of imaging spectrometer scans a scene by picture element (pixel). It measures the energy intensity for every wavelength over the range of the sensor one pixel at a time. The result is an entire spectrum for each pixel in the scene. The spectra from every pixel are then used to form an image when the data is analyzed. (See Figure 1)

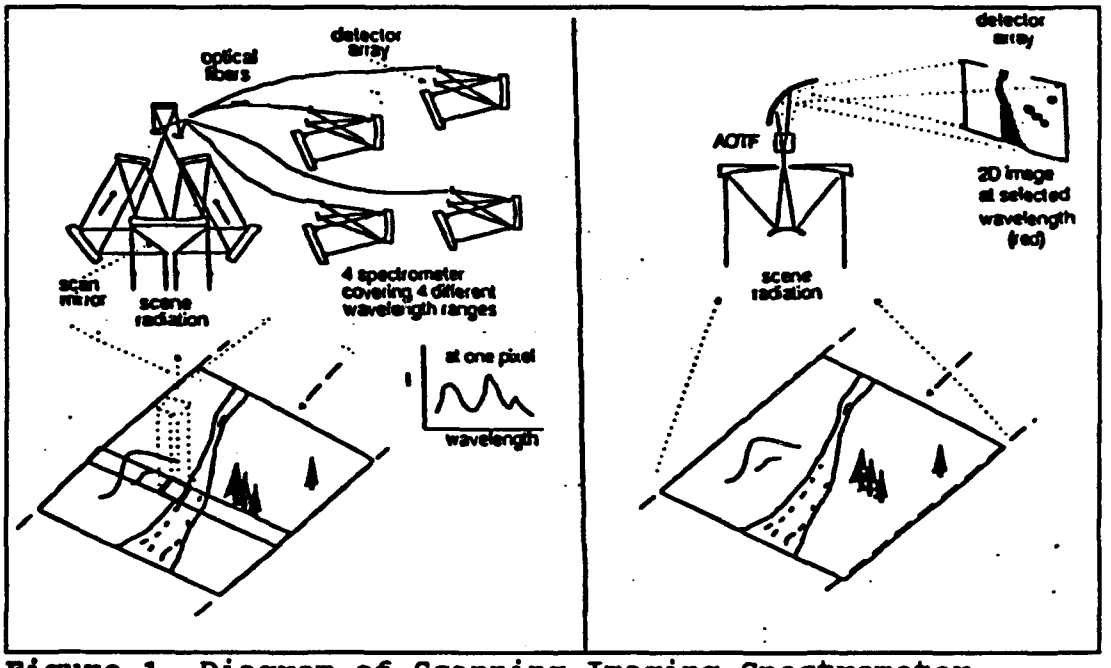


**Figure 1** Diagram of Scanning Imaging Spectrometer Versus AOTF Design

The AOTF type of sensor possesses unique properties which make it well-suited for intelligence collection. It simultaneously collects both spectral and polarimetric information. This polarization capability, not available on other existing systems, provides an added dimension to imagery analysis which could enhance target detection. The AOTF technique allows real time collection of only the data required for a specific purpose. For example, an AOTF system is not limited to collecting images for every wavelength within its range. It can be programmed to collect only the images for selected bands that will provide the most information about the target. This feature, combined with the ability to easily tune the sensor, enables operational flexibility in tailoring observation parameters. Additionally, the AOTF is compact and has no moving parts, making it versatile and reliable. [Ref. 2:p. 88]

The prototype AOTF hyperspectral imaging system used in the proof of concept experiment was designed and built by JPL engineers. It operates in the wavelength range between 0.48 and 0.76 microns with a field of view of 10.4 by 14.1 meters. At a power of 12 dBm the AOTF sensor has an integration time of one second. The AOTF system is composed of an AOTF, foreoptics, imaging optics and two silicon charge coupled device (CCD) cameras. The optics equipment and cameras planned for eventual airborne and space experiments are being

developed at MIT/LL and were not used in the ground-based experiment.

During the experiment, the foreoptics consisted of an ordinary camera zoom lens and a field lens was used for imaging optics. A 386 IBM-PC compatible computer was necessary for control and data acquisition. The prototype system also included an image grabber and a generator as an independent power supply. [Ref. 2:p. 89]

The AOTF uses a tellurium dioxide ($TeO_2$) crystal which splits a beam of light entering the sensor into a set of two narrow band, orthogonally polarized images for each wavelength determined by the acoustic frequency input to the crystal. The field lens is placed behind the AOTF and in combination with the zoom lens, generates the diffracted images, one directed at each focal plane array. The CCD cameras then detect the images and convert the measured analog information to digital data by assigning a digital number to the corresponding intensity for every pixel in the arrays. Thus, the arrays of pixel values create digital images for both polarizations at each of 33 different wavelengths.

## C. EXPERIMENT

In order to determine the capabilities of the prototype AOTF system, analysis of data collected during its proof of concept experiment is necessary. The experiment was conducted at Fort Huachuca, Arizona, where convenient sensor locations

were identified which allowed the AOTF system to easily image military targets with different types of backgrounds. Hilltops were selected for sensor locations tc simulate, as closely as possible, the geometry of sun and viewing angles such as an airborne sensor would detect a scene. During the AOTF experiment, spectral measurements of various targets and background features were made with a portable field spectrometer. The field spectrometer data is used to validate the hyperspectral imagery collected by the prototype AOTF system. The portion of the AOTF experiment data that contains camouflaged military equipment deployed in the desert is the focus of the spectral and polarimetric analysis accomplished in this thesis.

# II. THEORY

Before addressing the data analysis, it is important to understand the scientific basis that supports the study of the AOTF experiment data. This chapter introduces the physics behind the science of remote sensing, describes the AOTF sensor technology, and explains the concepts of spectral and polarimetric resolution.

## A. REMOTE SENSING

The physical phenomenon that makes remote sensing possible is electromagnetic radiation. By quantitatively measuring the properties of the electromagnetic radiation arriving at a sensor, scientists can gain an abundance of information about the earth's surface or atmosphere. Electromagnetic radiation collected by a remote sensor is characterized by the spectrum of its generating source, the atmosphere through which it propagates, and the reflecting surface from which it is received. How electromagnetic radiation from the source is changed by the reflecting surface and the atmosphere provides the information sought by remote sensing users. Therefore, understanding the properties of this radiation is necessary for analysis of remotely sensed data. [Ref. 3:p. 41]

### 1. Electromagnetic Waves

Energy is carried from its source by electromagnetic radiation, either directly through free space or indirectly by reflection and reradiation, at the speed of light [Ref. 3:p. 37]. This radiative energy moves through space as electromagnetic waves. These waves are propagated by alternating electric and magnetic field components which generate electric and magnetic fields. These fields are mutually orthogonal and oscillate with the same amplitude variations. (See Figure 2) [Ref. 4:pp.843-854]

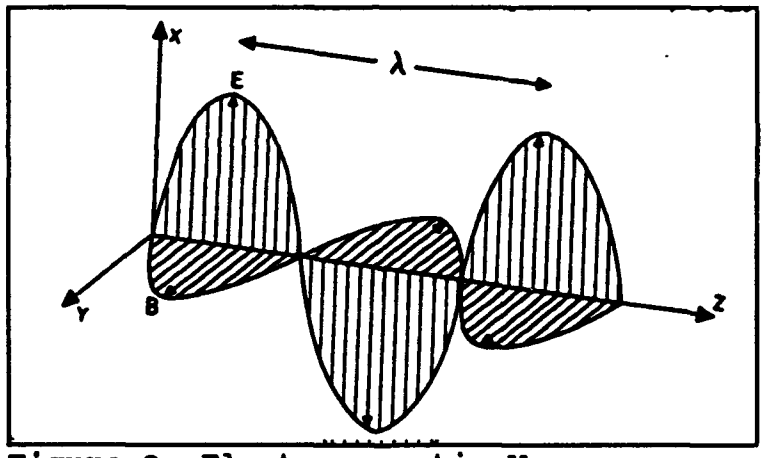


**Figure 2** Electromagnetic Wave
[Ref. 5:p. 34]

Because of its wave properties, electromagnetic radiation has a wavelength and frequency. The following relationship exists between wavelength, $\lambda$, frequency, $\nu$, and

the velocity of light in a vacuum, c:

$$\lambda=\frac{c}{v}.$$

When an electromagnetic wave penetrates matter, its velocity changes according to the index of refraction of the medium. This refractive index is the ratio of the velocity of light in a vacuum to the velocity of light in the medium. The frequency never changes, therefore, upon interaction with a medium, the wavelength must change. This causes a bending or refraction of the wave. [Ref. 6:p. 13]

Snell's Law defines the extent of the refraction for a denser medium as

$$n\sin\theta=n'\sin\theta',$$

where n is the index of refraction for a vacuum, $\theta$, is the angle of the incident ray from the normal, n' is the refractive index for the medium, and $\theta'$ is the angle of the refracted ray from the normal. If an electromagnetic wave interacts with a reflecting surface, the index of refraction remains the same and

$$\theta=\theta'.$$

Also, if the medium is isotropic, the incident ray, the normal to the surface, the reflected ray, and the refracted ray lie in the same plane. (See Figure 3) These laws hold true for

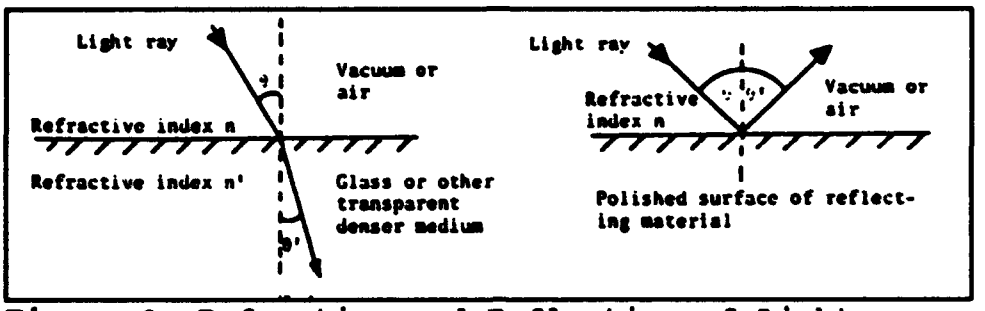


**Figure 3** Refraction and Reflection of Light
[Ref. 5:p. 35]

reflection or refraction of all electromagnetic radiation. [Ref. 5:pp. 34-35]

### 2. Electromagnetic Particles

The basic unit of radiative energy is the photon. Because waves also behave like particles, it is possible to quantify electromagnetic radiation according to the equation

$$Q=h\upsilon,$$

where Q is the radiant energy, h is Planck's constant and $\upsilon$ is frequency of the wave. This means that electromagnetic waves with longer wavelengths have photons with less energy than those with shorter wavelengths. Electromagnetic radiation is characterized by the propagation of photons at a velocity with a particular frequency, energy and wavelength.

### 3. Electromagnetic Spectrum

Electromagnetic radiation naturally provides a fast communications link between a sensor and its remotely located target [Ref. 3:p. 37]. The electromagnetic spectrum is a continuous distribution of electromagnetic waves arranged in order of wavelength which travel through space at a common speed. The accepted range of the electromagnetic spectrum spans wavelengths from $10^{-10}$ microns, where cosmic rays are emitted to $10^{10}$ microns, used for broadcast signals. (See Figure 4)

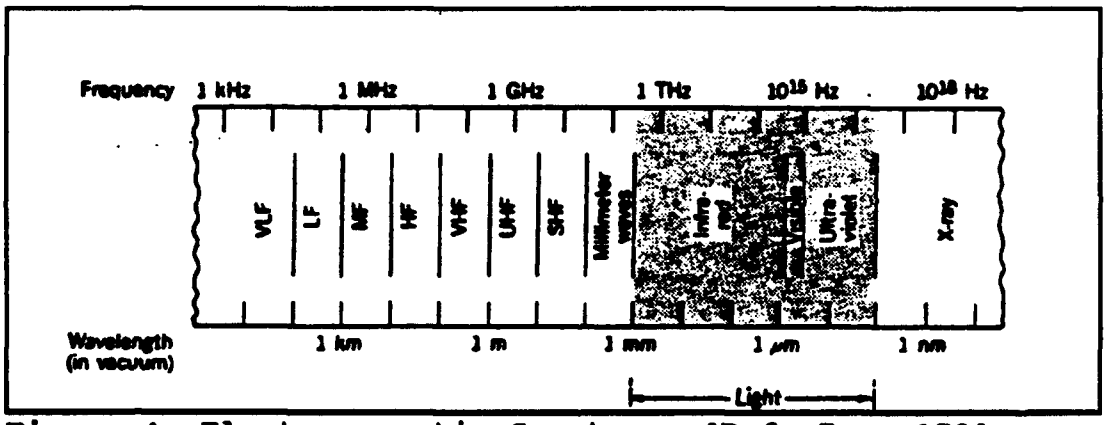


**Figure 4** Electromagnetic Spectrum [Ref. 7:p. 158]

The most useful wavelengths for remote sensing are the optical wavelengths which extend from 0.30 to 15 microns. The electromagnetic energy in this wavelength range can be reflected or refracted by mirrors or lenses built to precision tolerances for remote sensing systems. [Ref. 8:p. 33]

## 4. Geometry of Remote Sensing

Fundamental to the measurement of electromagnetic radiation by a remote sensor is the concept of solid angle geometry. Because the distances between radiation sources and sensors are finite and radiation does not actually move in parallel rays, electromagnetic energy diverges radially from its source. The mathematical representation of this reality is accomplished with solid angles. The basic idea is that if a sphere with radius, R, encloses a cone, the solid angle or volume of the cone is equal to the area of the circle created by the cone on the surface of the sphere, A, divided by the square of the sphere's radius. (See Figure 5)

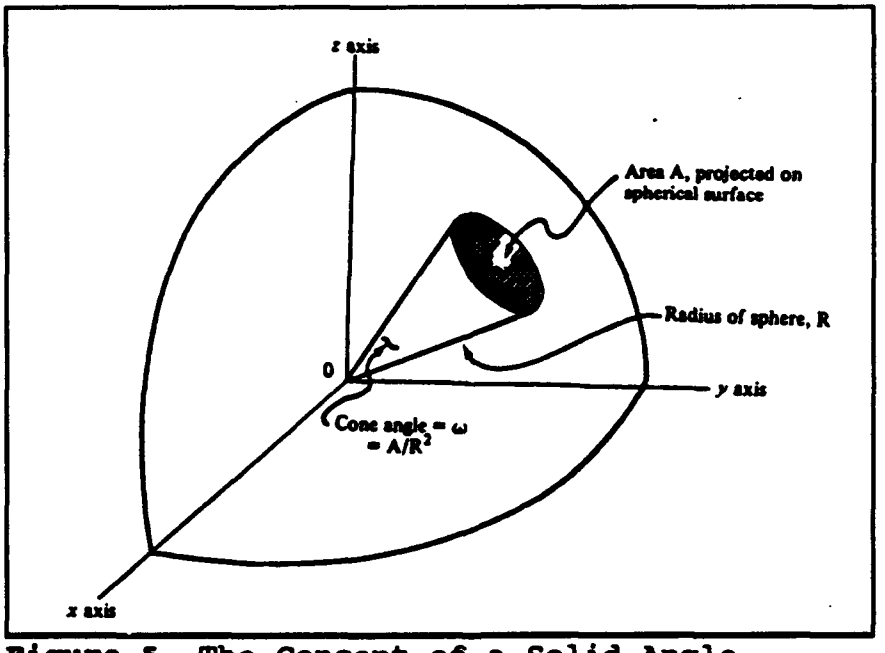


**Figure 5** The Concept of a Solid Angle
[Ref. 6:p. 16]

The unit of a solid angle is the steradian. Since the surface area of a sphere is $4\pi R^2$, a sphere contains $4\pi$ steradians of solid angle. [Ref. 6:pp. 17-18]

Consider a remote sensing system a distance away from an energy-emitting target. The system's sensor is a flat plate of a particular area. This area is used to calculate the solid angle of radiated energy even though the area of the flat plate is not exactly the same as the area of the circle cut by the diverging rays of energy. As long as the distance between the sensor and target is large compared to the size of the plate, this calculation is accurate enough for remote sensing purposes. [Ref. 3:p. 47]

### 5. Radiative Transfer Quantities

It is impossible to explain the radiative transfer concepts without first defining the radiometric quantities associated with remote sensing. Radiance is the radiant energy per unit time coming from a specific direction which passes through a unit area perpendicular to that direction. It is the intensity or brightness which a sensor measures. (See Figure 6) The symbol for radiance is L and its units are Watts per meter squared per steradian ($W/m^2$-sr).

Another important quantity is irradiance or radiant flux density, which is the total flux of photons flowing into a particular point per unit area from all directions. (See Figure 7) The radiant flux density leaving a surface is

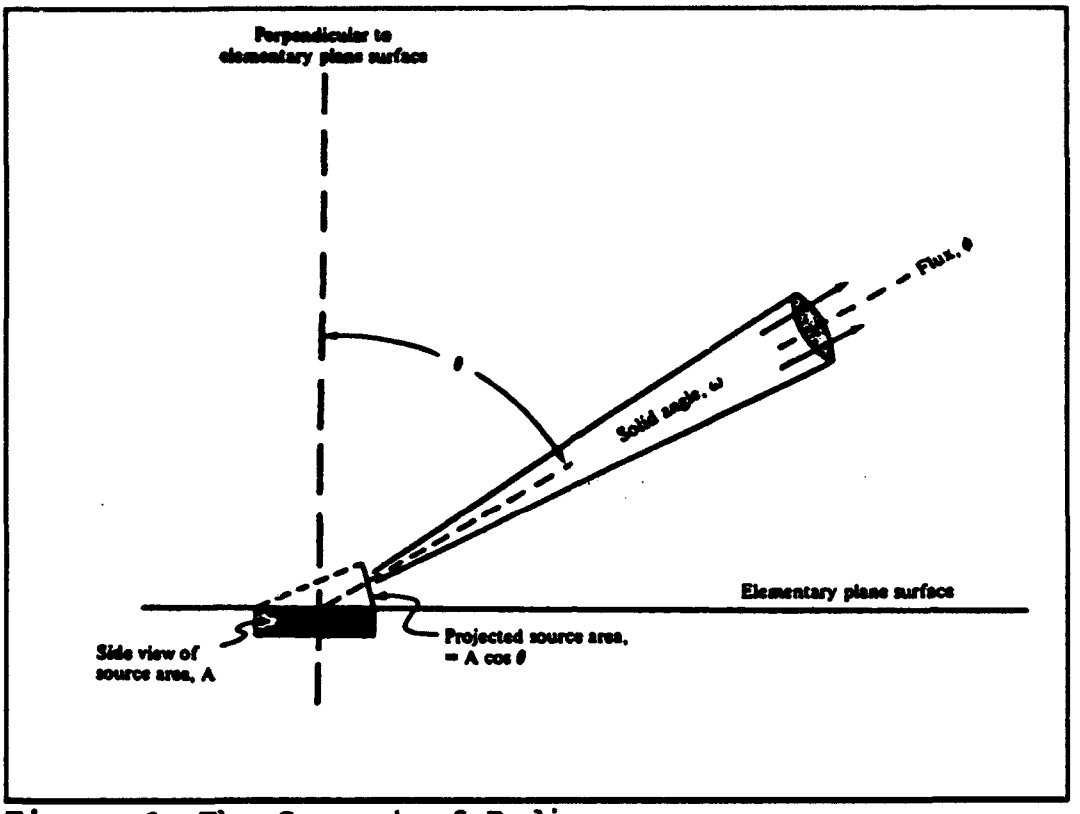


**Figure 6** The Concept of Radiance
[Ref. 6:p. 17]

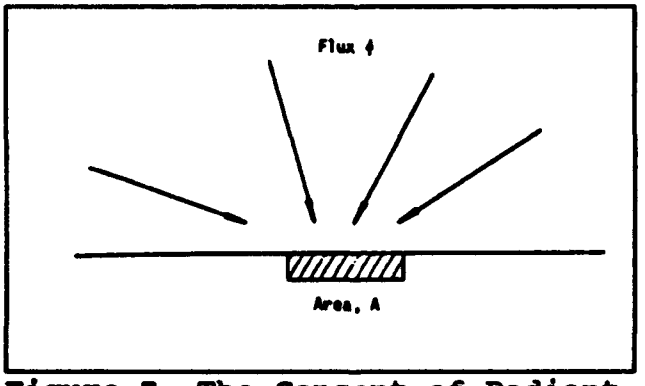


**Figure 7** The Concept of Radiant Flux Density [Ref. 3:p. 47]

called exitance, M. This quantity is important in remote sensing because knowing how different surfaces emit photons can help derive information about a target when its radiance is measured at a sensor. Normally, the quantity of electromagnetic radiation that sensors measure is spectral radiance, which is the radiance per wavelength. [Ref. 9]

### 6. Solar and Atmospheric Properties

In passive remote sensing, the primary source of electromagnetic radiation at visible wavelengths is the sun. The objective is to characterize a target's solar irradiance as it is modified by scattering, reflection, and absorption due to the earth's atmosphere and surface. Therefore, it is important to understand the sun's characteristics as they affect remote sensing. The sun's photosphere emits radiation as a near blackbody. This radiation travels through the solar system. Solar radiant flux output, though, is variable because the sun does not emit radiation as a perfect blackbody at all wavelengths. Therefore, the amount of solar radiation emitted depends on wavelength. Figure 8 illustrates this effect on the solar spectrum. [Ref. 5:pp. 38-39]

The earth's atmosphere is another important consideration in remote sensing because of its significant effect on electromagnetic radiation. The atmosphere between the sensor and the target and also between the radiation source and the target affects the radiance measured by the

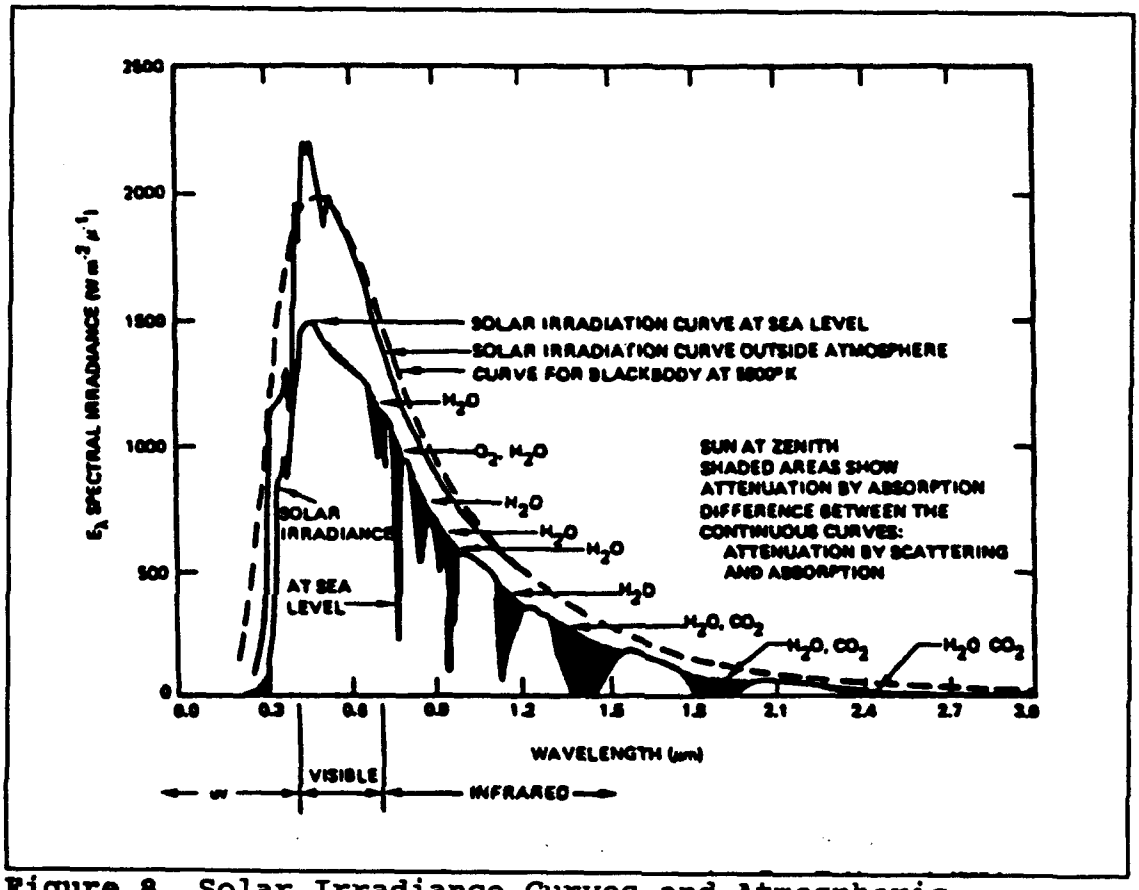


**Figure 8** Solar Irradiance Curves and Atmospheric Absorption Bands (From Chahine, et al., 1983)

remote sensor. Energy transmitted through the atmosphere may be scattered or absorbed. Scattering is the reflection or refraction of radiation by particles in the atmosphere. When radiation interacts with the atmosphere, photons can be absorbed by gases or other constituents. This absorption heats the atmosphere. Both scattering and absorption are

wavelength dependent and the extent of their influence on radiation is determined by the meteorological characteristics of the atmosphere. By conservation of energy, the irradiance absorbed, transmitted and reflected must add to equal the initial amount of irradiance. [Ref. 8:p. 35]

Atmospheric constituents that absorb electromagnetic energy are $CO_2$, $H_2O$, $O_2$, and $O_3$. The ranges for these absorption bands are also shown in Figure 8. For example, major water vapor absorbing regions exist at 1-3 microns and 5-7 microns. There are ranges in the electromagnetic spectrum where the atmosphere allows photons to be transmitted without absorption by any gases. These transmittance regions are called atmospheric windows. A window in the visible range exists between 0.3 and 0.7 microns. Sensors are designed to operate in ranges that take advantage of atmospheric windows. [Ref. 9]

### 7. Radiative Transfer Equation

An approach to quantifying the measurement of radiance of a remotely located sensor is illustrated by the radiative transfer equation model. By applying spherical coordinates to the concept of a solid angle, a frame of reference is created that models radiance emanating in a particular direction from an area on the earth's surface. With this frame of reference, an equation can be developed to represent all of the factors that influence the radiance measured by a sensor. The

equation for total radiance detected at the sensor as a function of wavelength and direction is

$$L_t(\lambda,\theta,\phi) = L_o(\lambda,\theta,\phi)\, e^{\frac{-\delta(\lambda)}{\mu}} + \int_0^{\delta(\lambda)} \frac{\sigma_s(\lambda,z)\, B[\lambda,T(z)]}{\sigma_e(\lambda,z)} e^{\frac{-\delta(z,\lambda)}{\mu}} \frac{d\delta}{\mu} +$$

$$+ \int_0^{\delta(\lambda)} \frac{\oint \gamma_s(\theta,\phi;\theta',\phi';\lambda,z)\, L(\theta',\phi';\lambda,z)\, d\Omega'}{\sigma_e(\lambda,z)} e^{\frac{-\delta(z,\lambda)}{\mu}} \frac{d\delta}{\mu}.$$

Although the radiative transfer equation appears complex, it is relatively simple to explain in words. The first term is the radiance transmitted from the earth's surface through the atmosphere to the sensor, at a specific wavelength. Anything in the atmosphere, in the path between the surface and the sensor, that has a temperature emits radiance in the direction of the sensor. The quantity of this radiance that is transmitted to the sensor without being scattered or absorbed is represented by the second term. The third term accounts for radiance that is scattered from all directions into the direction of the sensor anywhere in the path between the surface and the sensor. The radiative transfer equation shows that given knowledge of atmospheric characteristics and sources of electromagnetic radiation, measurements of the radiance at a remote sensor can be used to derive information about the earth's surface. [Ref. 7]

The relationship between measured radiance and the factors that influence it is the basic concept that supports the hyperspectral sensor experiment which is the focus of this thesis. The AOTF measures the total radiance received from an area on the earth's surface in a particular direction over a range of wavelengths. Through analysis of the data measured by the sensor, information about the targets in the imaged scenes may be derived.

## B. SPECTRAL CHARACTERISTICS

An important radiometric quantity, especially in imaging spectroscopy is spectral reflectance. Spectral reflectance is a function of wavelength and is determined by the manner in which solar radiation interacts with the earth's surface [Ref. 8:p. 38]. In order to characterize ground features, it is essential to know their spectral reflectances.

The spectral radiance at a sensor is the solar radiance reflected by a place on the earth's surface as modified by the atmosphere. By measuring this radiance, and knowing the quantity of atmospherically altered solar irradiance, the reflectance of the surface can be derived. Reflectance of a feature or target on the earth's surface is the ratio of the measured irradiance and the atmospherically altered solar irradiance. A spectrum of reflectance values for a target can be created by measuring the radiance over a range of wavelengths. This spectrum of reflectances is commonly

referred to as the spectral signature of the target. The ability to identify targets on the earth's surface through analysis of spectral signatures is the objective of imaging spectroscopy. (See Figure 9)

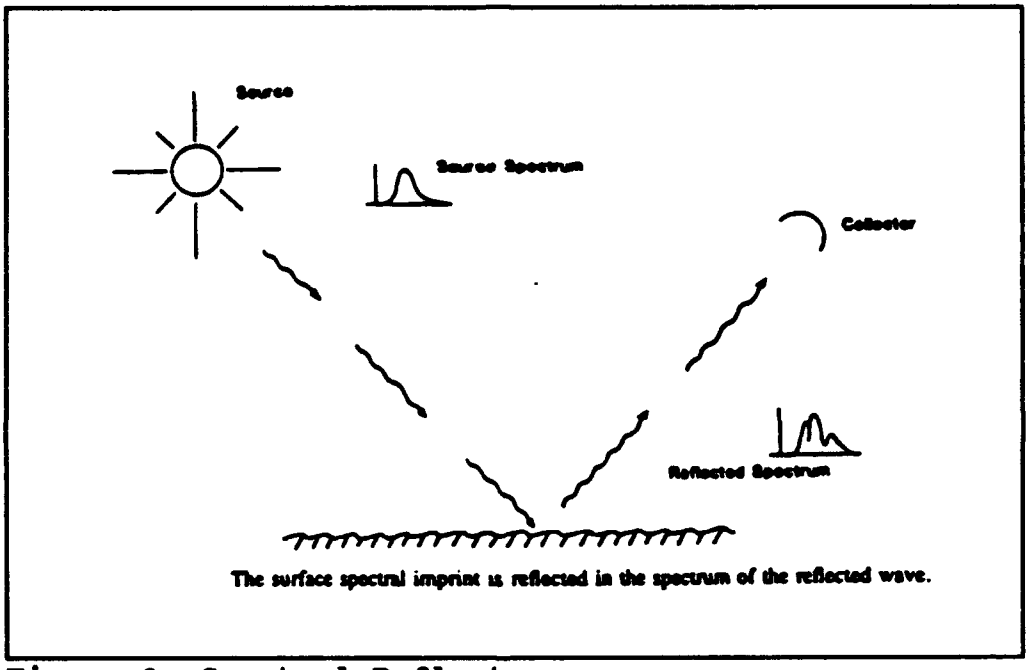


**Figure 9** Spectral Reflectance

Under ideal circumstances, spectral signatures could be used to accurately detect and locate targets on the earth's surface by analyzing hyperspectral data due to its high

spectral resolution. However, spectral signatures are not single valued or completely independent of other factors. A target's moisture content, background, and illuminating and viewing geometries, among other factors, like meteorological conditions, can alter its observed reflectance spectrum. Therefore, spectral analysis must be accompanied by spatial information in order to draw accurate conclusions about targets on the earth's surface. [Ref. 5:p. 97]

## C. POLARIZATION

Electromagnetic radiation propagates as plane polarized waves as shown in Figure 2. Conventionally, the plane of polarization for an electromagnetic wave is that of the electric field, but actually, the wave may polarize in any plane perpendicular to the direction it travels. Polarization of solar radiation occurs as a result of reflection and scattering by the earth's surface features. Anything that has a surface can cause polarization of radiation incident upon it through reflectance or scattering, especially in the spectral region between 0.18 and 3.0 microns where reflected and scattered radiation dominates. [Ref. 6:pp. 27-40]

Solids and liquids with a temperature emit polarized radiation. By applying Maxwell's equations to optical surfaces, Fresnel developed equations to describe this polarization for a smooth surface. According to Fresnel,

emissivity, $\epsilon$, has two components relative to the plane of emission, one parallel and one perpendicular such that,

$$\epsilon=\frac{1}{2}(\epsilon_{\parallel}+\epsilon_{\perp}),$$

$$\epsilon_{\parallel}=\left[\frac{2\sin\theta\cos\phi}{\sin(\theta+\phi)\cos(\phi-\theta)}\right]^2,$$

$$\epsilon_{\perp}=\left[\frac{2\sin\theta\cos\phi}{\sin(\theta+\phi)}\right]^2.$$

In these equations, $\theta$ is the angle of emission from the surface normal and $\phi$ is the angle of incidence for internally generated blackbody radiation. This relationship between emissivity and polarization is the basis for polarimetric analysis of AOTF hyperspectral data. [*Ref. 6:p. 29*]

The quantities of emissivity and reflectance are related such that,

$$\epsilon=1-\rho,$$

where $\rho$ is reflectance. Therefore, reflectance also possesses parallel and perpendicular components. The quantity of reflectance is derived from the radiance measured by the AOTF sensor in two different polarizations. This ability to separate reflectance values into its components allows polarimetric data analysis.

## D. AOTF DESIGN

The basic premise for the design of an acousto-optic tunable filter is that an optical medium's index of refraction can be altered by sound. An acoustic strain applied to a material creates a perturbation of the refractive index in the form of a wave. This causes the medium to become nonhomogeneous with a variable refractive index. The ability to influence diffraction of light through the application of sound is referred to as the acousto-optic effect. [Ref. 7:p. 857]

A set of parallel reflectors separated by the acoustic wavelength, $\Lambda$, will reflect light if the angle of incidence, $\theta$, satisfies the Bragg condition for constructive interference,

$$\sin\theta = \frac{\lambda}{2\Lambda},$$

where $\lambda$ is the wavelength of light in the medium. An optical wave composed of a broad spectrum of wavelengths can be filtered using this acousto-optic technique. The filter is tuned by changing the angle, $\theta$, or the sound frequency. [Ref. 7:pp. 856-863]

An AOTF consists of a piezo-electric transducer bonded to a properly oriented birefringent crystal. Applying an RF voltage to the transducer induces an acoustic wave in the crystal, periodically altering its index of refraction. This

traveling wave causes diffraction of light entering the crystal. If an AOTF is noncolinear, the diffraction of the optical wave is accompanied by a deflection at the tuned wavelength into two narrow beams exiting the crystal. The two beams are derived from orthogonal polarizations and are deflected at an angle to the optical wave. The output beams have wavelengths inversely proportional to the frequency of the acoustic field. Each beam is then intercepted by a detector. [Ref. 10:p. 133] (See Figure 10)

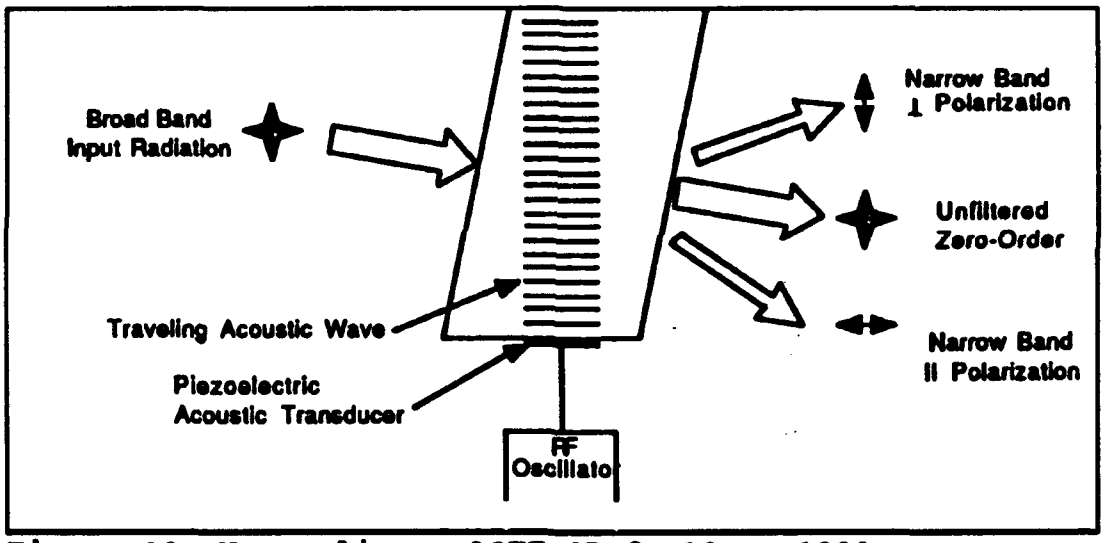


**Figure 10** Non-colinear AOTF [Ref. 10:p. 133]

In addition to providing the ability to select wavelengths by tuning the crystal, an AOTF sensor design allows simultaneous collection of both spectral and polarization information. These features make the AOTF hyperspectral

imaging system unique compared to imaging spectrometers like the Airborne Visible/Infrared Imaging Spectrometer (AVIRIS) and HYDICE systems that can only collect complete spectra by scanning a scene pixel by pixel.

# III. AOTF EXPERIMENT

The TERRA SCOUT II proof of concept experiment was conducted at Fort Huachuca on 23-26 April 1993. The experiment team consisted of two JPL engineers who assembled and operated the AOTF system, the project's principal investigator (PI) and assistant PI from DCD, an ASTRO representative, a technical advisor from Aerospace Corporation, a scientist from the University of Arizona who supplied and operated a portable field spectrometer, and the author. Over the four day period, the experiment team set up at four different sites and imaged twelve scenes. The scenes contained combinations of various targets and backgrounds. Halon panels were placed in each scene to be used for reference spectra in the eventual data correction and analysis. Also, each scene was photographed from the sensor location for ground truth. As the AOTF imaged the scene, spectral radiances for targets and backgrounds were measured with the field spectrometer to validate the accuracy of the collected data. A day by day description of the experiment follows.

## A. DAY 1

On 23 April 1993, Cemetery Hill, elevation 1650 meters, was the sensor location chosen for the first day of the experiment. The weather was conducive to a successful experiment with the exception of scattered high, thin clouds throughout the day and an average peak wind speed of 20 miles per hour. There was no precipitation and the average relative humidity was 18 percent. Also, the average temperature was 69 degrees Fahrenheit.

The AOTF system was deployed about 1.5 kilometers from a motor pool containing foreign military vehicles. Four scenes were imaged of different vehicles in the motor pool. The specific information on these four scenes is contained in Table 1.

**TABLE 1**

**EXPERIMENT INFORMATION**

| Target | Magnetic Bearing | Start Time | End Time | Elevation | File Name |
|---|---|---|---|---|---|
| Russian BMP | NE 54° | 1122 | 1152 | 1530 m | HCH |
| Russian Truck | NE 51.5° | 1241 | 1311 | 1530 m | CAN |
| Russian Tank | NE 39.5° | 1518 | 1548 | 1530 m | BTR |
| Chinese Truck | NE 48° | 1440 | 1511 | 1530 m | TRK |

These targets were chosen to obtain spectral information on foreign military equipment. Analysis of data collected on Day 1 of the experiment is not included in this thesis.

## B. DAY 2

The weather did not adversely affect the second day of the experiment, except for minor inconsistencies in measurements caused by occasional high, thin clouds. No precipitation was present on 24 April 1993. The average relative humidity was 15 percent and the average temperature was 65 degrees Fahrenheit.

The sensor location chosen was the Laundry Ridge antenna site at an elevation of 1550 meters. Four different scenes were imaged at this site. Two scenes contained aircraft on the runway of the Sierra Vista Airport, which was easily observed at a distance of approximately 2 kilometers from the sensor site. The other two scenes contained camouflaged U.S. military equipment deployed in the desert about 3.5 kilometers away from the sensor site. One scene had green camouflage nets and the other had brown nets. Table 2 shows the experiment details for these four scenes.

The two scenes of airplanes on the runway were selected for target variety, but will not be analyzed as part of this study. However, the image data for the two scenes with camouflage nets in a natural background will be studied to determine the AOTF's ability to detect military targets. The

two scenes of airplanes on the runway were selected for target variety, but will not be analyzed as part of this study. However, the image data for the two scenes with camouflage nets in a natural background will be studied to determine the AOTF's ability to detect military targets.

**TABLE 2**

**EXPERIMENT INFORMATION**

| Target | Magnetic Bearing | Start Time | End Time | Elevation | File Name |
|---|---|---|---|---|---|
| 2 C-130 Airplanes | NE 26.5° | 0923 | 0953 | 1430 m | C13 |
| 2 F-16 Airplanes | NE 31° | 1012 | 1043 | 1430 m | F16 |
| Green Camouflage | NE 34.9° | 1140 | 1210 | 1410 m | TNT |
| Brown Camouflage | NE 48° | 1322 | 1352 | 1420 m | BRT |

## C. DAY 3

Only one scene was imaged on 25 April 1993. It contained green camouflage nets concealing U.S. military equipment. Demonstration Hill, elevation 1490 meters, was the sensor site chosen for Day 3 of the experiment. From this location, the deployed equipment was well-camouflaged in a stand of trees at an elevation of 1450 meters. The sensor to target distance

was four kilometers at a magnetic bearing of NE 12° relative to the sensor site.

Weather conditions on the third day of the experiment were excellent for measuring spectral radiances. It was the clearest day of the experiment duration. No clouds were present to interfere with consistent measurements. There was no precipitation and the relative humidity was 16 percent. The average temperature was 67 degrees Fahrenheit.

The AOTF began imaging this scene at 1205 hours and finished at 1235 hours. The image data was stored in a file called VNT and completes the data set of camouflaged equipment with natural backgrounds which is the focus of the analysis conducted in this thesis.

### D. DAY 4

The last day of the experiment was 26 April 1993. Although there was no precipitation, significant cloud cover affected data collection on this day. The average relative humidity was 15 percent and average temperature was 70 degrees Fahrenheit.

Three scenes were imaged from the Huachuca Canyon Picnic Area at an elevation of 1610 kilometers. A pond about one kilometer from the sensor site was the target for the first scene. The second scene contained an OV-1D Mohawk airplane on static display in a field approximately three kilometers from the AOTF sensor. A motor pool with U.S. military vehicles was

the target for the third scene. The target/sensor distance for this scene was also about three kilometers. The experiment details for these three scenes are shown in Table 3.

**TABLE 3**

**EXPERIMENT INFORMATION**

| Target | Magnetic Bearing | Start Time | End Time | Elevation | File Name |
|---|---|---|---|---|---|
| Mohawk | NE 48° | 0955 | 1025 | 1460 m | MHK |
| Pond | NE 58.5° | 1055 | 1125 | 1510 m | PND |
| Motor Pool | NE 32.5° | 1217 | 1247 | 1475 m | MPL |

The image data collected on Day 4 of the experiment will be helpful in developing spectral libraries, but is not analyzed as part of this thesis.

# IV. METHODOLOGY

The purpose of this thesis is to analyze data collected during the experiment of a prototype AOTF hyperspectral imaging system in order to assess its potential for use in military applications. To determine the system's military utility, the experiment data selected for analysis are the three scenes which contain camouflaged equipment in natural settings. A complete and accurate assessment of the AOTF system requires processing, validation, and both spectral and polarimetric analysis of the data.

## A. DATA PROCESSING

Fundamental to processing data is understanding its format. Hyperspectral imagery forms a series of digital images. A digital image is the properly ordered array of digital numbers recorded for a remotely sensed scene. The advantage of digital imagery is that with appropriate tools it is relatively easy to manipulate. Data transmission, display and analysis of digital imagery are accomplished quickly with current communications and information systems technology.

Imaging spectroscopy provides the ability to collect digital images for each of many bands over a range of wavelengths. A basic hyperspectral data set has three

dimensions. It can be visualized as a stack of digital images at different spectral bands or channels. Hyperspectral data can also be thought of as a properly ordered array of spectra, one for each pixel. (See Figure 11) Thus, hyperspectral data adds a new dimension to digital imagery analysis with the contribution of spectral information.

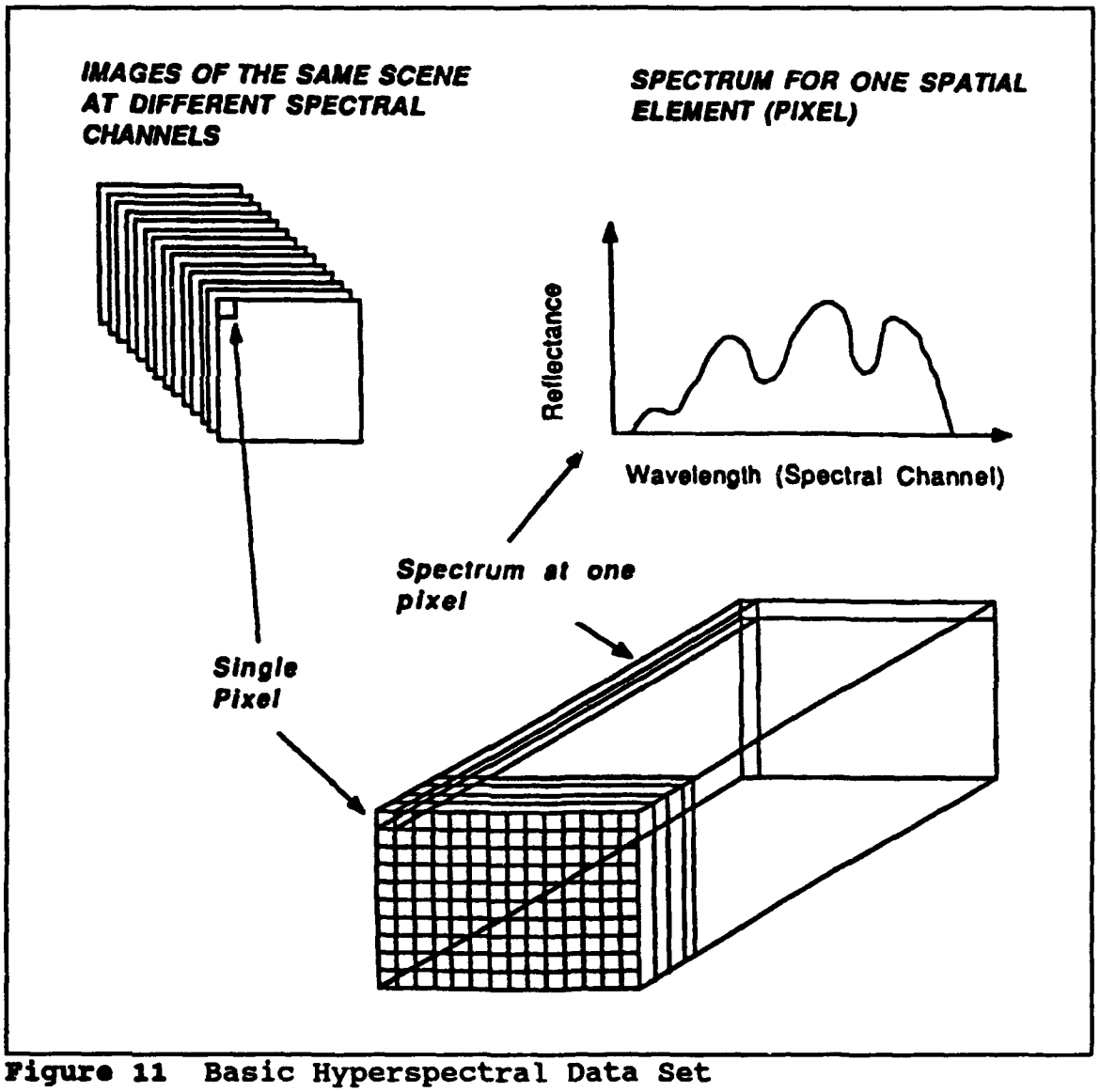


**Figure 11** Basic Hyperspectral Data Set

### 1. AOTF Experiment Data

The AOTF hyperspectral imaging system collects 33 different bands of image data over a wavelength range of 0.51 to 0.77 microns. Because of its ability to collect two different polarizations, the AOTF design provides additional information to the basic hyperspectral data set. The system acquires two digital images for each band. The two images represent orthogonally polarized views of the same scene. One polarization, annotated in the data files as *dt0*, is the image resulting from the electromagnetic waves parallel to the AOTF surface. The images created by measuring the radiance of the waves perpendicular to the AOTF's optical lens are stored in data files with *dt1* extensions to the file names. Each image file is made up of 250 samples and 350 lines which form an array of 87,500 digital numbers representing the image's pixels.

The AOTF collects the data for a scene one band at a time. For each wavelength, the system creates and stores two digital image files, one for each polarization. Chapter II described how the AOTF's wavelengths are tuned by altering the acoustic frequency input to the crystal. Thus, for each scene, the AOTF system creates 66 different digital image files. Data in this format, where the files are ordered one band at a time and each file contains a spatial image of a specific wavelength is called band sequential or BSQ. [Ref. 11:p. 5] A BSQ formatted cube allows easy access to the data

for processing and analysis, however, it is necessary to know the wavelengths that correspond to each band's data file. For the AOTF experiment data, a list of the band and file numbers with their corresponding acoustic frequency and wavelengths at each polarization is in Table 4.

### 2. Data Processing and Analysis Tools

The processing and analysis of digital imagery require the appropriate computer system and associated software. These requirements are intensified for hyperspectral data sets because of the need to visualize the spatial images as well as the spectral aspect. A computer system must be capable of storing and manipulating the many files, made up of huge arrays of digital numbers, that form this data set. The software must provide a means to read and view the data both spatially and spectrally.

The computer system used in this research was a Sun Sparc 10 workstation. It is a Unix-based machine with enough memory for responsive data manipulation and adequate data storage. The workstation's monitor is capable of displaying high quality images necessary for analysis of digital imagery.

The software system chosen to process and analyze the AOTF experiment data is called Interactive Data Language (IDL). It allows interactive analysis and display of scientific data. This software was designed for scientists

## TABLE 4

## AOTF DATA INFORMATION

| Band Number | File Number | Acoustic Frequency (Mhz) | Wavelength dt0 (nm) | Wavelength dt1 (nm) |
|---|---|---|---|---|
| 1 | 133 | 80 | 512.49 | 511.45 |
| 2 | 132 | 79 | 517.18 | 516.06 |
| 3 | 131 | 78 | 522.01 | 520.81 |
| 4 | 130 | 77 | 526.98 | 525.70 |
| 5 | 129 | 76 | 532.10 | 530.75 |
| 6 | 128 | 75 | 537.38 | 535.95 |
| 7 | 127 | 74 | 542.81 | 541.31 |
| 8 | 126 | 73 | 548.41 | 546.84 |
| 9 | 125 | 72 | 554.18 | 552.55 |
| 10 | 124 | 71 | 560.14 | 558.44 |
| 11 | 123 | 70 | 566.29 | 564.53 |
| 12 | 122 | 69 | 572.63 | 570.81 |
| 13 | 121 | 68 | 579.18 | 577.29 |
| 14 | 120 | 67 | 585.94 | 583.99 |
| 15 | 119 | 66 | 592.93 | 590.92 |
| 16 | 118 | 65 | 600.16 | 598.08 |
| 17 | 117 | 64 | 607.64 | 605.49 |
| 18 | 116 | 63 | 615.37 | 613.15 |
| 19 | 115 | 62 | 623.38 | 621.09 |
| 20 | 114 | 61 | 631.68 | 629.30 |
| 21 | 113 | 60 | 640.27 | 637.81 |
| 22 | 112 | 59 | 649.18 | 646.63 |
| 23 | 111 | 58 | 658.42 | 655.78 |
| 24 | 110 | 57 | 668.02 | 665.26 |
| 25 | 109 | 56 | 677.98 | 675.11 |
| 26 | 108 | 55 | 688.33 | 685.34 |
| 27 | 107 | 54 | 699.10 | 695.97 |
| 28 | 106 | 53 | 710.29 | 707.02 |
| 29 | 105 | 52 | 721.95 | 718.51 |
| 30 | 104 | 51 | 734.10 | 730.48 |
| 31 | 103 | 50 | 746.76 | 742.95 |
| 32 | 102 | 49 | 759.97 | 755.95 |
| 33 | 101 | 48 | 773.76 | 769.51 |

and engineers and has a relatively simple structured syntax. It "combines an immediate-mode interactive compiler, a powerful set of array-oriented operators and functions, and extensive graphic and image display capabilities into a truly interactive system." [Ref. 11:p. 1-2] The data processing and analysis conducted in this thesis is accomplished by interactive programs written in IDL. These programs are listed in Appendix A.

Because of the spectral dimension of hyperspectral data sets, the ability to display the spectra for pixels in an image is necessary. A software package that provides this capability is the Spectral Imagery Processing System (SIPS), designed by the University of Colorado's Center for the Study of Earth from Space (CSES). SIPS is written in IDL and is an excellent tool for displaying, processing and analyzing hyperspectral data sets. It was specifically designed for analysis of imaging spectrometer data at full spatial and spectral resolution. [Ref. 12:p. 3]

SIPS consists of three modules that support hyperspectral processing and analysis from data correction to final output. The first module, *SIPS_View*, is an interactive program that provides the user access to the data for viewing and manipulation both spatially and spectrally. The second module contains the SIPS utilities which consist of programs for data processing that include formatting, calibration, and tape reading. SIPS analysis programs make up the third module

that allow detailed, full-cube analysis of hyperspectral data sets. Tools from each of these modules are necessary for complete processing and spectral analysis of the AOTF experiment data. [Ref. 11:p. 1]

### 3. Data Correction

Before data analysis can be accomplished, the accuracy of the data must be determined. False results could be derived if the hyperspectral data sets are not corrected. The need for data correction is a result of the geometry of the sensor optics and the solar and atmospheric effects on the data.

#### *a. Spectral Geometry Correction*

In order to create accurate spectra for pixels in an image, each pixel must represent the same place in every other image for all the bands. The raw AOTF data does not meet this criteria. The AOTF sensor measures the radiance of a scene as it is detected on the focal plane array. Due to the Bragg condition for constructive interference, the change in acoustic frequency that tunes a new wavelength causes a very small change in the angle of incidence of the refracted beams onto the focal plane array. Although the change is small, it is significant enough to alter the pixel positions on the focal plane array between bands. This misalignment between the images of each band must be corrected to ensure accurate spectral analysis.

An interactive program called *band_shift.pro*, written in IDL, was developed to line up the images offset by the change in wavelength. This program correlates the pixels between bands by calculating the offset, shifting the lines of pixels, and creating a new aligned image. First, the program allows the user to select a particular data file and polarization view. The image data for that file is then read from files stored in an accessible directory. Next, the image for spectral Band 13, which is the reference band used to compare with the rest of the bands is displayed. At this point, the user selects a level or line of pixels in the image with the mouse to establish a reference line. A comparison of the pixel values across this line in the reference band with the same line in the other bands determines the offset error for each band. Michael Hamilton of Jet Propulsion Laboratory developed a function called *crosco* to calculate the number of pixels offset between bands by measuring the linear relationship between the reference line of Band 13 and the reference line of the other 32 bands. This function utilizes an IDL library module called *CORRELATE* and determines the number of pixels that must be shifted for the reference line in each band to best match the reference line of Band 13. The results of this function are used to properly align the entire image for each spectral band. Finally, the aligned images are written to files, creating a geometrically corrected BSQ cube.

### *b. Atmospheric and Solar Correction*

After geometry errors are corrected, the atmospheric effects on the data must be removed for accurate spectral analysis. Also, the characterization of spectral signatures requires analysis of spectral reflectance. The AOTF data is a measure of spectral radiance as a result of the sun's influence on the surface reflectance. Therefore, radiance must be converted to reflectance, by removing the solar spectrum from the data.

Correction for the atmosphere and the sun are accomplished at the same time with SIPS utilities. Because halon panels were placed in the scenes imaged by the AOTF system, a technique for data correction called flat field calibration can be used. This technique allows the removal of a reference spectrum that contains only solar irradiance and atmospheric effects from an entire image cube [Ref. 11:p. 38]. The spectrum of the halon panels is a relatively accurate representation the solar spectrum as influenced by atmospheric effects. Scientifically, flat fielding is not considered to be the most desirable data correction technique and a better approximation would result from a radiative transfer equation approach. However, for the purpose of this research, flat fielding is adequate and most practical.

Flat field correction of the AOTF experiment data is accomplished using SIPS. The first step requires converting the data cube into a SIPS formatted cube with the

*cvt2sips* utility. Then, a wavelength file must be created so *SIPS_View* can associate each band with the correct wavelength. This will enable *SIPS_View* to plot spectra by wavelength as well as band number. The wavelength file is an ASCII file with three columns. The columns contain the band number, wavelength and full-width-half-max band width value. Processing of the AOTF data requires two wavelength files, one for *dt0* files and one for *dt1* files. [Ref. 11:p. 5]

*SIPS_View* is used with the SIPS formatted data cube and appropriate wavelength file to display the image. At this point, the data is viewed band by band to verify its quality. It is important to identify any bands that may have disproportional bright or dark images to avoid errors in spectral and polarimetric analysis. These bad bands are saved and stored in a file. *SIPS_View* recognizes this bad bands list and filters the data by ignoring the files containing bad bands.

Next, a class is defined for the pixels representing halon panels. The spectrum for each pixel in the class is displayed in the *View Spectra* window and the mean spectrum for the halon panels is saved into a spectrum file. This file is the removal spectrum file used in the *flat_field* utility to correct the data. The *flat_field* utility then outputs a file containing the reflectance data. The BSQ data cube is now corrected and ready for spectral analysis.

### *c. Polarimetric Geometry Correction*

Although the BSQ cubes are sufficiently corrected for spectral analysis after the above procedures, one more correction is necessary before polarimetric analysis can be accomplished. Because the AOTF crystal is anisotropic, the angles of incidence for the refracted beams of each polarity onto the two separate focal plane arrays are not necessarily equal. This means that a pixel in an image recorded for one band is not likely to represent the same place in the differently polarized image for the same band. Comparison of the two different polarizations is not possible until the images between polarizations are aligned.

The procedure that aligned the images between bands can be used to align the images between polarizations. The IDL program that corrects the offset between polarizations is called *view_shift.pro*. This program is basically the same as *band_shift.pro* in that it uses the same correlation function to create a new BSQ cube with properly shifted images. The difference is that *view_shift.pro* reads two BSQ files, one for each polarization. It compares a reference line in each band of the data cube for one polarization to the same line and band of the data cube for the other polarization. The *dt0* cube is the reference cube and a new cube is created by shifting the images of each band by the calculated offset for the *dt1* cube. After applying these procedures to the six BSQ cubes that make up the data set for the three scenes of

interest, the AOTF experiment data is finally prepared for analysis.

## B. VALIDATION

In order to prove the concept of the AOTF hyperspectral system, it is important to establish the validity of the data it collects. Toward this end, field spectrometer measurements of various targets and backgrounds were recorded during the experiment. By comparing graphs of the target and background spectra produced from the field spectrometer data to spectra graphs of the same features using AOTF data, the data's validity can be determined. The field spectrometer data is shown in Appendix B.

SIPS provides the ability to create spectra files by defining classes of features. It allows the user to select pixels that represent a particular feature and save the resulting mean spectrum to a file. This file can be used to print a graph of the feature's spectrum. Spectral graphs of the field spectrometer data are compared to those of the AOTF data to validate the experiment results. Appendix C contains the spectra graphs of selected features for each AOTF data set.

## C. SPECTRAL ANALYSIS

The objective of the spectral analysis performed on the experiment data is to determine the AOTF system's ability to

distinguish military targets from the natural background in a scene. Two different methods are used to analyze the data's spectral characteristics. One method utilizes a SIPS analysis program, called Spectral Angle Mapper (SAM), which compares the similarity of a reference spectrum to the spectra in an entire scene. The other method is a technique that involves combining ratios of carefully selected bands to highlight a particular feature within a scene.

1. **SAM**

The SAM program in SIPS compares the spectrum of a reference pixel, r, to the spectrum of every other pixel in a data cube, t, using the equation,

$$\theta=\cos^{-1}\left(\frac{\sum_{i=1}^{nb} t_i r_i}{\sqrt{\sum_{i=1}^{nb} t_i^2}\sqrt{\sum_{i=1}^{nb} r_i^2}}\right),$$

where nb is the number of bands in the data cube. This method calculates the angular difference between two spectra, creating a new image that highlights the most spectrally similar pixels. The SAM processed output image is viewed in the *SAM Viewer* window. It is displayed in gray scales with two threshold controls for fine tuning the image. If the high threshold is lowered, pixels less similar to the reference spectrum become darker. If the low threshold is raised, all

pixels within the scene become brighter. The threshold adjustments allow the bright pixels that are most similar to the input spectrum to be contrasted with the rest of the pixels in the image. [Ref. 11:p. 18]

In order to use the SAM analysis tool within *SIPS_View*, a band interleaved by pixel (BIP) formatted data cube must be created. A BIP data cube stores the data as a properly ordered array of spectra. [Ref. 11:p. 5] This format allows the program ready access to the spectra for each pixel without calculating them from the BSQ image cube. *SIPS_View* is then used to identify a reference spectrum. The spectrum for the target of interest within a scene is the reference spectrum. This is accomplished by creating a class of pixels representing the target and saving the mean spectrum to a file. Next, the SAM function is selected under the *View Spectra* menu in the *SIPS_View* program. The reference spectrum is then loaded into the SAM function and processed. The SAM program compares the spectrum of every pixel in the data cube to the reference spectrum and calculates the angular difference between them. The result is an image that highlights the pixels with spectra most similar to the reference spectrum. The contrast of the output image is adjusted using the threshold controls in the *SAM Viewer* window to highlight the results. The pixels with spectra most like the target's spectrum are brightest while the darker pixels have less similar spectra.

### 2. Band Ratios

Another approach to spectral analysis of hyperspectral data is band ratioing. In this method, an image is created by combining ratios of carefully selected bands which displays a target distinguished from its background. The spectra of the surface features within a scene are used to determine the bands which provide the largest spectral differences between a target and its background. By adding or subtracting the images resulting from ratios of particular bands, a target of interest is highlighted, while the background features are subdued.

The best combination of bands to ratio is determined by comparisons of the spectra for a target and the background features that dominate a scene. The spectral graphs used in the validation of the AOTF experiment data provide the information necessary for proper band selection. The first ratio must highlight the target of interest. The two bands selected for this ratio are the bands with the highest and lowest relative reflectance recorded for the target spectrum. Ideally, the target's spectrum possesses a large difference in reflectance values for these bands compared to the difference in reflectance values for the other features within the scene. An array of pixel values is created, if the higher reflectance band is divided by the lower one. The resulting image contains relatively high pixel values for the target. Thus, in a gray scale image, the target appears bright.

However, other features with similar spectral curves may also show up as brightly as the target. In order to subdue these bright features yet highlight the target, another ratio of bands is subtracted from the band ratio image. A comparison of the target spectrum and the spectral curves for the features is necessary to determine the bands for the second ratio. The two bands with the largest difference in reflectance recorded for the background features but the smallest difference in reflectance for the target are chosen for the second ratio. By subtracting this ratio from the first ratio, an image is created in which the target remains bright while the previously highlighted background features are subdued. Ratios of selected bands are combined in this manner until the target is distinguished from all its background features.

As a result of dividing one band by another, the numbers in the image array are very small. There is little difference between the maximum and minimum pixel values. Thus there is a loss of contrast and clarity in the band ratio images. However, these images can be enhanced by applying a logarithmic scale to the ratios. The band ratio image arrays are replaced with the base ten logarithm for each pixel value. This increases the total range of pixel values and the ability to detect features in the band ratio images. Applying the base ten logarithm to the band ratio images enhances the

quality of their display and improves the results achieved by the band ratio technique.

An IDL program called *ratio.pro* was developed to perform this band ratio method of spectral analysis on the AOTF experiment data. The interactive program allows the user to select a data set and up to three pairs of spectral bands. It divides the array of pixel values for the first band by the array of pixel values for the second band. The base ten logarithm is calculated for the resulting array, which creates an image. The logarithms of the second and third ratios are then subtracted from the first ratio. The result is an image which highlights the target of interest within a scene.

## D. POLARIMETRIC ANALYSIS

A polarimetric analysis of the AOTF experiment data is necessary to determine the utility of a scene's polarimetric characteristics in distinguishing between targets and background features. Theoretically, man-made targets polarize differently than natural ones. Therefore, a comparison of the polarization differences for each wavelength is the method for polarimetric analysis used in this thesis.

An IDL program called *polarize.pro* was developed to perform polarimetric analysis on the AOTF experiment data. The program allows the user to select a particular data set. It then reads both *dt0* and *dt1* BSQ data cubes for the selected scene. The *dt1* pixel values are subtracted from the *dt0*

image, creating an image representing the difference between polarizations for each wavelength. The program displays both polarization view images and also the image for the difference between them, band by band.

A comparison of the spectral graphs of the target's spectrum for both polarizations illustrates the wavelengths with the largest polarization difference. The IDL program can be used to view the images of the polarization difference for these spectral bands and thus, determine the target's polarimetric characteristics.

# V. RESULTS

This chapter describes the results of performing the processing and analysis procedures shown in Chapter IV on the AOTF experiment data. Spectral and polarimetric analysis provide information about a scene that allows the targets to be distinguished from the background. This ability to identify features within a scene is illustrated for each of the three AOTF data sets containing camouflaged military equipment deployed in the desert. The results include an assessment of the data validation, spectral analysis and polarimetric analysis for the scenes of interest. Also, an algorithm developed to combine the information gained from spectral and polarimetric analysis is addressed in this chapter.

## A. SCENE 1

The first AOTF data set to be analyzed is the scene called TNT. It contains a communications site with four separate camouflaged pieces of equipment. Figures 12 and 13 show the two different corrected polarization images for Band 14. A dark green camouflage net conceals the smaller piece of equipment in the middle of the scene. The other equipment is concealed under woodland camouflage nets that are patterned

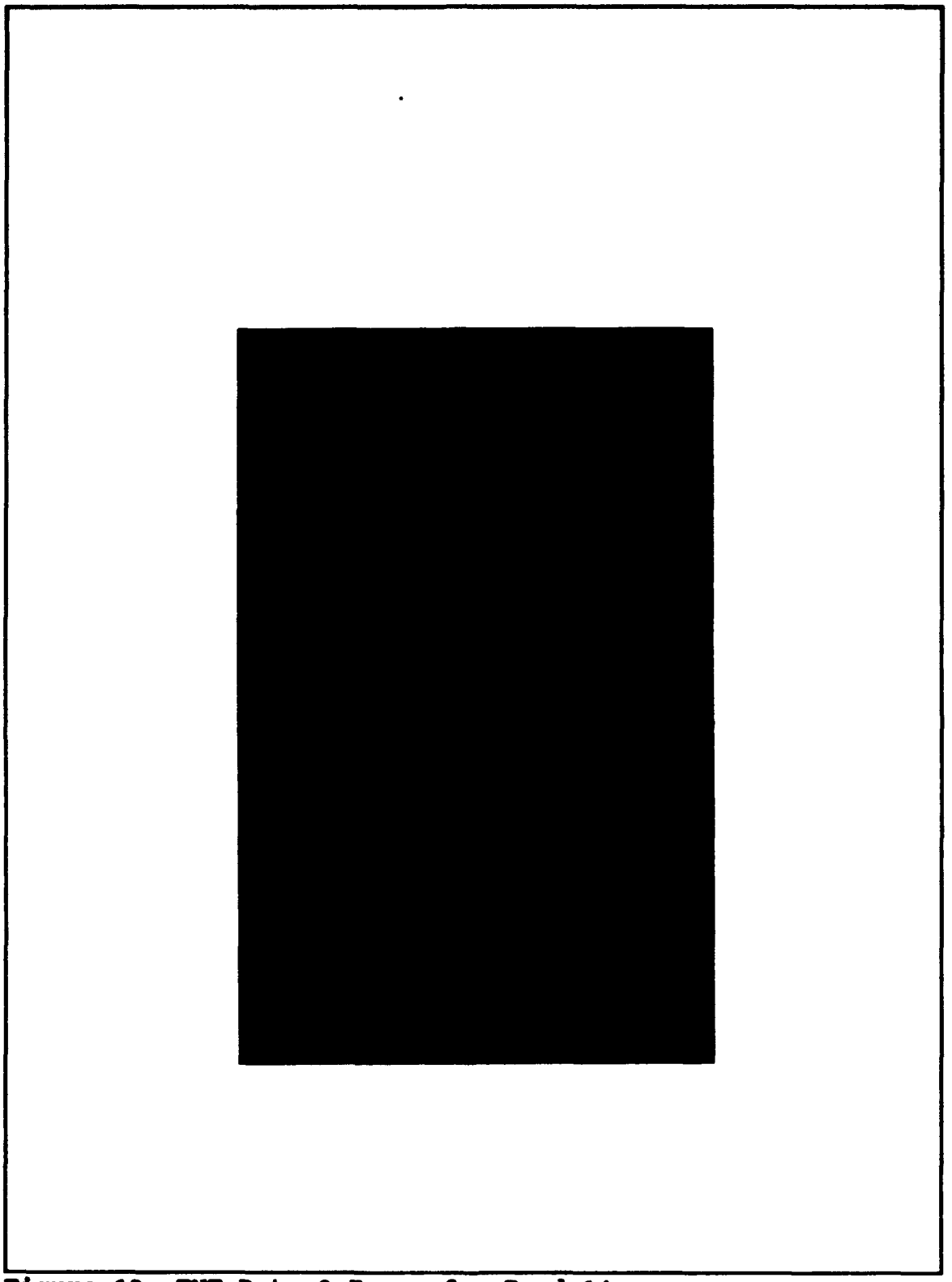

**Figure 12 TNT Data 0 Image for Band 14**

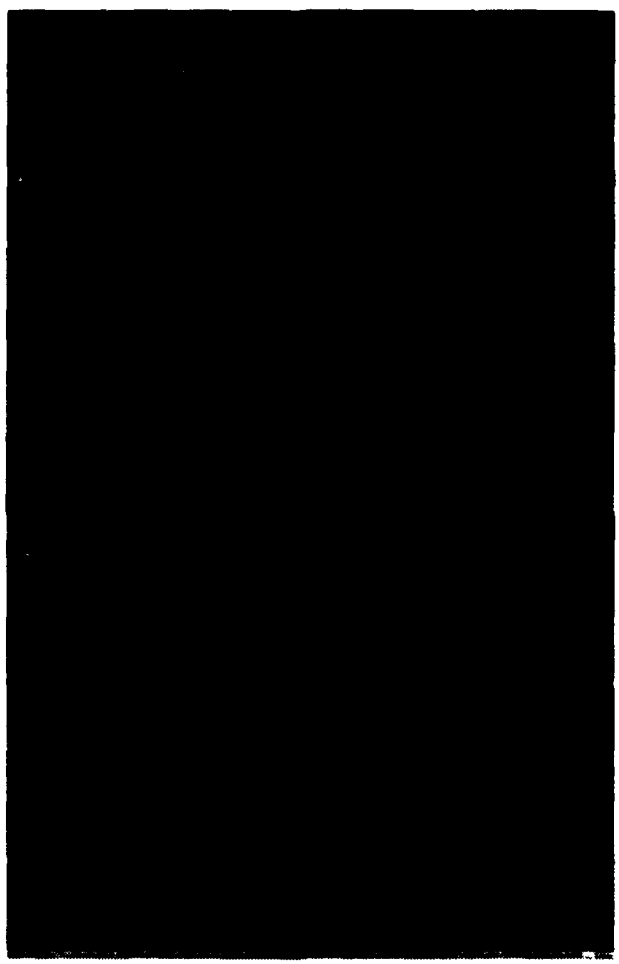

**Figure 13** TNT Data 1 Image for Band 14

shades of browns and greens. There are yucca cactus in the foreground and different types of grass, dirt, plants and bushes in the background.

1. Data Validation

As described in Chapter IV, a simple way to verify that the prototype AOTF system collected accurate spectral information is to compare spectral graphs of the AOTF data with those produced from the field spectrometer measurements. Figure 14 shows the field spectrometer spectral curve for the dark green camouflage net in the scene. The AOTF data's spectrum for the same net is shown in Figure 15. The curves are relatively similar and the differences between them are easily explained. The spike in the AOTF curve at 0.62 microns is the result of a bad band. The entire image recorded by the sensor for Band 18 is significantly brighter than the images for all the other bands. Therefore, the spectra for every pixel in the *dt0* scene have a similar spike at this wavelength. The field spectrometer spectrum appears smooth compared to the AOTF curve. This is due to the fact that there are three times as many data points in the field spectrometer curve. The AOTF system collects images for only 33 different wavelengths while the field spectrometer collects spectral radiances over a range of 100 wavelengths from 0.4 to 1.2 microns. In order to facilitate comparison with the AOTF data, the spectral graph for the camouflage net was plotted

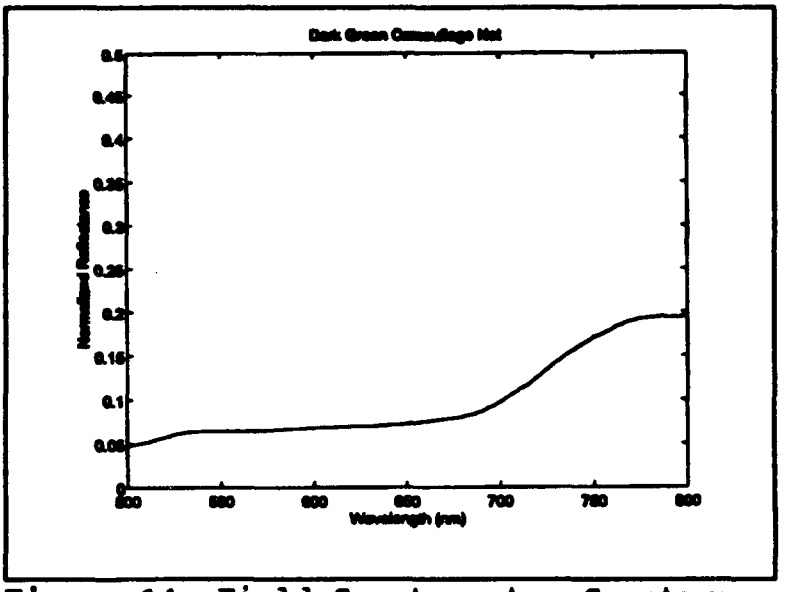


**Figure 14** Field Spectrometer Spectrum for Dark Green Camouflage Net

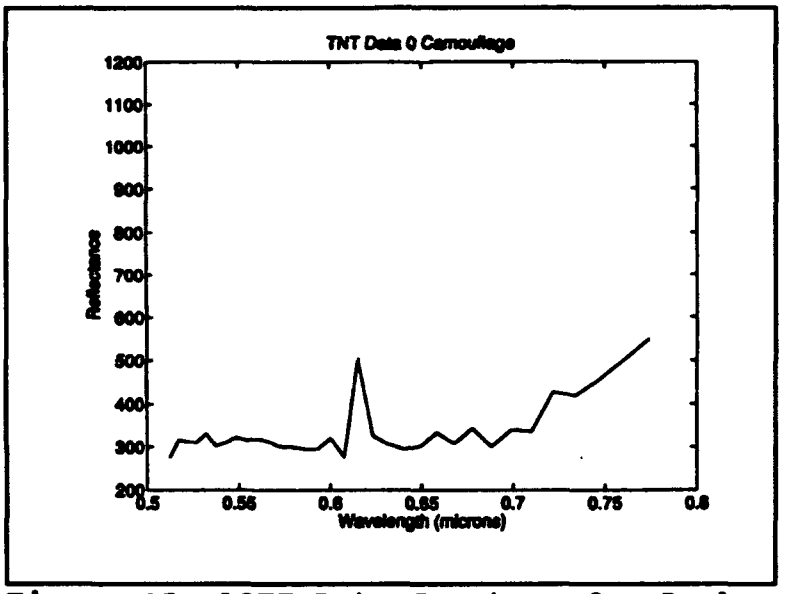


**Figure 15** AOTF Data Spectrum for Dark Green Camouflage

only between 0.5 and 0.8 microns. Considering the reasonsfor the differences between the two curves, a distinct similarity is apparent and therefore, the data can be considered valid.

### 2. Spectral Analysis

#### a. *SAM*

Figure 16 shows the image created by the Spectral Angle Mapper analysis tool in SIPS. The input spectrum used to compare with every pixel in the image is the mean spectrum calculated from the spectral curves for selected pixels representing each of the four camouflage nets in the scene. Portions of the camouflaged equipment appear bright in the SAM image. However, the image does not clearly define the shapes of the targets. Because the shapes are not discernable, it is difficult to distinguish the bright areas representing the target from those of the background features. The colored patterns of the camouflage nets are too variable for the sensitivity of the SAM utility. For this reason, the SAM utility in SIPS may not be a useful tool for accomplishing spectral analysis.

#### b. *Band Ratios*

By carefully selecting bands to ratio and combine, an image can be created that highlights a particular feature based on its spectral characteristics. An image illustrating this technique applied to the *dt0* polarization for the TNT data is shown in Figure 17. The bands selected for the first

**Figure 16** TNT Data 0 Spectral Angle Mapper Image

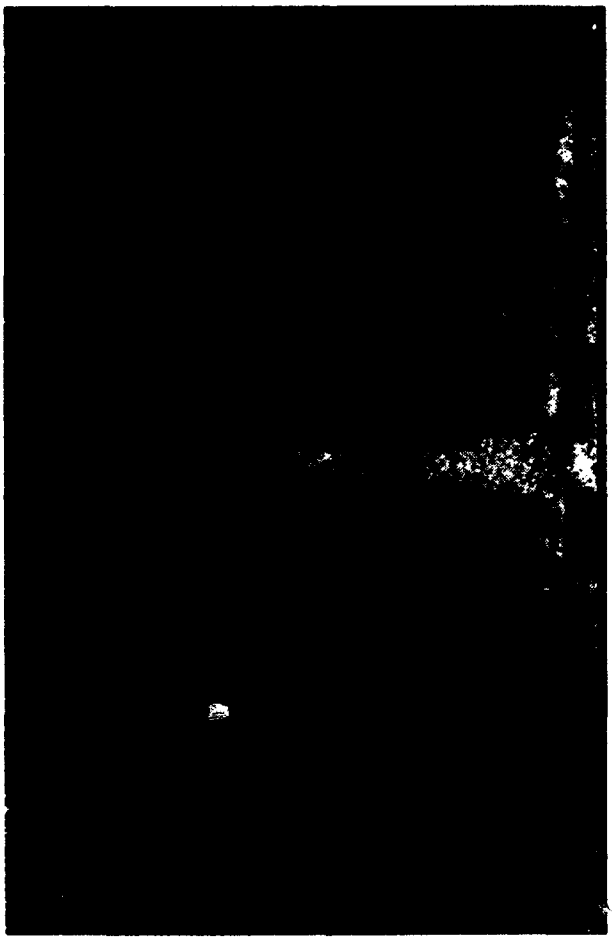

**Figure 17 TNT Data 0 Band Ratio Image**

ratio are Band 25 and Band 9. They represent images at wavelengths of 0.68 and 0.55 microns respectively. These two bands were chosen to create an image that makes the camouflaged equipment appear bright relative to the background features. The second ratio is Band 23 divided by Band 32, while the third is the ratio of Band 30 to Band 3. These bands were determined by comparing the mean spectrum for the camouflage nets to the mean spectral curves for the dominant background features in the same scene. Bands which result in a large difference between reflectance values for grass and plants, but a relatively small difference in reflectance values for the camouflage nets are chosen for these ratios. The second and third ratios are subtracted from the first ratio in order to subdue background features in the image that appear as bright as the camouflage nets.

The image of the combination of band ratios clearly highlights the camouflaged equipment compared to the background. The entire surface area of the camouflaged equipment is represented by brighter pixels than the background such that the shapes of the targets are distinguishable. The band ratio approach is much more effective in detecting the camouflaged equipment in this scene than the SAM analysis tool in SIPS.

## 3. Polarimetric Analysis

The ability of the AOTF hyperspectral imaging system to collect both spectral and polarimetric data allows the performance of another type of analysis to derive information about surface features from remotely sensed imagery. To analyze the polarimetric characteristics of surface features, given data from two orthogonally polarized images, the difference between the polarizations can provide information. An effective way to visualize the difference between the parallel and perpendicular polarized data collected by the AOTF system is to create an image by subtracting the polarization view for one band from the other for the same band. Figure 18 shows the image resulting from the subtraction of the *dt1* image from the *dt0* image for the TNT data set at Band 14. A comparison of the spectral curves for the camouflage nets in this scene at each polarization shows that the polarization difference is relatively large in Band 14 or at 0.58 microns.

The difference in polarization provides information about certain features within the scene. The halon panels register quite well in the polarization difference image. The panels were placed at 90 degree angles to one another. One was placed flat on the ground while the other was propped up to face the sensor directly. The very dark pixels in the right center of the image represent the large negative difference between polarizations as a result of the panels

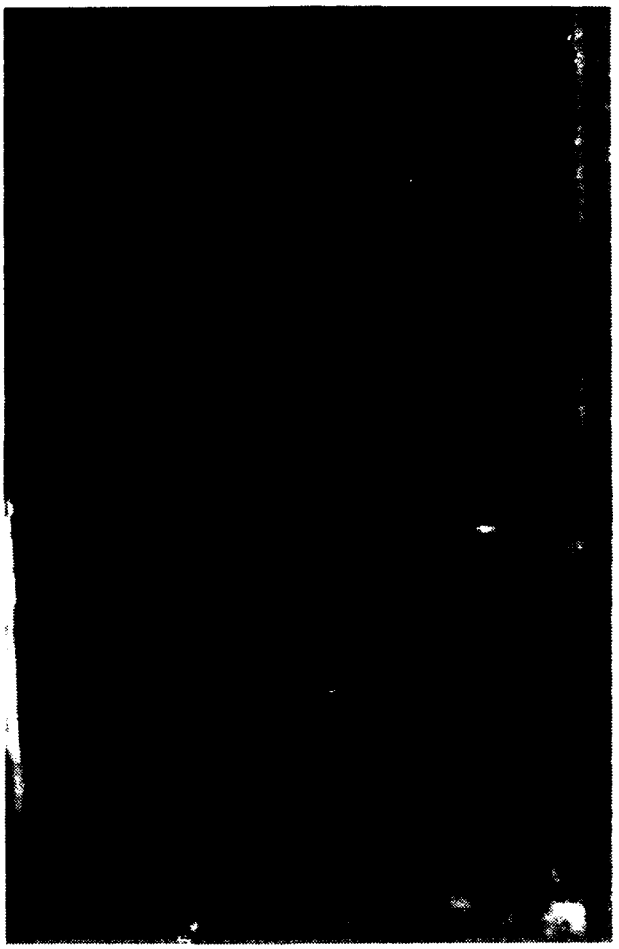

**Figure 18** TNT Band 14 Polarization Difference Image

perpendicular to the AOTF lens. Similarly, the very bright pixels immediately below the dark ones represent the large positive difference between polarizations as a result of the reflectance off of the halon panel parallel to the AOTF sensor. The smooth surface of the panels caused the reflected sunlight to polarize more significantly than that reflected off of the other features in the scene.

The polarization difference image also highlights the shapes of the camouflaged equipment. The top edges of the nets are represented by bright pixels and the bottom edges where the camouflage nets meet the ground are darker. Features like plants, bushes, and the contour of the land have surfaces that reflect light in a way which causes it to polarize. Significant features within a scene can be detected in this manner.

An interesting result is the clarity with which the periscoping antenna protruding from the far left camouflage net in the scene is detected. Its distinct shape and smooth surface polarize the reflected light, allowing it to be easily distinguished from its background in the polarization difference image.

## B. SCENE 2

The AOTF data set called BRT contains another communications site deployed in the desert. However, the equipment in this scene is concealed under desert or tan

colored camouflage nets. There are three separate camouflaged pieces of equipment on the left side of the image and three more camouflage nets concealing equipment further away on the right side of the image. The scene contains grass, plants and shrubs in the foreground with buildings and trees in the distant background. A satellite dish antenna painted dark green is barely discernable in the image between the two sets of camouflaged equipment. Figures 19 and 20 show the corrected images for each polarization in Band 13.

### 1. Data Validation

A comparison of the spectra from the AOTF image data to the spectra resulting from the field spectrometer measurements for features in this scene confirms the validity of the data. The spectra for the tan camouflage nets illustrate the similarity between the spectral curves for each data source. (See Figures 21 and 22)

Although, the overall similarity between the spectra for the tan camouflage nets is evident, it is important to note the spikes at 0.62, 0.65 and 0.70 microns. Again, the abnormally high reflectance values represent bad bands at these particular wavelengths. The bad bands are caused by slight errors in sensor alignment and are a common occurrence in hyperspectral data collection. Also, the AOTF spectrum is not as smooth as the field spectrometer curve due to the fewer number of data points available for the AOTF data set.

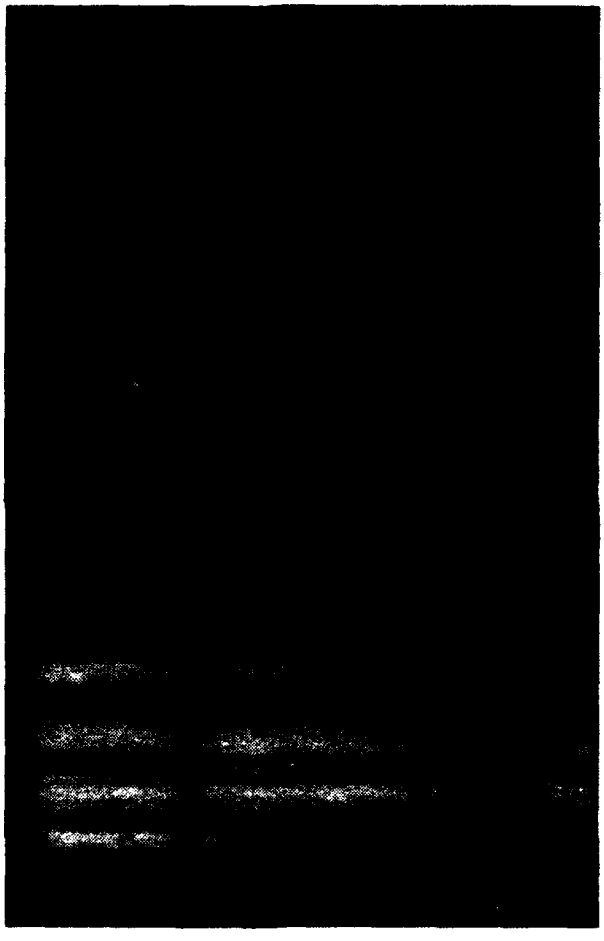

**Figure 19** BRT Data 1 Image for Band 13

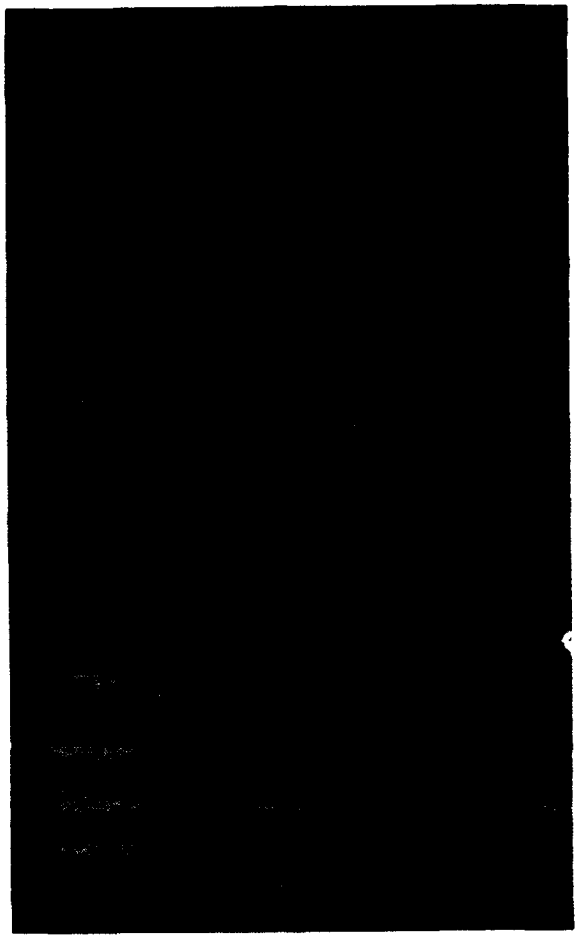

**Figure 20** BRT Data 0 Image for Band 13

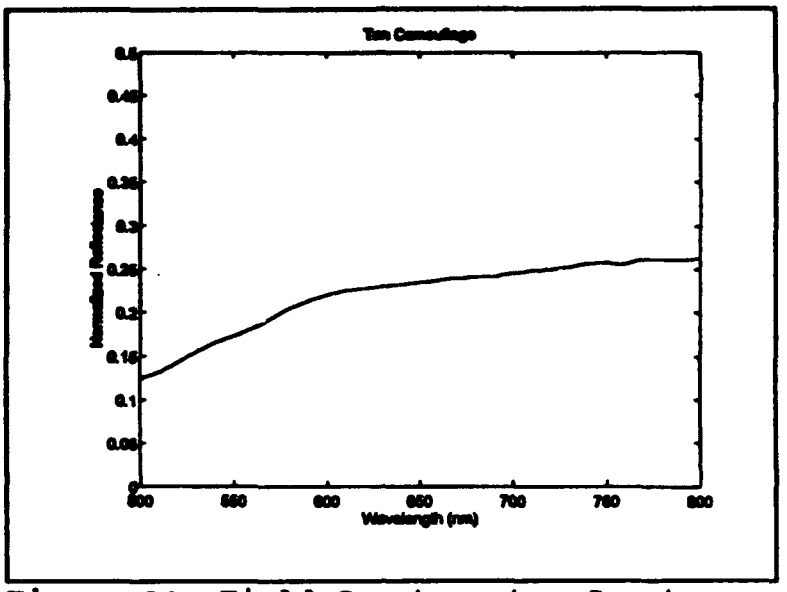


**Figure 21** Field Spectrometer Spectrum for Tan Camouflage Net

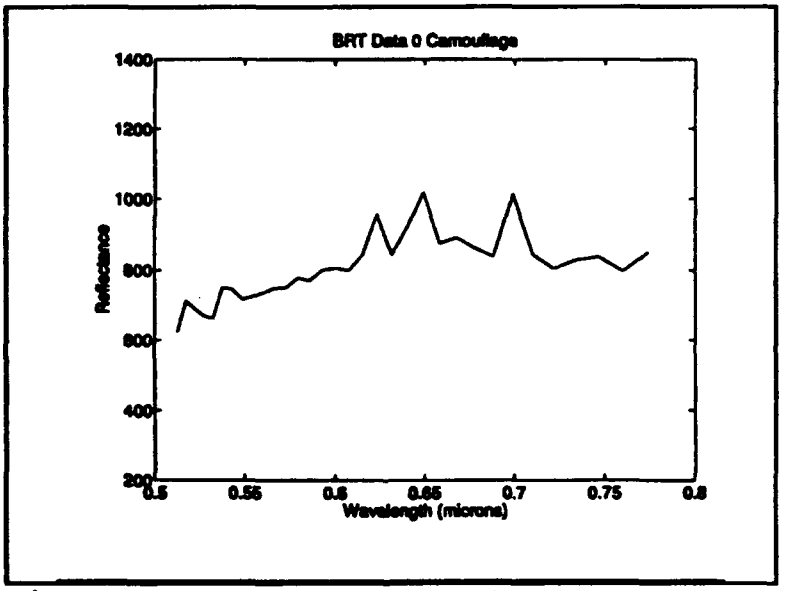


**Figure 22** AOTF Data Spectrum for Tan Camouflage Net

However, the basic shape of both curves is the same which indicates that the BRT data set is valid.

2. Spectral Analysis

*a. SAM*

The SAM image that SIPS produced by comparing the input spectrum of the tan camouflage nets with the spectrum for each pixel in the scene is shown in Figure 23. The spectrum used as input for the SAM function is the mean calculated from selected pixels representing the tan camouflage nets.

Unlike the TNT data set, the SAM analysis tool is relatively effective in highlighting the tan camouflage nets in the BRT scene. The SAM image shows these targets with significantly brighter pixels than most of the background features. Even the shapes of the camouflaged equipment are discernable. However, some of the pixels that represent grass in the image appear as bright as the camouflage nets. This is a result of the spectral similarity between the tan camouflage nets and the desert grass. Figures 24 and 25 illustrate the mean spectra for each surface feature. The SAM method as applied to the BRT data set is successful in identifying the targets because the input spectrum for the tan camouflage nets is consistent over the entire area of each of the targets.

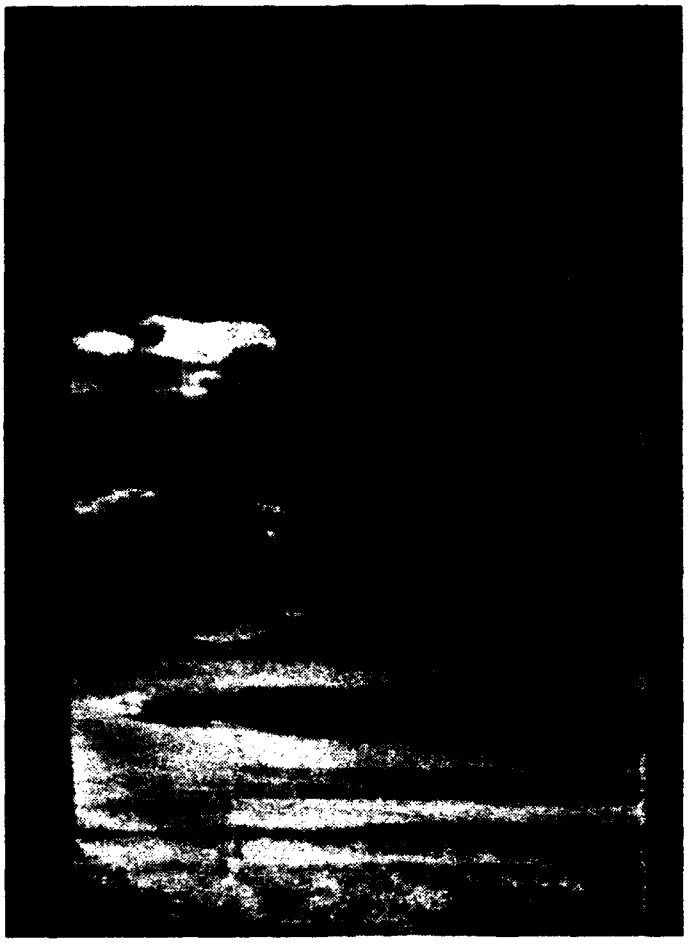

**Figure 23 BRT Spectral Angle Mapper Image**

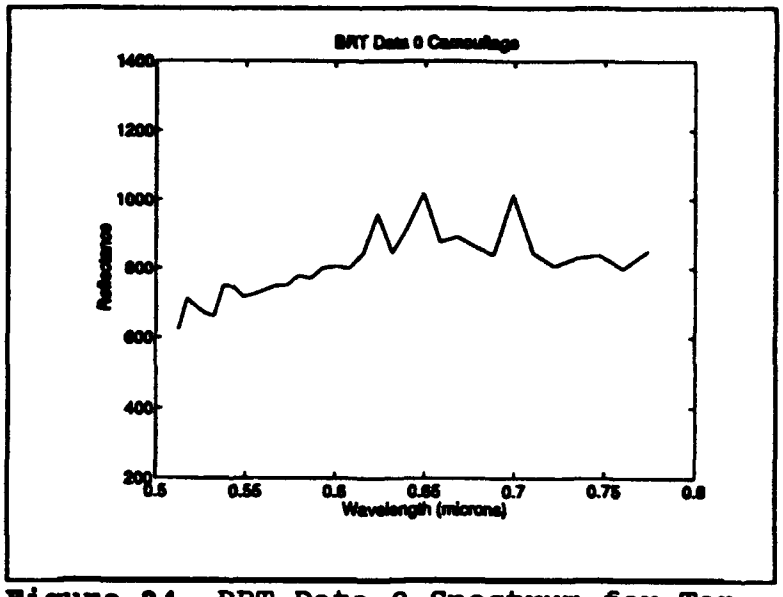


**Figure 24** BRT Data 0 Spectrum for Tan Camouflage

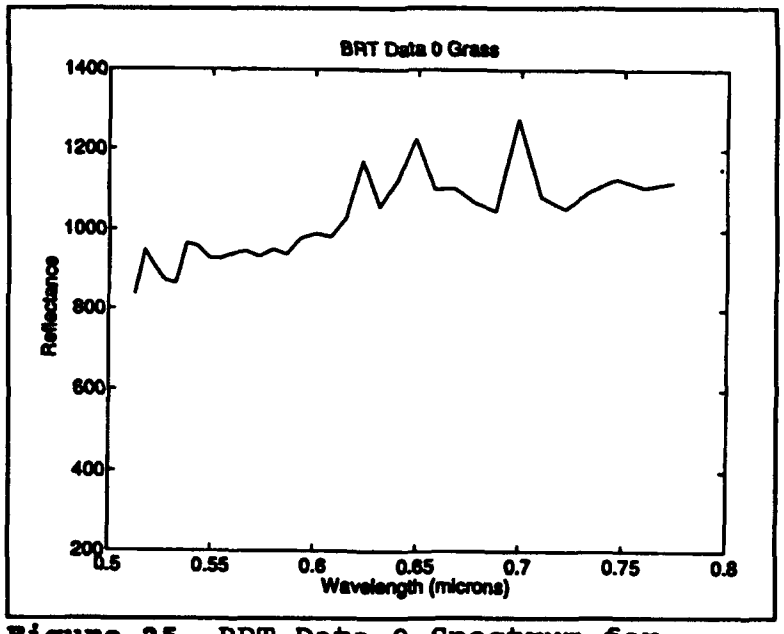


**Figure 25** BRT Data 0 Spectrum for Desert Grass

*b. Band Ratios*

Due to the spectral similarity between the tan camouflage nets and the desert grass that dominates the BRT scene, it is difficult to sharply contrast these features even by combining the ratios of bands. Finding bands that highlight the differences between the reflectance values for the tan camouflage relative to the grass is the problem. The best combination of band ratios is:

$$BandRatio = \log\left(\frac{Band24}{Band2}\right) - \log\left(\frac{Band32}{Band13}\right) - \log\left(\frac{Band31}{Band25}\right).$$

The image resulting from this combination of band ratios is shown in Figure 26.

The camouflaged equipment in the band ratio image appears slightly brighter than most of the background features. The shapes of the targets on the left side of the image are well-defined and the tops of the nets on the right side of the image are even discernable. The band ratio technique is as effective in distinguishing the camouflage background as the SAM approach for the BRT data set.

**3. Polarimetric Analysis**

An image created by subtracting the BRT Band 13 *dt1* polarized image from the *dt0* image is shown in Figure 27. Like the polarization difference image for the TNT data set, the visualization of the difference between the parallel and

**Figure 26** BRT Data 0 Band Ratio Image

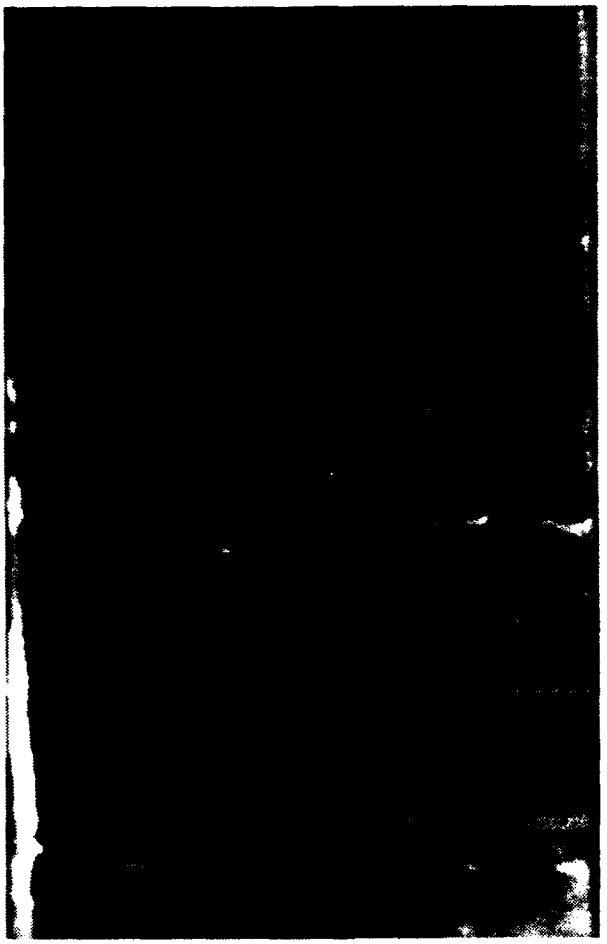

**Figure 27** BRT Band 13 Polarization Difference Image

perpendicular polarizations provides information about the features within the scene. It shows the outlines of the features with surfaces that reflect light such that the difference in polarization is detected. The same polarimetric characteristics of the halon panels are evident in the BRT scene as in the TNT polarization difference image. Also, the camouflaged equipment on the right side of the image is distinctly outlined. The top edges of the camouflaged netting appear dark while the place where the level of the surface meets the netting is shown with very bright pixel values. Places in the scene where the contour of the land causes features to appear closer to the sensor than they actually are have a very strong difference in polarization as illustrated in the BRT polarization difference image.

## C. SCENE 3

The last data set to be analyzed in this research are the VNT files. They contain a scene with military equipment concealed under woodland camouflage nets deployed in a stand of trees. There are tall trees with full leafy branches in the foreground and desert grass, dirt and plants in the background of the scene. Also, a lone mesquite tree is visible in the center of the AOTF images. (See Figures 28 and 29) In this data set, the camouflaged military equipment cannot be distinguished from the trees in which they are hidden. Although it is not apparent, the tops of three

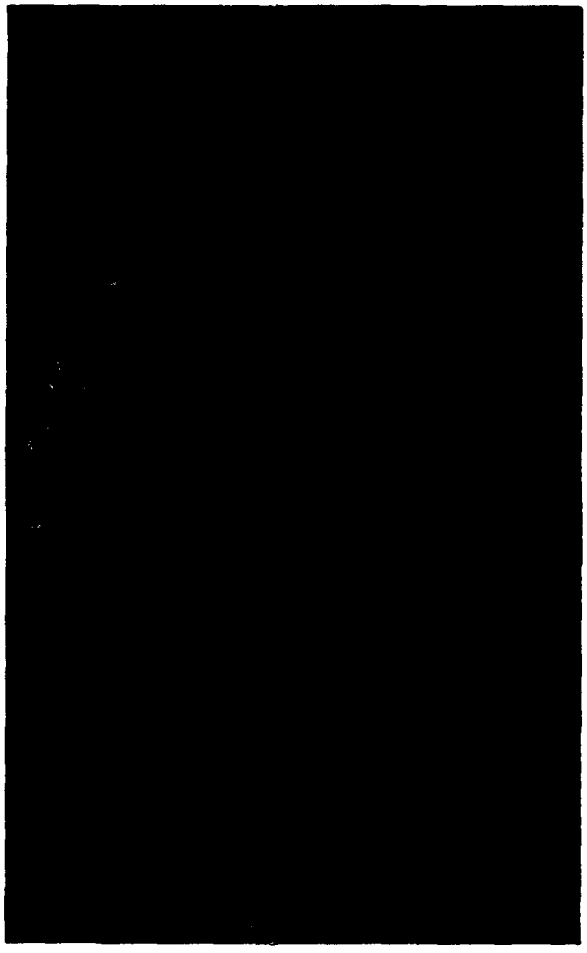

**Figure 28** VNT Data 0 Image for Band 7

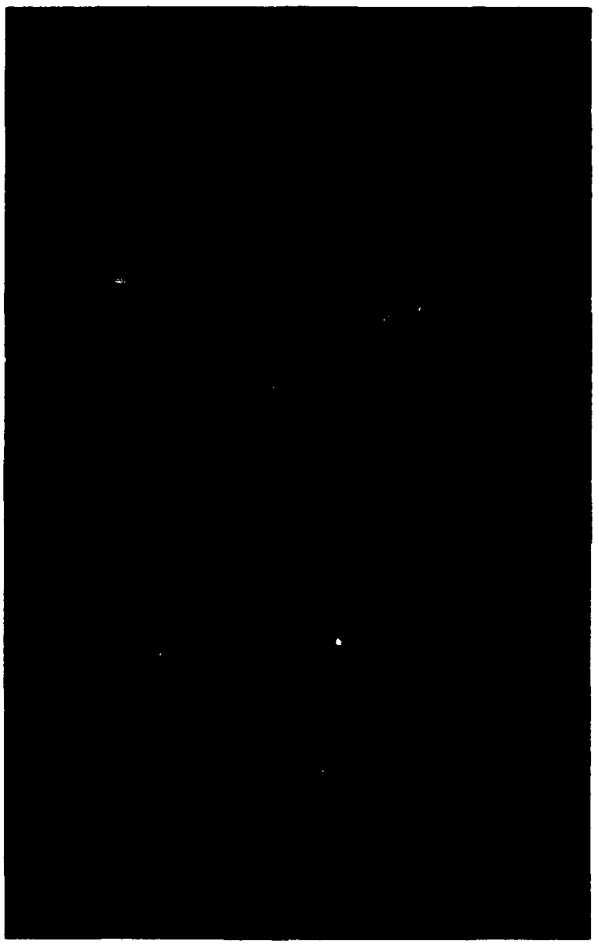

**Figure 29** VNT Data 1 Image for Band 7

camouflage nets concealing military exist in the area of the image enclosed by the box.

### 1. Data Validation

A comparison of the field spectrometer spectral curve and AOTF data spectrum for a mesquite tree is used to determine the accuracy of the VNT data set. (See Figures 30 and 31) There are no apparent bad bands in the VNT data set, but one difference between the two curves is again a result of the difference in the number of data points. Even considering this explanation, there is still a fairly significant difference between the spectra from the two sources. One reason for the difference is that the distance of the AOTF sensor from the mesquite tree combined with the relative size of the mesquite tree branches allow other features like leaves, grass and dirt to be represented in the same pixel as the mesquite tree. A mixture of these features in one pixel interferes with the true spectral curve of the tree. Also, the field spectrometer measurements of the mesquite branches were made on a different day and, therefore, under different meteorological conditions than when the AOTF system collected the TNT data set. This could account for the differences in the mesquite tree spectra as well. For the most part, the curves are enough alike to consider the data valid.

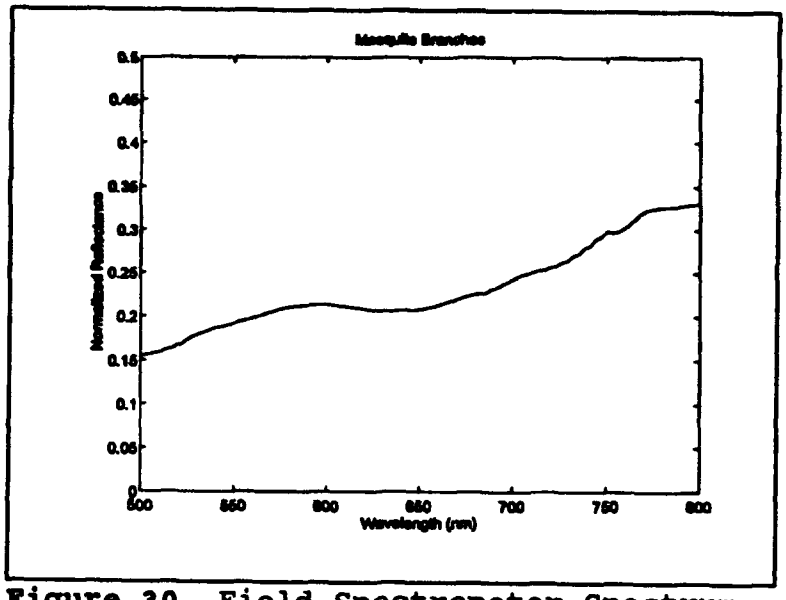


**Figure 30** Field Spectrometer Spectrum for Mesquite Branches

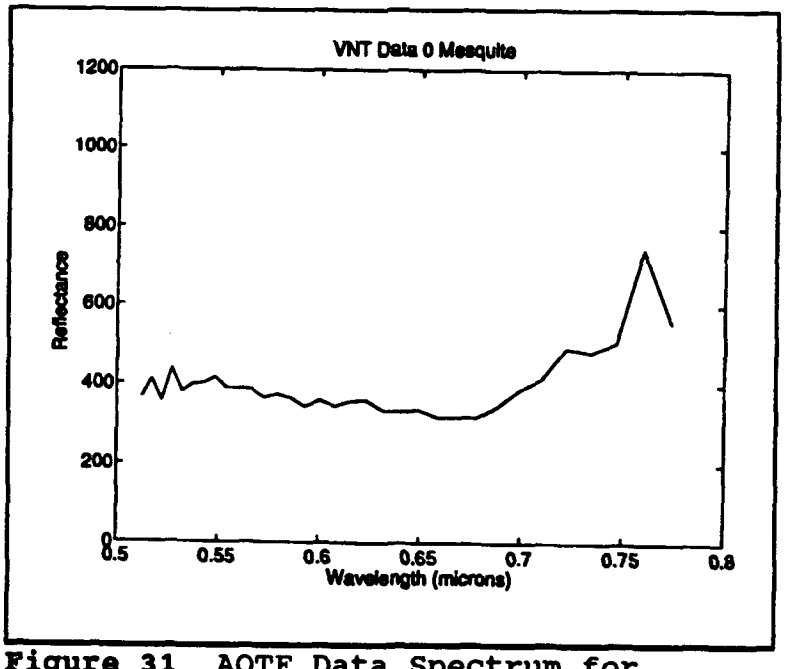


**Figure 31** AOTF Data Spectrum for Mesquite Tree

## 2. Spectral Analysis

### a. *SAM*

Since the pixels representing camouflage nets cannot be identified in order to define a class and create a library file for its mean spectrum, the spectral library file for woodland camouflage from the TNT data set is the input spectrum used in the SAM analysis of the VNT data set. The image created by the SAM utility in SIPS is shown in Figure 32. This image is a result of comparing the input spectrum for the camouflage nets to every pixel's spectrum in the VNT scene. The brighter pixels in the SAM image represent features with spectra most similar to the input spectrum and the darker pixels have spectra least like the input spectrum.

The SAM image considered by itself does not appear to accurately identify the camouflaged equipment in the scene. There are very bright areas in the image that obviously do not represent the targets of interest. However, when the SAM image is compared to the original corrected AOTF image for Band 7, bright areas that appeared to be trees are evident. These brighter areas represent the camouflaged equipment. It is even possible to discern the shapes of the tops of the camouflage nets after comparing the SAM image to the original.

### b. *Band Ratios*

The bands selected for ratioing to highlight the camouflaged equipment in the VNT data should be similar to

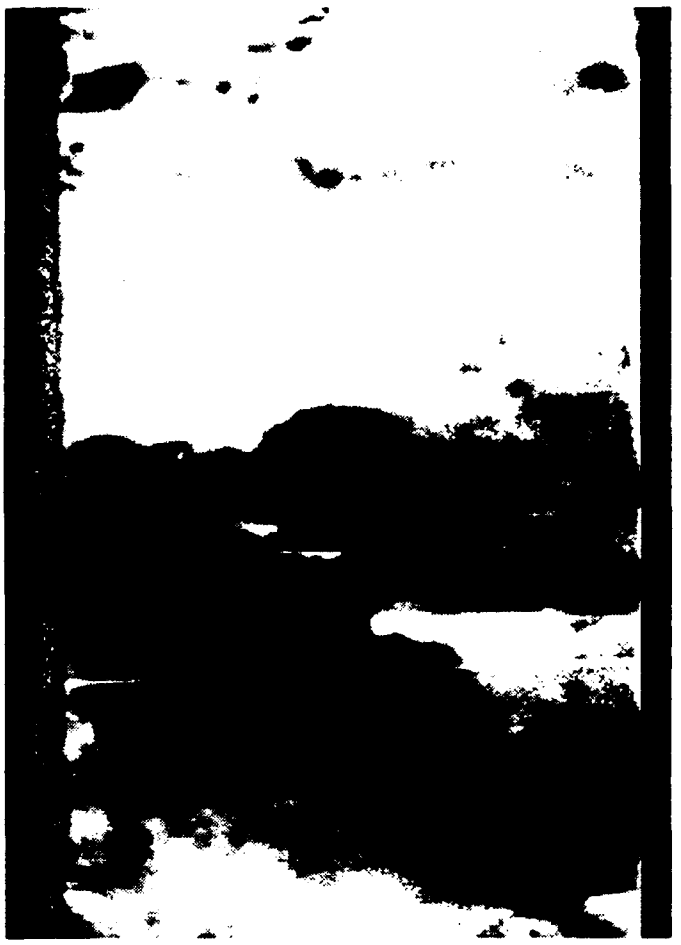

**Figure 32** VNT Data 0 Spectral Angle Mapper Image

those selected for the TNT scene since the target of interest is the same. But minor adjustments in band selection is necessary due to the difference in the background features between the scenes. In order to determine the appropriate bands to ratio and combine, the mean spectrum for the woodland camouflage nets from the TNT data set is compared to the spectra for the dominant background features like trees and grass in the VNT scene. The equation,

$$BandRatio=\log\left(\frac{Band24}{Band8}\right)-\log\left(\frac{Band22}{Band31}\right)-\log\left(\frac{Band29}{Band24}\right),$$

describes the combination of ratios used to distinguish the camouflaged equipment from the background in the VNT *dt0* scene. (See Figure 33)

Although the desert grass and dirt in the foreground and background of the band ratio image appears bright, the area within the box shows brighter pixels than those representing the trees. These brighter pixels form shapes that are indicative of the tops of camouflage nets concealing military equipment. The ability to identify these targets is enhanced when the band ratio image is compared to the original corrected AOTF image of the VNT *dt0* data set.

### 3. Polarimetric Analysis

The polarization difference image at Band 7 is shown for the VNT data set in Figure 36. The image does not provide

**Figure 33** VNT Data 0 Band Ratio Image

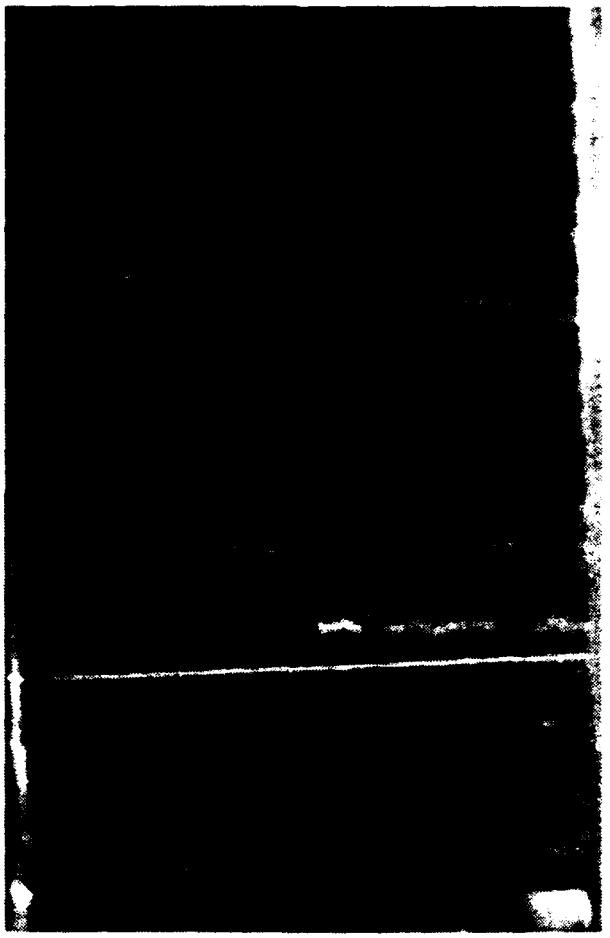

**Figure 34** VNT Band 7 Polarization Difference Image

enough information to identify the camouflaged equipment in the scene. Because the targets are so well-camouflaged in the trees and the polarimetric signature of camouflage nets is quite similar to that of the trees, the polarization difference does not significantly highlight the target features. The size and shape, as well as the surface characteristics of the trees are basically the same as those of the tops of the camouflage nets. The distance and viewing angle affect the amount of polarization detected.

The polarization image does, however, illustrate polarimetric characteristics similar to those described in the previous polarimetric analysis results. The halon panels in the upper left portion of the image posses the same appearance as in the other data sets with the darker pixels immediately above the brighter ones. Also, the difference in polarizations adds a depth perception to the image which is not evident in the band ratio image.

## D. CONVOLUTION ALGORITHM

The information provided by separate spectral and polarimetric analysis of the experiment data indicates that combining these results to better distinguish targets from the background features is desirable for assessing the AOTF system's utility. A simple algorithm that accomplishes this convolution of the spectral and polarimetric results was developed. By adding the band ratio image to a filtered

polarization difference image, a new image is created which should highlight the camouflaged military equipment in the scene. Images can be enhanced using techniques to smooth and sharpen them. Filtering is an example of one image processing technique that outlines of the shapes of features within the image. The filtering process requires converting the image data into the frequency domain using a fast Fourier transform. Then, applying a bandpass filter to the image data removes the very high and low values that clutter the image. After converting the filtered data back into the spatial domain, the resulting image is added to the band ratio image. The filtered polarization difference array values and band ratio array values are weighted before summation so that each image is equally represented in the convolved image. An IDL program called *convolution.pro* was written to accomplish this convolution process.

The image resulting from the algorithm applied to the TNT data set is shown in Figure 35. This image is an improvement over both the band ratio image and the polarization difference image shown in Figures 17 and 18. It displays the camouflaged equipment with pixels brighter than the background features and also sharpens the appearance of the target shapes. For the TNT scene, the algorithm is successful in combining the information derived from spectral and polarimetric analysis to create an image where the targets are easily distinguished from the background features.

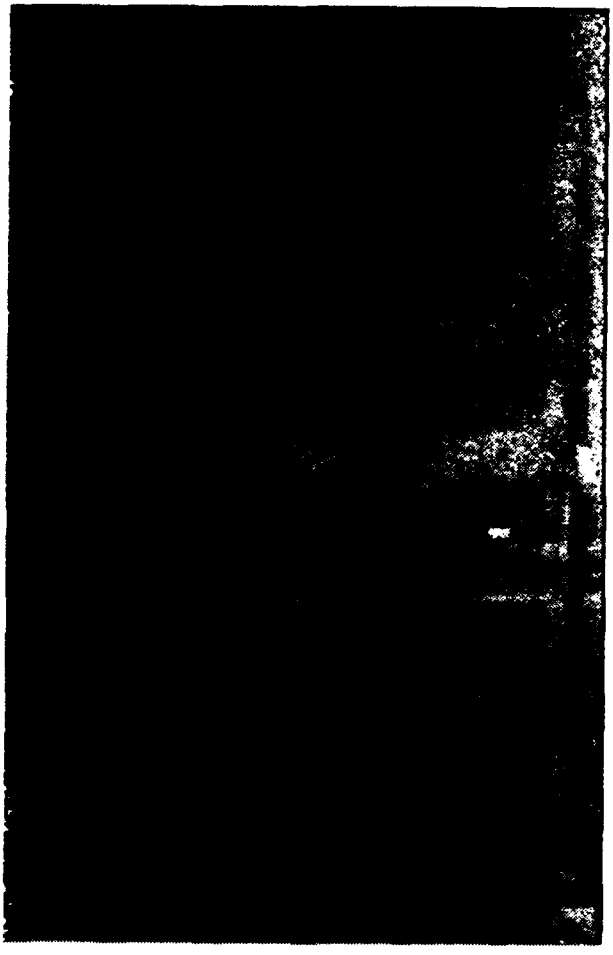

**Figure 35** TNT Data Set Convolution Image

Figure 36 shows the convolution algorithm applied to the BRT data set. Again, the image combining the spectral and polarimetric information provides a better display of the targets within the scene compared to the band ratio and polarization difference images in Figures 26 and 27. As a result of the information contributed by the band ratio image, the camouflaged equipment appears brighter than the background features. The filtered polarization difference image provides the edge enhancement that highlights the outlines of shapes in the scene. Together, this information allows the camouflaged equipment to be easily distinguished from the natural background.

Applying the convolution algorithm to the VNT data set results in the image shown in Figure 37. Since the polarization difference did not provide information to enhance the detection of the camouflaged equipment, combining it with the band ratio image does not improve the appearance of the targets compared to the background features. The VNT band ratio and polarization difference images are shown in Figures 33 and 34, respectively. In the case of the VNT scene, the band ratio image alone is best for distinguishing the camouflaged equipment.

When both spectral and polarimetric analysis provide significant information about a scene, the convolution algorithm is quite effective in combining the results. It is successful in producing an image that equally displays the

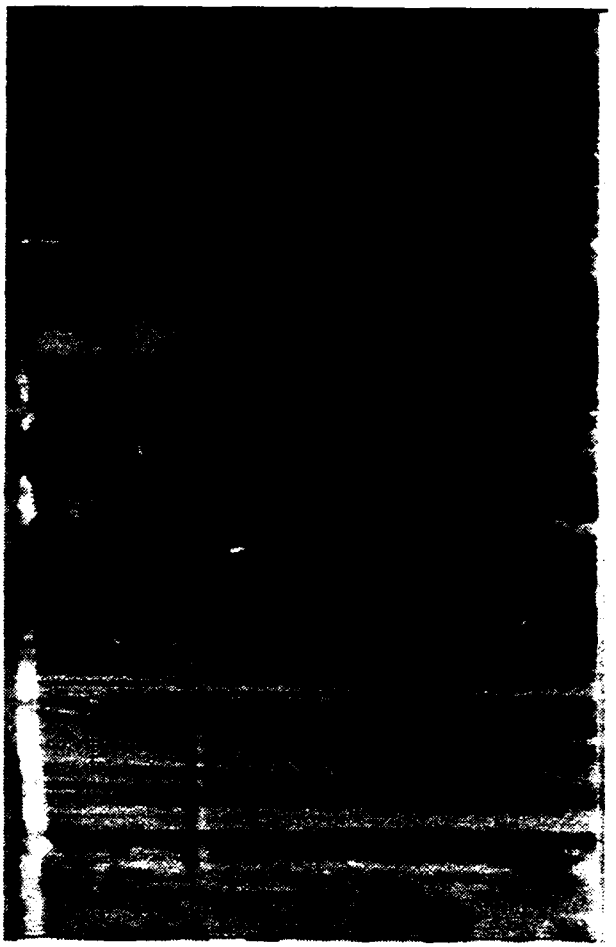

**Figure 36** BRT Data Set Convolution Image

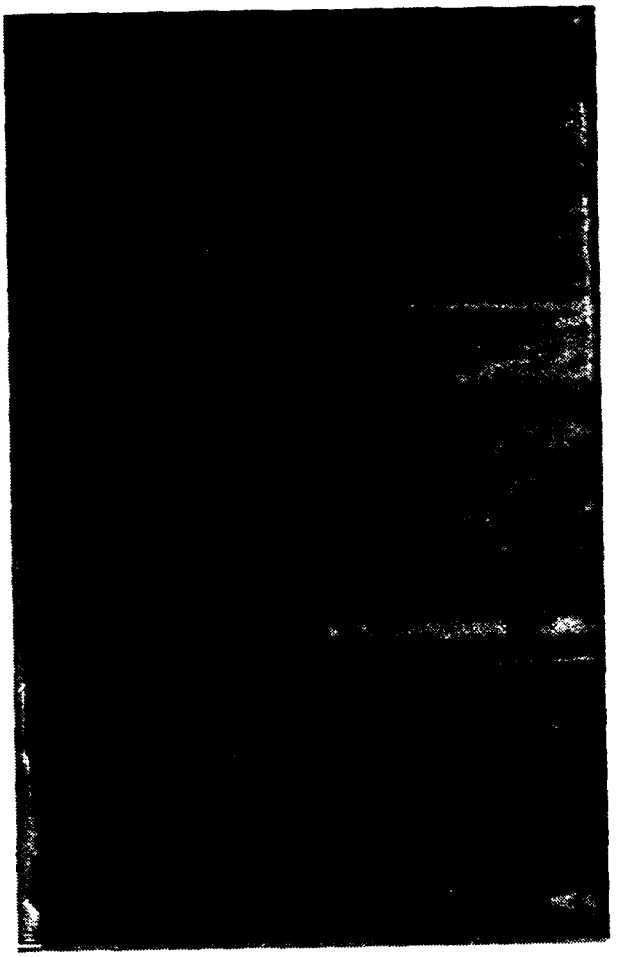

**Figure 37** VNT Data Set Convolution Image

highlighted features contributed from the separate analytical approaches. The ability to visualize the combined effects of spectral and polarimetric resolution in this manner introduces a simple and efficient procedure for distinguishing targets from background features in analysis of AOTF hyperspectral data.

# VI. CONCLUSIONS

Analysis of the AOTF experiment data shows that the potential exists to utilize this technology in military applications. The capability to collect digital imagery that allows the contribution of information derived from both spectral and polarimetric analysis provides a new dimension to imagery interpretation. This chapter discusses the conclusions drawn as a result of the analysis performed on the AOTF experiment data. Also, recommendations for proceeding with future efforts in the AOTF system development process are addressed.

## A. SPECTRAL CHARACTERISTICS

After spectral analysis of the AOTF experiment data, it is determined that the ability to distinguish targets like camouflaged military equipment from the background features within a scene by comparing spectra validates the concept of the system. Also, of the two spectral analysis methods, the band ratio technique is preferred. The SAM analysis tool in SIPS is not always as effective at identifying targets as the band ratio technique. The results show that the SAM utility is overly sensitive to the variations between the input spectrum and the spectra for the pixels in the scene. Thus,

it does not recognize pixels that actually represent the target. Also, because the spectra for the camouflaged equipment and the dominant background features in the AOTF data sets are very similar due to the range of the sensor system, the SAM function displays pixels not representing the target as brightly as those that actually are the target pixels. Overall, the band ratio technique was much more successful in distinguishing the targets from their backgrounds for each of the scenes. Careful selection of a few bands even in the limited range of the prototype AOTF system allowed the camouflaged equipment to be identified as a result of its spectral characteristics.

Spectral analysis of data using both techniques is limited by two different constraints. The first is the spatial resolution of the system. A direct relationship exists between spatial resolution and the uniqueness of spectral signatures. High spatial resolution insures that pixels represent only the homogeneous target of interest without spectral interference from other features. An improvement in the AOTF system's spatial resolution capability would increase the effectiveness of both spectral analysis methods.

The other limitation on the ability to derive information about targets within a scene by spectral analysis is the wavelength range of the sensor. The field spectrometer data shows that at higher wavelengths, more unique spectral features are present. The prevalence of these unique spectral

features allows the isolation of a particular target as a result of its spectrum which increases the effectiveness of band ratioing and methods like the SAM analysis tool. Widening the AOTF system's range would also improve the results achieved through spectral analysis using both methods.

With adequate spectral resolution, it is possible to associate unique spectral characteristics with a particular target type. The narrow bandwidth data collected by hyperspectral imaging systems provide the capability to isolate specific variations in spectral curves. From data measured by a sensor, given prior knowledge of a feature's spectral variations, information is derived that allows its detection and identification. The ability to distinguish targets from background features in an image using ratios of only several bands that highlight the target's unique spectral variations instead of its complete spectrum makes the AOTF design attractive for military applications. This design takes advantage of the information provided by data in narrow bandwidth yet overcomes the problem of collecting huge amounts of redundant or unused data associated with existing hyperspectral systems.

The spectral characteristics analyzed for each data set illustrated in this thesis were applied to the *dt0* polarization. It is important to note that the results of the spectral analysis techniques are basically the same when applied to the *dt1* polarization. Whether analysis of *dt0* or

*dt1* data is considered, the same conclusions are drawn concerning the accuracy and capabilities of the AOTF system.

## B. POLARIMETRIC CHARACTERISTICS

The polarimetric analysis of the AOTF data provides information about the polarimetric characteristics of surface features, though its contribution to detecting camouflage nets is not necessarily significant. Any information that can lead to a better understanding of how features affect the polarity of the light reflected off their surfaces is valuable in determining the worth of the AOTF system. The results of the polarimetric analysis show that a feature's shape and surface characteristics influence the polarity of the light it reflects. Also, the sun angle, viewing geometry, and sensor to target distance affect the polarimetric measurements.

Since this thesis only addresses the AOTF experiment data containing camouflaged military equipment, the analysis of polarimetric characteristics was severely limited. Targets with more distinct shapes and different types of surface features must be considered for an accurate assessment of the contribution made by polarimetric analysis of the AOTF data. Because camouflaged equipment possesses a polarimetric signature very similar to the trees in which these targets are normally concealed, the determination of the utility of polarization information should not be based on research limited to analysis of only this target type.

The polarimetric characteristics of features in other data sets collected during the experiment show that polarization data could be used to derive information for target identification. The shapes and surface characteristics of vehicles and planes have distinct polarimetric signatures like those of the antennas in the TNT and BRT scenes. More analysis and research must be done to properly categorize polarimetric characteristics and determine its usefulness in target detection and identification.

## C. RECOMMENDATIONS

The military should pursue development of hyperspectral imagery technology, especially the AOTF design, to enhance current intelligence collection capabilities. An airborne test of a system similar to the prototype AOTF system discussed in this thesis with the improved capabilities of a wider wavelength range and better spatial resolution is necessary to accurately determine the utility of an AOTF hyperspectral system for military applications. A plan already exists for conducting an airborne experiment of an AOTF system with increased capabilities over the prototype used in the ground-based test. The proposed system for the airborne experiment includes improved optics, cameras and a new crystal to increase the wavelength range of the sensor. These modifications to the AOTF design would provide enhanced

spatial and spectral resolution in addition to the temporal responsiveness necessary for an airborne sensor.

More valuable information would be gained from analysis of data collected by an airborne system than in the ground-based experiment. The geometry of an airborne experiment allows the sensor to target distance, sun angle, and viewing angle to remain constant over the entire scene, resulting in spatial uniformity. This condition is necessary for an accurate assessment of the spectral and polarimetric target characteristics.

With proper libraries containing spectral and polarimetric information and preprogrammed batch processing procedures an AOTF hyperspectral system could provide unprecedented imagery support to commanders. The major problem in current imagery procedures is the time delay caused by the analysis process. A system utilizing AOTF technology could eliminate this delay by tailoring the collection requirements to the bands determined most appropriate for the target of interest. Real-time collection and near real-time analysis is a feasible future capability of such a system. From an airborne platform or space, a sensor could downlink tailored image data directly to the user's processing system. Batch processing by running the data through a preprogrammed set of procedures that include an algorithm similar to the one developed in this thesis could accomplish fast data correction and analysis.

Design features of the AOTF system could provide this type of simple and rapid imagery support to tactical commanders.

The experiment to test the prototype system proves the concept of AOTF hyperspectral technology. The AOTF system displays outstanding potential for enhancing current intelligence capabilities and development of this technology could benefit a wide variety of applications.

# APPENDIX A

```
;*****************************************
;                                        *
;          band_shift.pro                *
;                                        *
;*****************************************

; The program listed here reads the raw data from the
; AOTF files and performs the geometric correction
; between bands for the user selected data set and
; polarization.  A properly aligned integer data file
; is produced by this procedure.


function crosco, v1, v2
  n = n_elements(v1)
  out = fltarr(n/2)
  for ishift = -n/4, n/4 - 1  do begin
     temp = shift(v2, ishift)
     out(ishift+n/4) = correlate(v1, temp)
   endfor
  w = where(out eq max(out))
wset, 3
plot, out
 return, w(0) - n/4
end


pro init,  max_colors
max_colors = 254
device, pseudo_color = 8, retain = 2
window, 0, xsize= 520, ysize = 400, colors=max_colors
loadct, 0
tvlct, r,g, b, /get
r(0) = 255 & g(0) = 255 & b(0) = 255
r(1) = 0   & g(1)  = 0  & b(1) = 0
tvlct, r, g, b
line_color = 1
!p.color = 1
window, 1, xsize = 260, ysize = 400
window, 2, xsize = 400, ysize = 300
window, 3, xsize = 200, ysize = 200
return
```

```
end


pro      get_data, files
index = 6
dirs = [ 'tnt', 'brt', 'vnt','2ss', 'hal', 'rj2', 'rj3', 'rjp', 'tjp', 'tnk']
print, dirs
read, 'enter index 0 to 9 ', index

   path = '/opt/sturgeon/'+dirs(index)

dir=path
print, dir
; filename = pickfile(path=dir, filter='*.dt1')
zero_or_one = 0
read, ' enter 0 or 1  for dt0 or dt1 ', zero_or_one

  if zero_or_one eq 0 then begin
      suffix = 'dt0'
        endif else begin
     suffix = 'dt1'

endelse
 files = findfile(dir+'/*.'+suffix)
index = 32 - indgen(33)
help, files

out_file =  dir+'/'+suffix+'_int_bsq.cub'
print, ' bsq file = ', out_file

openw, 4, out_file
return
end

init,    max_colors
 loop:
get_data,  files
n_max = n_elements(files) -1


wset, 0
loadct, 0

ifile = 19
ifile = 33 - ifile
filename = files(ifile)
openr, 2, filename
data0 = intarr(350, 250)
```

```
FORRD, 2, data0
close, 2

byteorder, data0, /sswap
print, min(data0), max(data0)
data0 =   rotate(data0,3)

byt_data0 = data0
wset, 0
!p.color = 250

refline = intarr(350)
refline = data0(*, 195)
help, refline

wset, 0
tvscl, byt_data0
plots, [0, 300],[195, 195], /device, color = 250
print, 'choose level with mouse'

cursor, x, y, /device
print, y,' is the new vertical level '
refline = data0(*, y)

plots, [0, 300], [y, y], /device, color = 250


for ifile = 0, n_max do begin

ifile = 32 - ifile

n_to_shift = 10
wset, 0
loadct, 0

filename = files(ifile)
openr, 2, filename
data1 = intarr(350, 250)
FORRD, 2, data1
close, 2
byteorder, data1, /sswap
print, ifile, min(data1), max(data1)
data1 =   rotate(data1,3)


byt_data1 = ( data1 )

line = intarr(350)
```

```
line = data1(*, y)
help, line
wset, 2

plot_io, refline, yrange = [10, 1e3], ystyle = 1
oplot, line

wset, 0

n_to_shift = crosco(refline, line)

byt_data1 = shift(byt_data1, n_to_shift, 0)
print, 'shifted data1 by ', n_to_shift

wset, 0
erase

tvscl, byt_data0
xyouts, 10, 360, 'scene 13', /device

tvscl, byt_data1, 260, 0
xyouts, 270, 360, 'scene'+ string(ifile, format ="(i3)" ), /device

goto, skip_rgb

skip_rgb:

forwrt, 4, ( rotate(byt_data1,7) )

ifile = 32 - ifile


endfor

close, 4

cont = ' '

 close, 2
 close, 3

END
```

```
;*********************************
;                                *
;      view_shift.pro            *
;                                *
;*********************************

; This program reads the two band corrected data
; files, one for each polarization, of the data
; set selected by the user.  It accomplishes the
; geometric correction between polarizations.  The
; program outputs a byte data image file for the
; dt1 polarization that is aligned with the dt0 data.


function crosco, v1, v2
  n = n_elements(v1)
  out = fltarr(n/2)
  for ishift = -n/4, n/4 - 1  do begin
     temp = shift(v2, ishift)
     out(ishift+n/4) = correlate(v1, temp)
   endfor
  w = where(out eq max(out))
wset, 3
plot, out

 return, w(0) - n/4
end

pro init,  max_colors
max_colors = 254
device, pseudo_color = 8, retain = 2
window, 0, xsize= 520, ysize = 400, colors=max_colors
loadct, 0
tvlct, r,g, b, /get
r(0) = 255 & g(0) = 255 & b(0) = 255
r(1) = 0   & g(1)  = 0  & b(1) = 0
tvlct, r, g, b
line_color = 1
lp.color = 1
window, 1, xsize = 260, ysize = 400
window, 2, xsize = 400, ysize = 300
window, 3, xsize = 500, ysize = 200
window, 4, xsize = 260, ysize = 400
return
end

pro      get_data, dir, file0, file1
```

```
index = 6
dirs = [ 'tnt', 'brt', 'vnt','2ss', 'hal', 'rj2', 'rj3', 'rjp', 'tjp', 'tnk']
print, dirs
read, 'enter index 0 to 9 ', index

   path = '/opt/sturgeon/'+dirs(index)

dir=path
print, dir

file0 = path+'/dt0.bsq'
file1 = path+'/dt1.bsq'
openr, 10, file0
openr, 11, file1
file3 = path+'/dt1.shft'
openw, 13, file3
return
end

init,    max_colors
 loop:
get_data,  dir, file0, file1
print, 'files open in directory ', dir

n_max = 32

dt0 = assoc(10, intarr(250, 350) )
dt1 = assoc(11, intarr(250, 350) )

wset, 0
loadct, 0

min_data = 10
max_data = 300
ifile = 13

byt_data0 =  dt0(ifile)
help, byt_data0
max_data = .95 * max(byt_data0)
help, max_data

wset, 0
tv, bytscl(byt_data0, min = min_data, max = max_data)

byt_data1 = dt1(ifile)
help, byt_data1
wset, 0
tv, bytscl( byt_data1, min = min_data, max = max_data), 260, 0
```

```
wset, 0
!p.color = 250

refline = intarr(350)
refline = byt_data0(*, 195)
;help, refline

wset, 0
plots, [0, 300],[195, 195], /device, color = 250
print, 'choose level with mouse'

cursor, x, y, /device
print, y,' is the new vertical level '
refline = byt_data0(*, y)

plots, [0, 300], [y, y], /device, color = 250

for ifile = 0, n_max do begin
byt_data0 = dt0(ifile)
byt_data1 = dt1(ifile)

n_to_shift = 10
wset, 0
loadct, 0

line0 = byt_data0(*,y)
line1 = byt_data1(*,y)

wset, 2

plot_io, line0, yrange = [10, 1e3], ystyle = 1
oplot, line1

wset, 0

n_to_shift = crosco(line0, line1)

byt_data1 = shift(byt_data1, n_to_shift, 0)
print, 'shifted data1 by ', n_to_shift

wset, 0
erase

tv, bytscl( byt_data0, min = min_data, max = max_data)

xyouts, 10, 360, 'dt0', /device
xyouts, 100, 360, string(ifile), /device
tv, bytscl( byt_data1, min = min_data, max = max_data), 260, 0
```

```
xyouts, 270, 360, 'dt1', /device

forwrt, 13, byt_data1

result = bytscl(byt_data0 - byt_data1)

wset, 1
tv, result

skip_rgb:

endfor

close, 10
close, 11
close, 13

END
```

```
;*****************************************
;                                        *
;        ratio.pro                       *
;                                        *
;*****************************************

; This program allows the user to select a data set
; and six bands for ratios to produce an image that
; results from combining the base ten logarithm of
; the ratios.


pro init,  max_colors
max_colors = 254
loadct, 0
window, 0, xsize= 520, ysize = 400, colors=max_colors
window, 1, xsize = 260, ysize = 400, xpos = 5, ypos = 10, $
  title = 'Ratio of 2 bands - dt0'
return
end

pro      get_data, dir, file0, file1
index = 6
dirs = [ 'tnt', 'brt', 'vnt','2ss', 'hal', 'rj2', 'rj3', 'rjp', 'tjp', 'tnk']
print, dirs
read, 'enter index 0 to 9 ', index

   path = '/opt/sturgeon/'+dirs(index)

dir=path
print, dir

file0 = path+'/dt0.bsq'
file1 = path+'/dt1.shft'
openr, 10, file0
openr, 11, file1
return
end

init,    max_colors
 loop:
get_data,  dir, file0, file1
print, 'files open in directory ', dir

n_max = 32
dt0 = assoc(10, intarr(250, 350) )
dt1 = assoc(11, intarr(250, 350) )
```

```
wset, 0
min_data = 10
max_data = 300
ifile = 13

byt_data0 =  dt0(ifile)
help, byt_data0
byt_data1 = dt1(ifile)
help, byt_data1
wset, 0

band1 = 10  &  band2 = 30
band3 = 15  &  band4 = 5
band5 = 16  &  band6 = 1

read, 'enter two bands to ratio in dt1 (e.g. 10, 30)', band1, band2

band_1 = dt0(band1) + 1
band_2 = dt0(band2) + 1
print, min(band_1), max(band_1), '  min, max of band ', band1
print, min(band_2), max(band_2), '  min, max of band ', band2
read, 'enter two more bands to ratio in dt1 (e.g. 15, 5)', band3, band4
band_3 = dt0(band3) + 1
band_4 = dt0(band4) + 1
read, 'enter two more bands to ratio in dt1 (e.g. 16, 1)', band5, band6
band_5 = dt0(band5) + 1
band_6 = dt0(band6) + 1

ratio_1 = alog10(float(band_1)/float(band_2))
ratio_2 = alog10( float(band_3)/float(band_4))
ratio_3 = alog10(float(band_5)/float(band_6))

ratio = ratio_1 - ratio_2
ratio = ratio - ratio_3

s_array = ratio( 50:200, 50:200)
min_sc = min(s_array)
max_sc = max(s_array)
help, min_sc, max_sc

tmp = bytscl(ratio, min = min_sc, max = max_sc)

wset, 1
tv, tmp
close, 10
close, 11

END
```

```
;*************************************************
;                                                *
;                                                *
;            polarize.pro                        *
;                                                *
;                                                *
;*************************************************

; This program reads the corrected data file for both polarizations
; of a data set selected by the user and produces an image that
; represents the difference between the polarizations for each band.


pro init,  max_colors
max_colors = 254
device, pseudo_color = 8, retain = 2
window, 0, xsize= 520, ysize = 400, colors=max_colors
loadct, 0
tvlct, r,g, b, /get
r(0) = 255 & g(0) = 255 & b(0) = 255
r(1) = 0   & g(1)  = 0  & b(1) = 0
tvlct, r, g, b
line_color = 1
!p.color =
window, 1, xsize = 260, ysixe = 400, xpos = 0, ypos =10
window, 2, xsize = 260, ysize = 400, xpos = 270, ypos = 10

return
end

pro      get_data, dir, file0, file1

index = 6
dirs = [ 'tnt', 'brt', 'vnt','2ss', 'hal', 'rj2', 'rj3', 'rjp', 'tjp', 'tnk']
print, dirs
read, 'enter index 0 to 9 ', index

  path = '/opt/sturgeon/'+dirs(index)

dir=path
print, dir

file0 = path+'/dt0.bsq'
file1 = path+'/dt1.shft'
openr, 10, file0
openr, 11, file1

return
end
```

```
init,    max_colors
 loop:
get_data,  dir, file0, file1
print, 'files open in directory ', dir

n_max = 32

dt0 = assoc(10, intarr(250, 350) )
dt1 = assoc(11, intarr(250, 350) )

ifile = 13

byt_data0 =  dt0(ifile)
help, byt_data0

wset, 0
tv, bytscl(byt_data0)

byt_data1 = dt1(ifile)
help, byt_data1

wset, 0
tv, bytscl( byt_data1), 260, 0

for ifile = 0, n_max do begin
    byt_data0 = dt0(ifile)
    byt_data1 = dt1(ifile)

     wset, 0
    erase

     tv, bytscl(byt_data0)
     xyouts, 10, 360, 'dt0', /device
     xyouts, 100, 360, string(ifile), /device
     tv, bytscl(byt_data1), 260, 0
     xyouts, 270, 360, 'dt1', /device

      result =( byt_data0 - byt_data1)

sub_array = result(50:200, 50:200)
min_scl = min(sub_array)
max_scl = max(sub_array)
help, min_scl, max_scl

tmp = bytscl(result, min = min_scl, max = max_scl)

wset, 1
tv, tmp
```

```
\vset, 2

tv, hist_equal(sharp)

endfor

close, 10
close, 11


END
```

```
;*************************************************
;                                                *
;                convolution.pro                 *
;                                                *
;*************************************************

; This program applies an algorithm that combines the band ratio
; image with the polarization difference image for the data set,
; bands to ratio and bands to subtract selected by the user.
; It produces a convolved image in which the information provided
; by the combination of band ratios and the difference in
; polarizations are weighted equally.


pro init,  max_colors
max_colors = 254
window, 0, xsize= 520, ysize = 400, colors=max_colors
loadct, 0
window, 1, xsize = 260, ysize = 400, xpos = 5, ypos = 10, $
  title = 'Ratio of 2 bands - dt0'
window, 2, xsize = 260, ysize = 400, xpos = 270, ypos = 10, $
  title = 'Polarization difference'

window, 4, xsize = 260, ysize = 400, xpos = 5+265*2, ypos = 10, $
  title = 'convolution'

return
end

pro     get_data, dir, file0, file1

index = 6
dirs = [ 'tnt', 'brt', 'vnt','2ss', 'hal', 'rj2', 'rj3', 'rjp', 'tjp', 'tnk']
print, dirs
read, 'enter index 0 to 9 ', index

   path = '/opt/sturgeon/'+dirs(index)

dir=path
print, dir

file0 = path+'/dt0.bsq'
file1 = path+'/dt1.shft'
openr, 10, file0
openr, 11, file1

return
```

```
end

init,    max_colors
 loop:
get_data,  dir, file0, file1
print, 'files open in directory ', dir

n_max = 32

dt0 = assoc(10, intarr(250, 350) )
dt1 = assoc(11, intarr(250, 350) )

wset, 0
loadct, 0

min_data = 10
max_data = 300
ifile = 13

byt_data0 =  dt0(ifile)
help, byt_data0

byt_data1 = dt1(ifile)
help, byt_data1

band1 = 10  &  band2 = 30
band3 = 15  &  band4 = 5
band5 = 16  &  band6 = 1

read, 'enter two bands to ratio in dt1 (e.g. 10, 30)', band1, band2

band_1 = dt0(band1) + 1
band_2 = dt0(band2) + 1
print, min(band_1), max(band_1), '  min, max of band ', band1
print, min(band_2), max(band_2), '  min, max of band ', band2
read, 'enter two more bands to ratio in dt1 (e.g. 15, 5)', band3, band4
band_3 = dt0(band3) + 1
band_4 = dt0(band4) + 1
read, 'enter two more bands to ratio in dt1 (e.g. 16, 1)', band5, band6
band_5 = dt0(band5) + 1
band_6 = dt0(band6) + 1

ratio_1 = alog10(float(band_1)/float(band_2))
ratio_2 = alog10( float(band_3)/float(band_4))
ratio_3 = alog10(float(band_5)/float(band_6))

ratio = ratio_1 - ratio_2
ratio = ratio - ratio_3
```

```
s_array = ratio( 50:200, 50:200)
min_sc = min(s_array)
max_sc = max(s_array)
help, min_sc, max_sc

tmp = bytscl(ratio, min = min_sc, max = max_sc)

;help, ratio_1, ratio_2


wset, 1
tv, tmp

for ifile = 0, n_max do begin

    byt_data0 = dt0(ifile)
    byt_data1 = dt1(ifile)

     wset, 0
     erase

     tvscl, byt_data0
     xyouts, 10, 360, 'dt0', /device
     xyouts, 100, 360, string(ifile), /device

     tvscl, byt_data1, 260, 0
     xyouts, 270, 360, 'dt1', /device

     difference = byt_data0 - byt_data1

     help, difference

subarray = difference( 50:200, 50:200)
min_scl = min(subarray)
max_scl = max(subarray)
help, min_scl, max_scl

     polar = bytscl( difference, min = min_scl,  max = max_scl)

help, polar


transform = fft(polar,1)
freq = dist(250, 350)
;filter = 1/(1 + (freq/30)^2)     ; these are optional filters that
;filter = 1/(1 + (20/freq)^2)     ; can be applied to the image.
filter = 1/(1 + ((freq - 230)/25)^2)
sharp =  fft(filter * transform, -1)
```

```
su_array = sharp(50:200, 50:200)
min_sc = min(su_array)
max_sc = max(su_array)
help, min_sc, max_sc

sharp = bytscl(sharp, min = min_sc, max = max_sc)

      wset, 2
      tv, polar


tmp2 =3*tmp + 3*polar
help, tmp2

sub_tmp2 = tmp2(50:200, 50:200)
scl_min = min(sub_tmp2)
scl_max = max(sub_tmp2)
help, scl_min, scl_max

tmp2 = bytscl(tmp2, min = scl_min, max = scl_max)

wset, 4
tv, tmp2

endfor          ; end of loop for ifile = 0, # files

close, 10
close, 11

END
```

# APPENDIX B

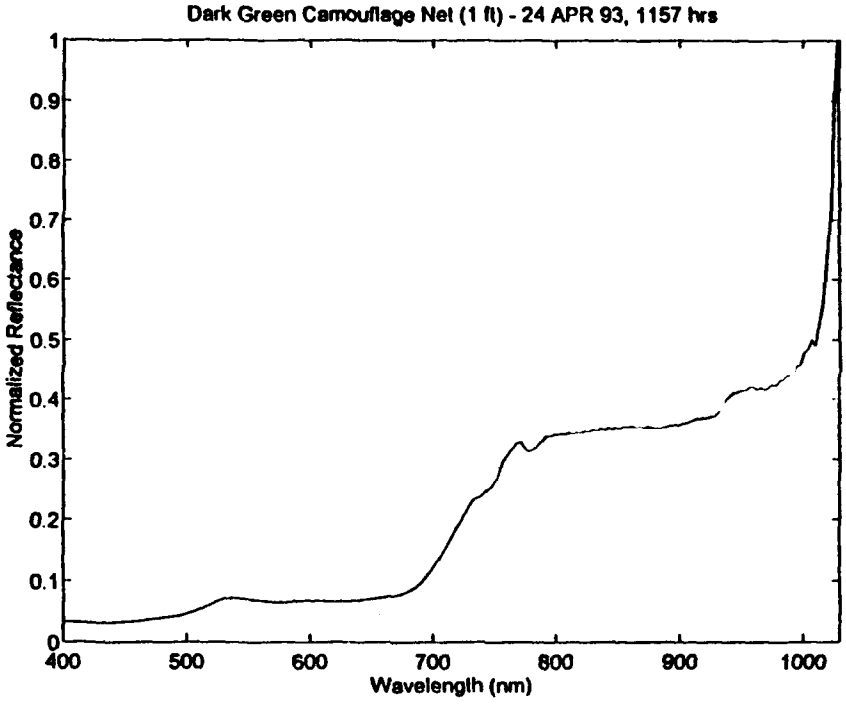
Dark Green Camouflage Net (1 ft) - 24 APR 93, 1157 hrs
Normalized Reflectance
Wavelength (nm)
0
0.1
0.2
0.3
0.4
0.5
0.6
0.7
0.8
0.9
1
400
500
600
700
800
900
1000

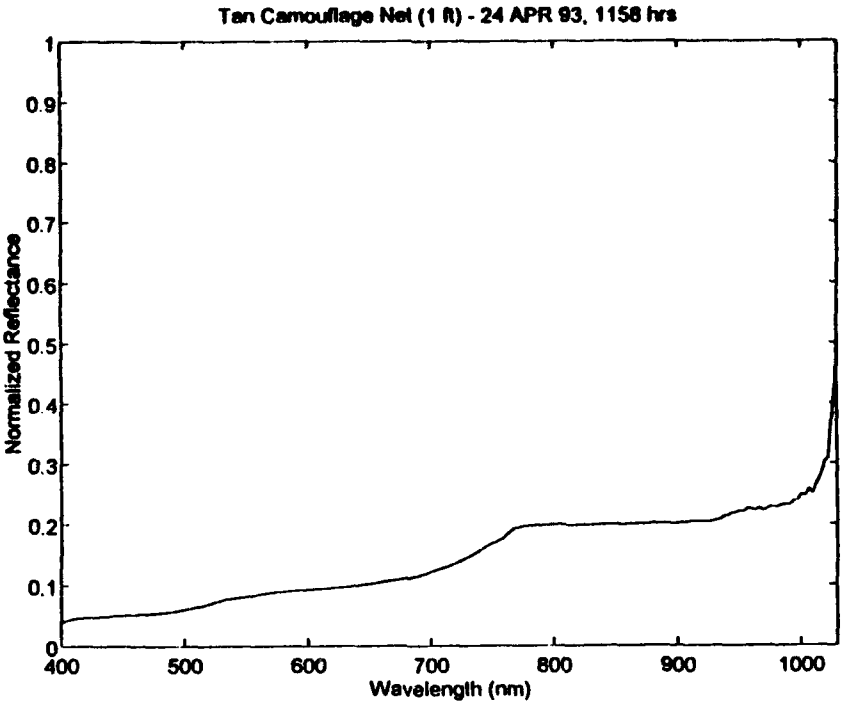
Tan Camouflage Net (1 ft) - 24 APR 93, 1158 hrs
Normalized Reflectance
Wavelength (nm)
0
0.1
0.2
0.3
0.4
0.5
0.6
0.7
0.8
0.9
1
400
500
600
700
800
900
1000

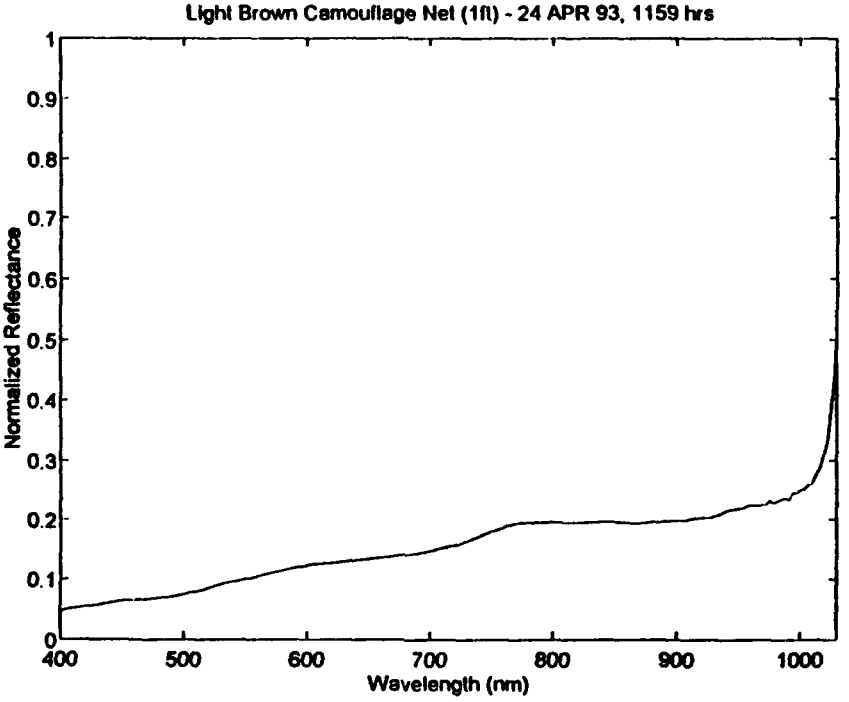
Light Brown Camouflage Net (1ft) - 24 APR 93, 1159 hrs
Normalized Reflectance
Wavelength (nm)
0
0.1
0.2
0.3
0.4
0.5
0.6
0.7
0.8
0.9
1
400
500
600
700
800
900
1000

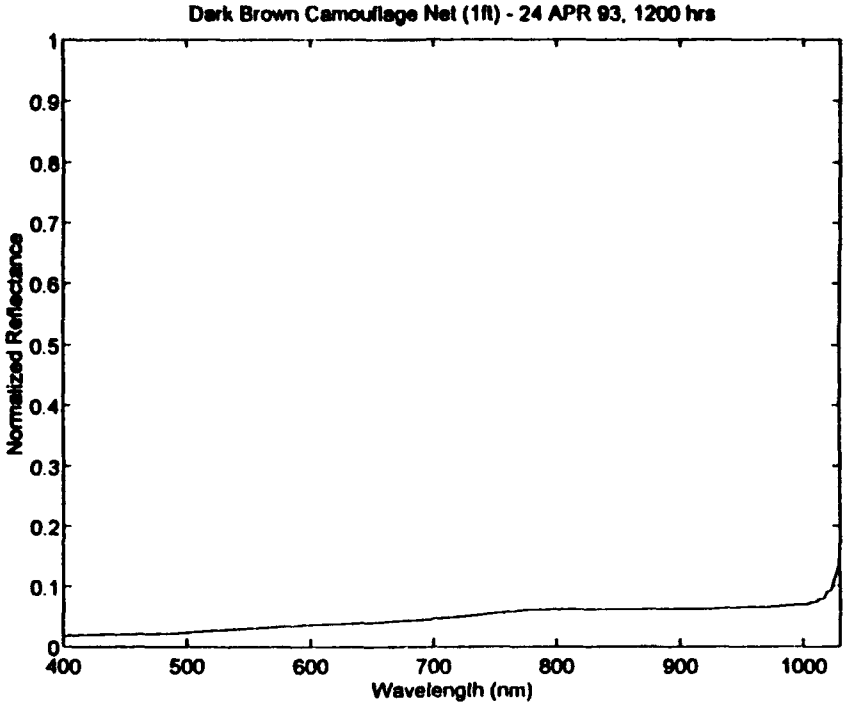
Dark Brown Camouflage Net (1ft) - 24 APR 93, 1200 hrs
Normalized Reflectance
Wavelength (nm)
0
0.1
0.2
0.3
0.4
0.5
0.6
0.7
0.8
0.9
1
400
500
600
700
800
900
1000

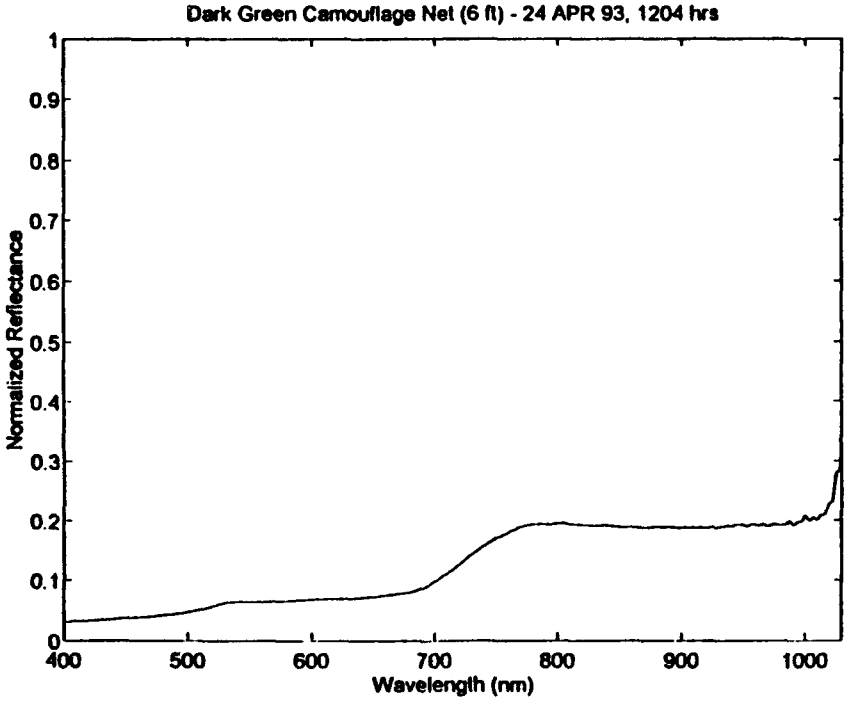
Dark Green Camouflage Net (6 ft) - 24 APR 93, 1204 hrs
Normalized Reflectance
Wavelength (nm)
0
0.1
0.2
0.3
0.4
0.5
0.6
0.7
0.8
0.9
1
400
500
600
700
800
900
1000

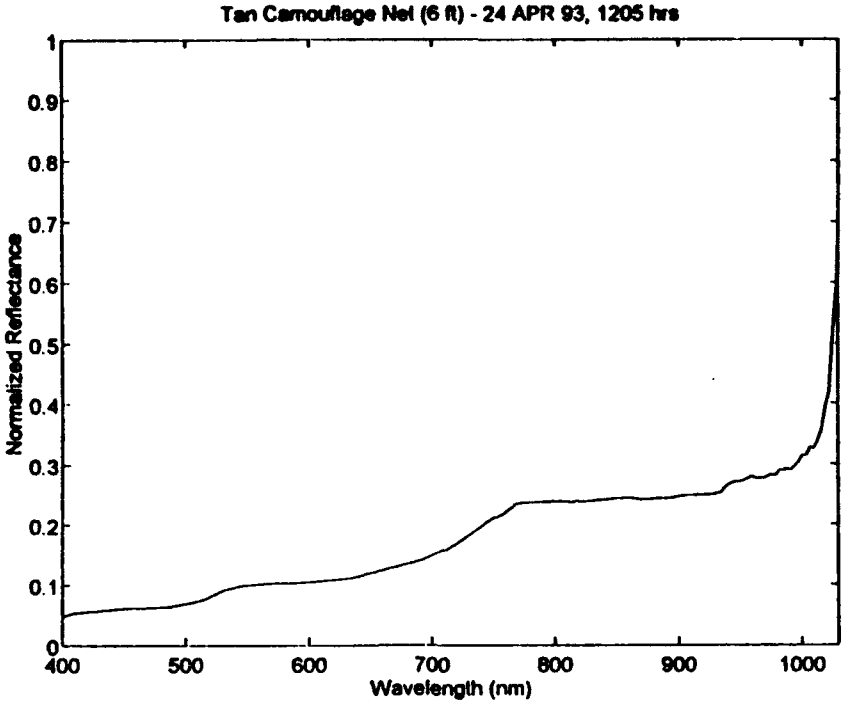
Tan Camouflage Net (6 ft) - 24 APR 93, 1205 hrs
Normalized Reflectance
Wavelength (nm)
0
0.1
0.2
0.3
0.4
0.5
0.6
0.7
0.8
0.9
1
400
500
600
700
800
900
1000

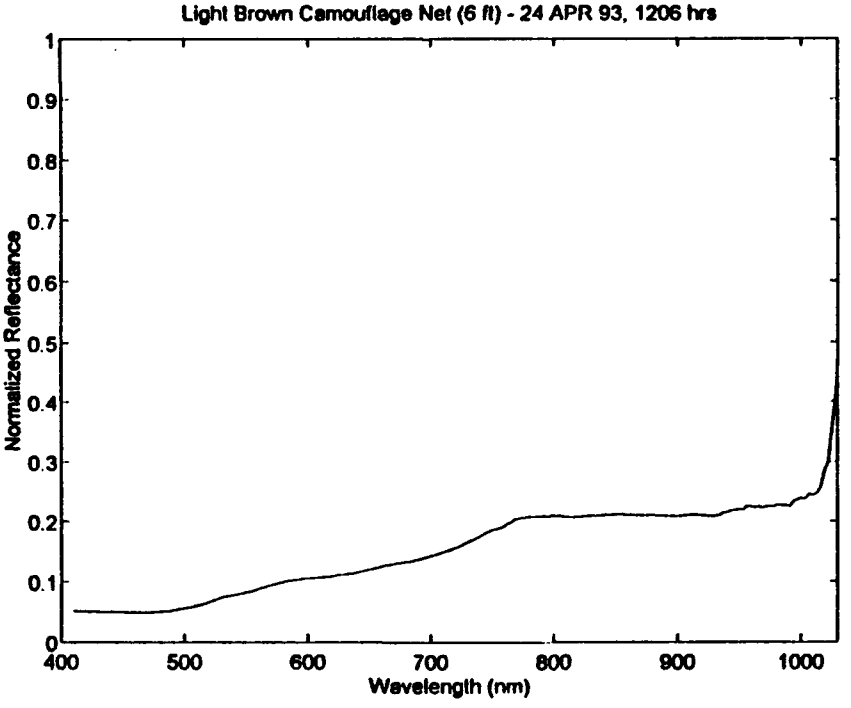
Light Brown Camouflage Net (6 ft) - 24 APR 93, 1206 hrs
Normalized Reflectance
Wavelength (nm)
0
0.1
0.2
0.3
0.4
0.5
0.6
0.7
0.8
0.9
1
400
500
600
700
800
900
1000

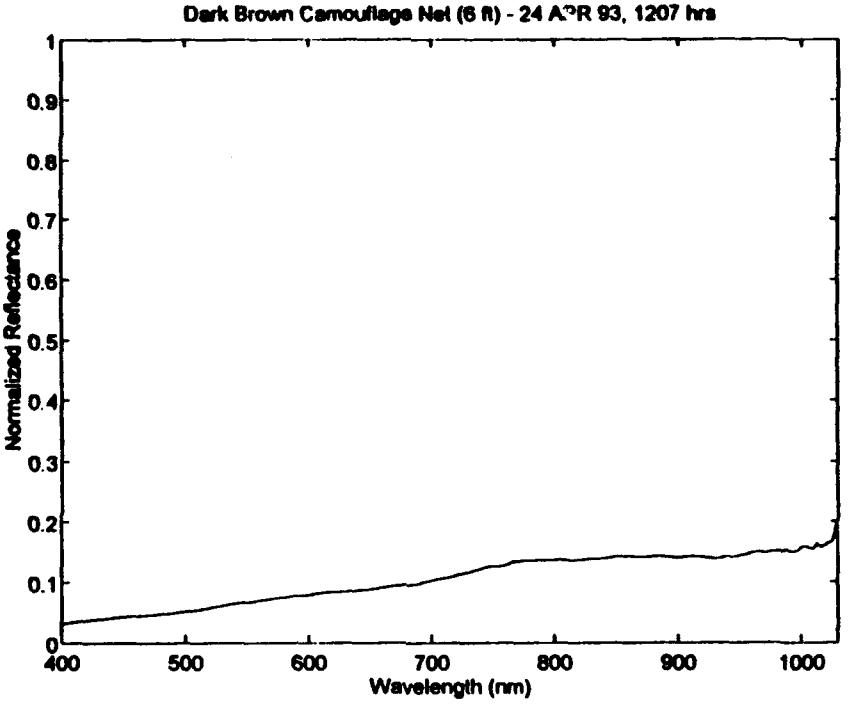
Dark Brown Camouflage Net (6 ft) - 24 APR 93, 1207 hrs
Normalized Reflectance
Wavelength (nm)
0
0.1
0.2
0.3
0.4
0.5
0.6
0.7
0.8
0.9
1
400
500
600
700
800
900
1000

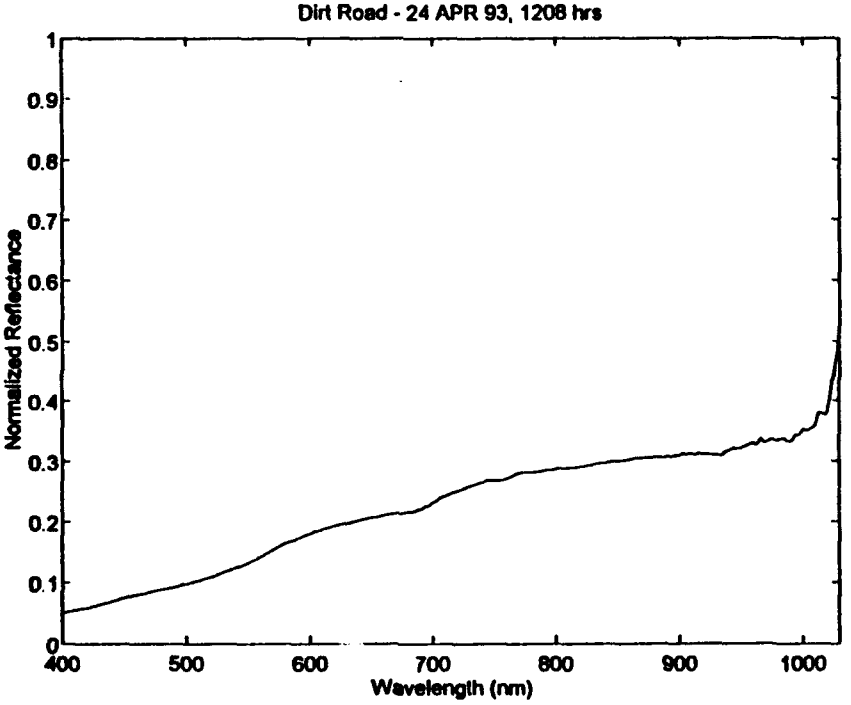
Dirt Road - 24 APR 93, 1208 hrs
Normalized Reflectance
Wavelength (nm)
0
0.1
0.2
0.3
0.4
0.5
0.6
0.7
0.8
0.9
1
400
500
600
700
800
900
1000

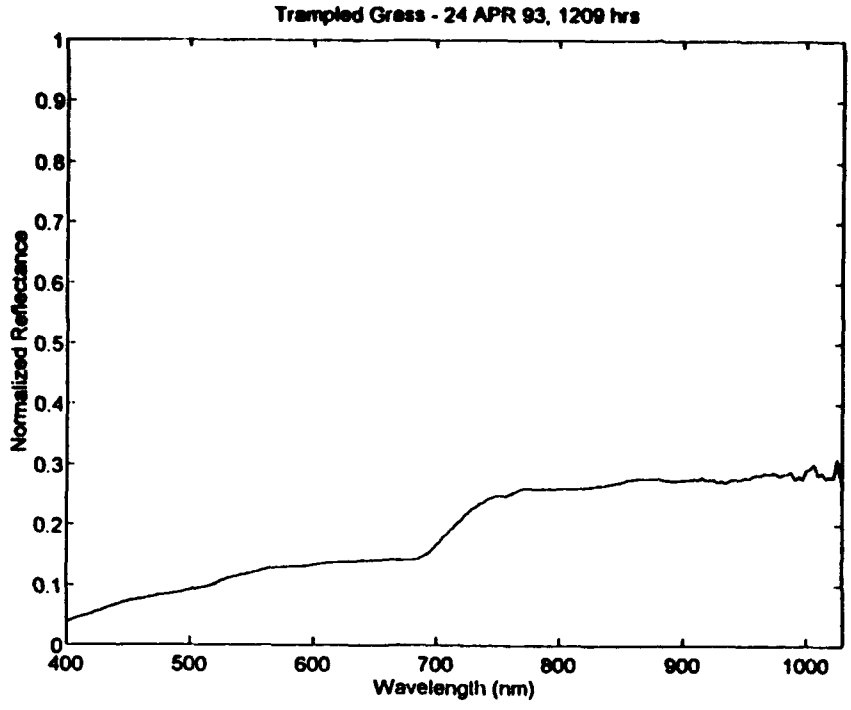
Trampled Grass - 24 APR 93, 1209 hrs
Normalized Reflectance
Wavelength (nm)
0
0.1
0.2
0.3
0.4
0.5
0.6
0.7
0.8
0.9
1
400
500
600
700
800
900
1000

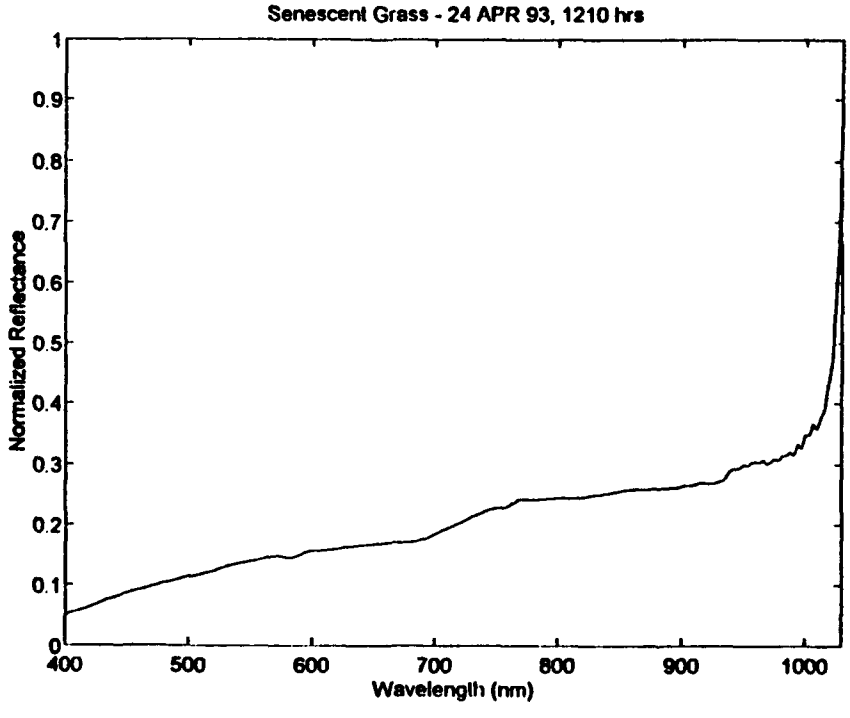
Senescent Grass - 24 APR 93, 1210 hrs
Normalized Reflectance
Wavelength (nm)
0
0.1
0.2
0.3
0.4
0.5
0.6
0.7
0.8
0.9
1
400
500
600
700
800
900
1000

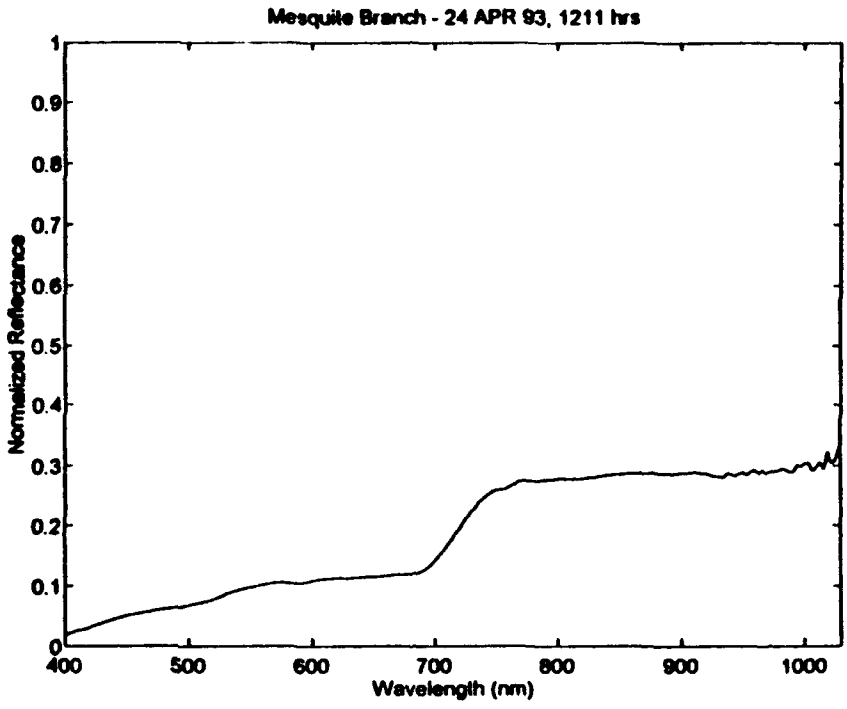
Mesquite Branch - 24 APR 93, 1211 hrs
Normalized Reflectance
Wavelength (nm)
0
0.1
0.2
0.3
0.4
0.5
0.6
0.7
0.8
0.9
1
400
500
600
700
800
900
1000

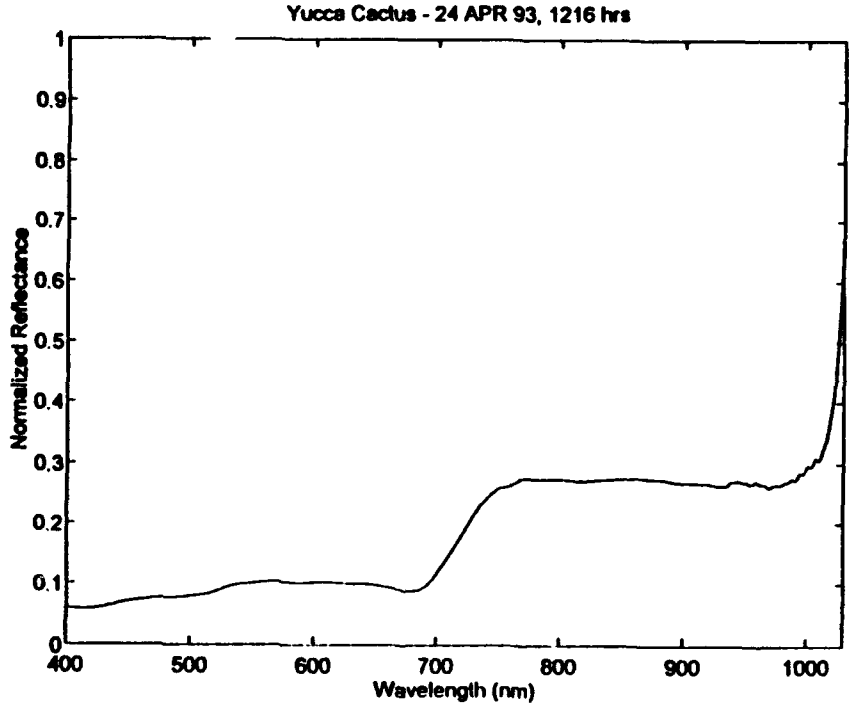
Yucca Cactus - 24 APR 93, 1216 hrs
Normalized Reflectance
Wavelength (nm)
0
0.1
0.2
0.3
0.4
0.5
0.6
0.7
0.8
0.9
1
400
500
600
700
800
900
1000

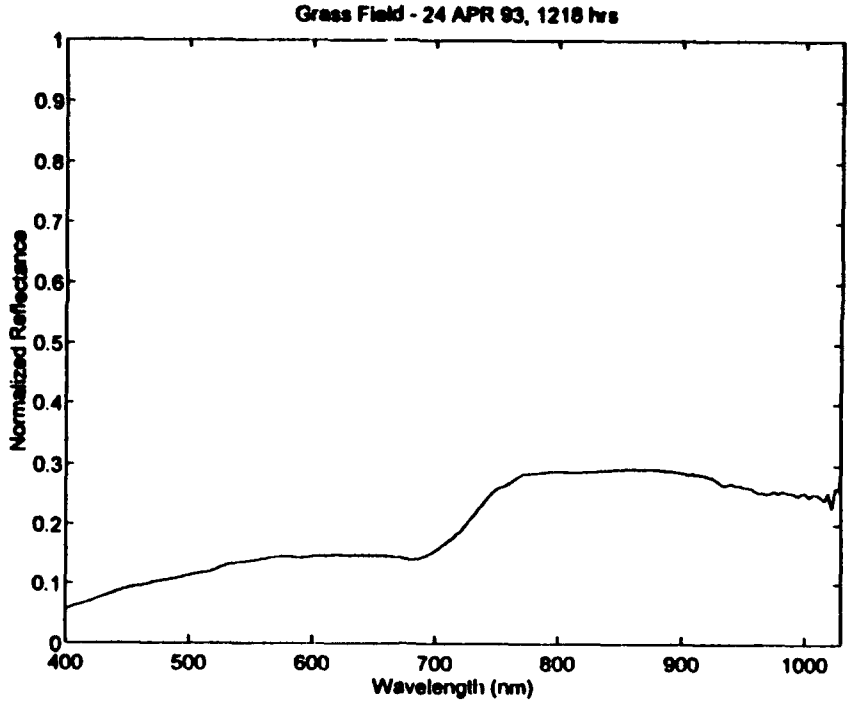
Grass Field - 24 APR 93, 1218 hrs
Normalized Reflectance
Wavelength (nm)
0
0.1
0.2
0.3
0.4
0.5
0.6
0.7
0.8
0.9
1
400
500
600
700
800
900
1000

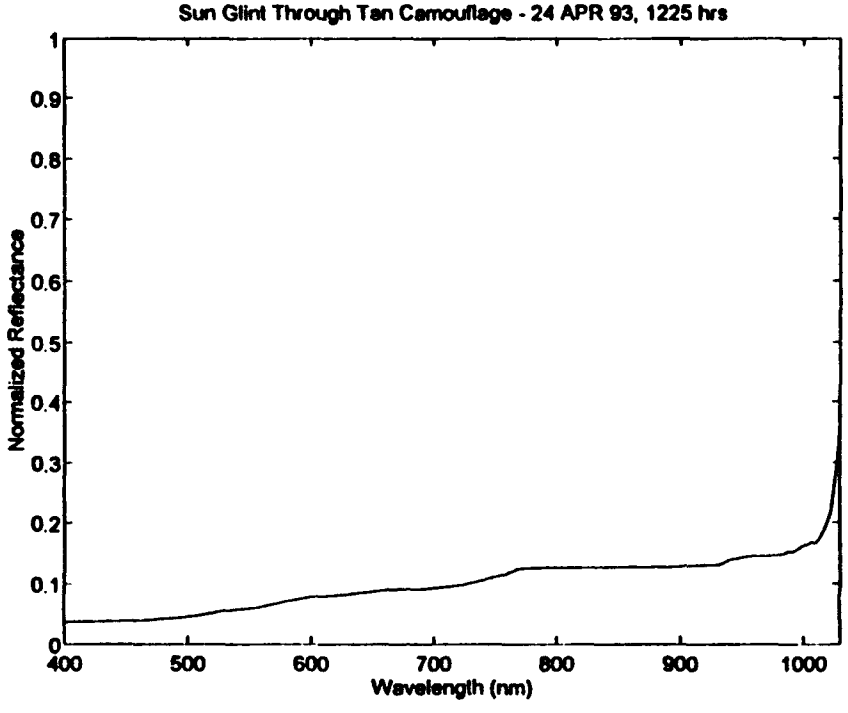
Sun Glint Through Tan Camouflage - 24 APR 93, 1225 hrs
Normalized Reflectance
Wavelength (nm)
0
0.1
0.2
0.3
0.4
0.5
0.6
0.7
0.8
0.9
1
400
500
600
700
800
900
1000

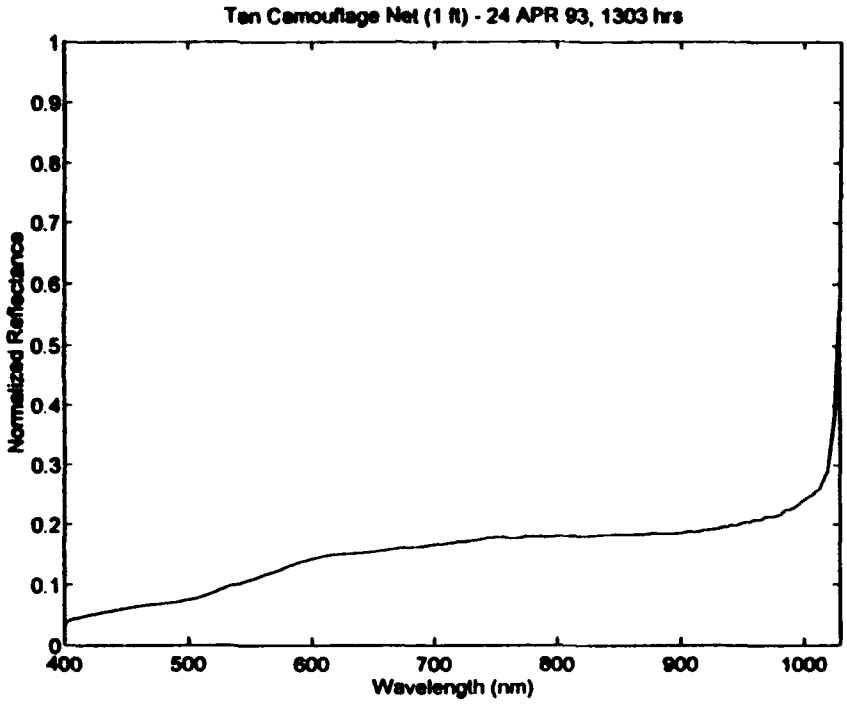
Tan Camouflage Net (1 ft) - 24 APR 93, 1303 hrs
Normalized Reflectance
Wavelength (nm)
0
0.1
0.2
0.3
0.4
0.5
0.6
0.7
0.8
0.9
1
400
500
600
700
800
900
1000

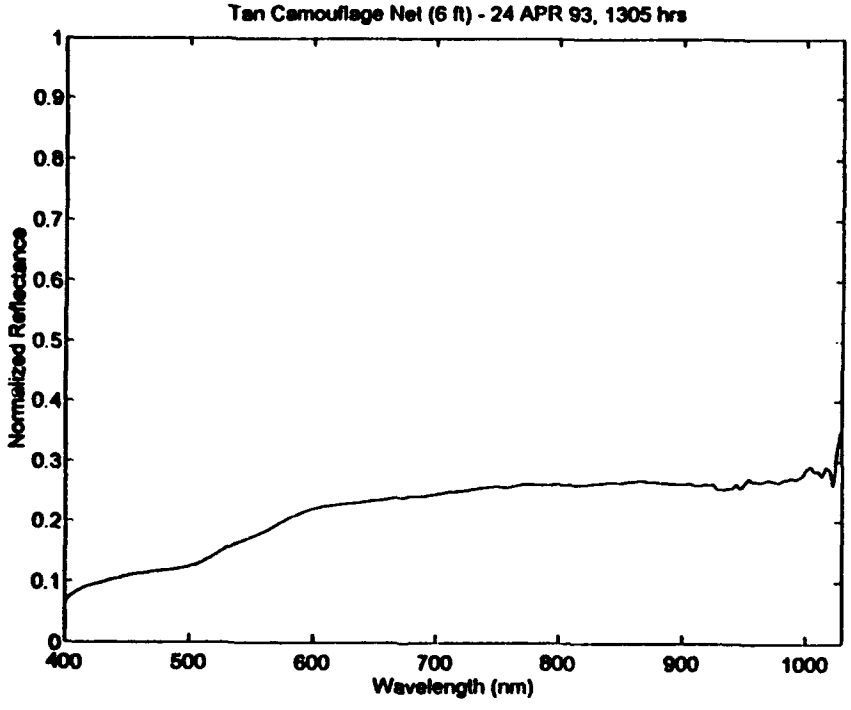
Tan Camouflage Net (6 ft) - 24 APR 93, 1305 hrs
Normalized Reflectance
Wavelength (nm)
0
0.1
0.2
0.3
0.4
0.5
0.6
0.7
0.8
0.9
1
400
500
600
700
800
900
1000

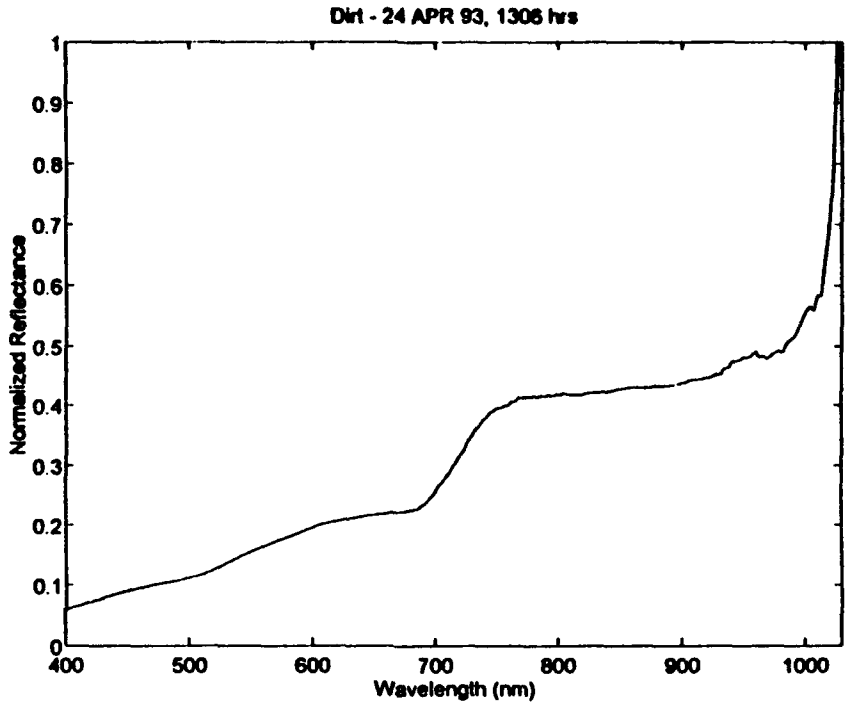
Dirt - 24 APR 93, 1306 hrs
Normalized Reflectance
Wavelength (nm)
0
0.1
0.2
0.3
0.4
0.5
0.6
0.7
0.8
0.9
1
400
500
600
700
800
900
1000

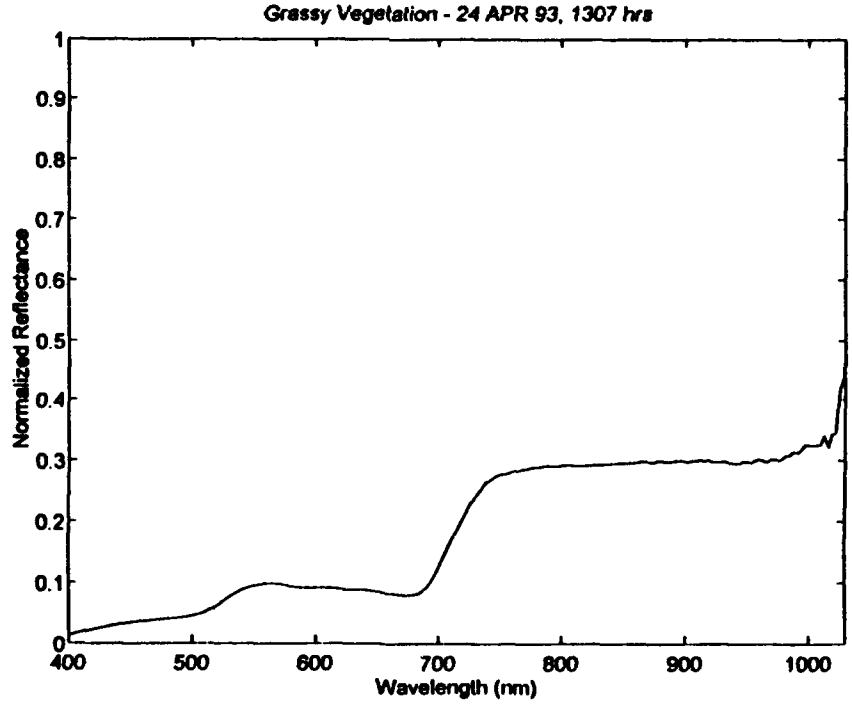
Grassy Vegetation - 24 APR 93, 1307 hrs
Normalized Reflectance
Wavelength (nm)
0
0.1
0.2
0.3
0.4
0.5
0.6
0.7
0.8
0.9
1
400
500
600
700
800
900
1000

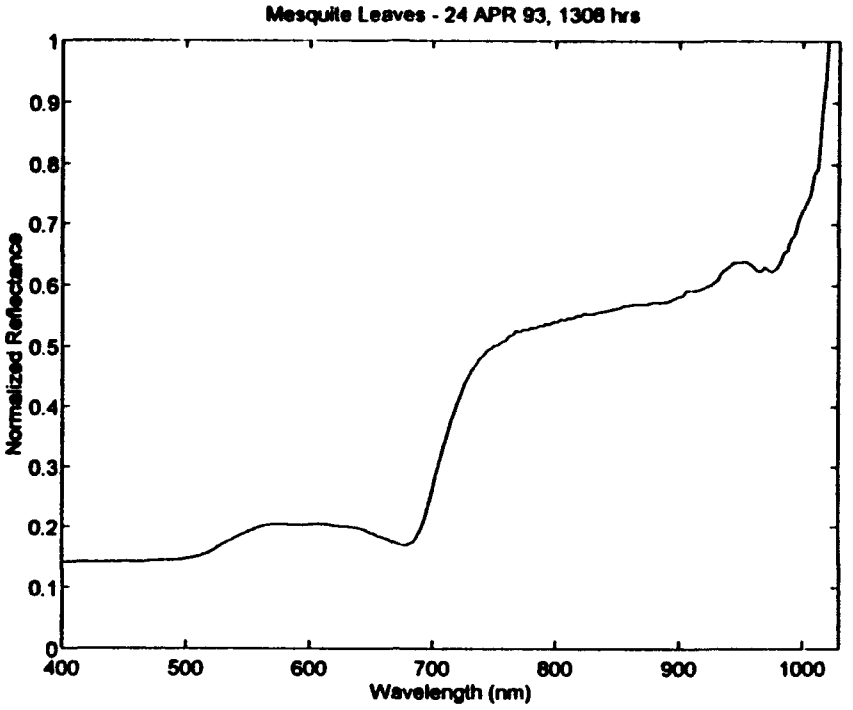
Mesquite Leaves - 24 APR 93, 1308 hrs
Normalized Reflectance
Wavelength (nm)
0
0.1
0.2
0.3
0.4
0.5
0.6
0.7
0.8
0.9
1
400
500
600
700
800
900
1000

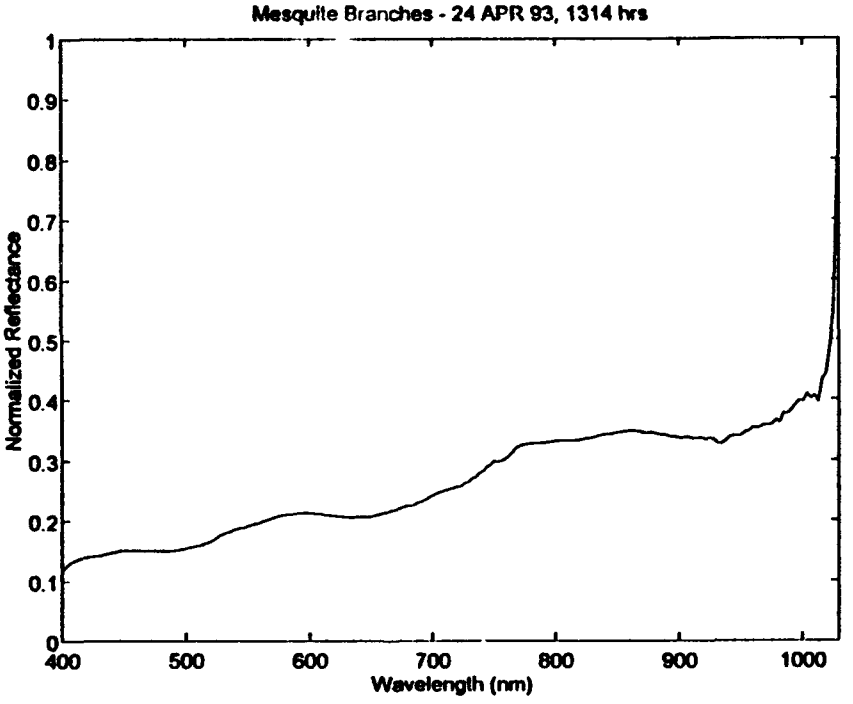
Mesquite Branches - 24 APR 93, 1314 hrs
Normalized Reflectance
Wavelength (nm)
0
0.1
0.2
0.3
0.4
0.5
0.6
0.7
0.8
0.9
1
400
500
600
700
800
900
1000

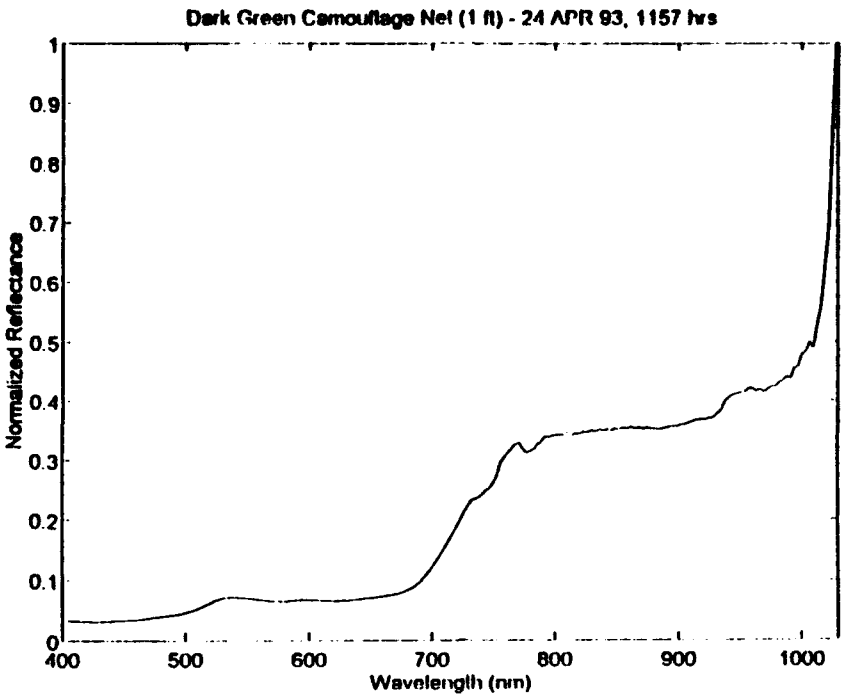
Dark Green Camouflage Net (1 ft) - 24 APR 93, 1157 hrs
Normalized Reflectance
Wavelength (nm)
0
0.1
0.2
0.3
0.4
0.5
0.6
0.7
0.8
0.9
1
400
500
600
700
800
900
1000

# APPENDIX C

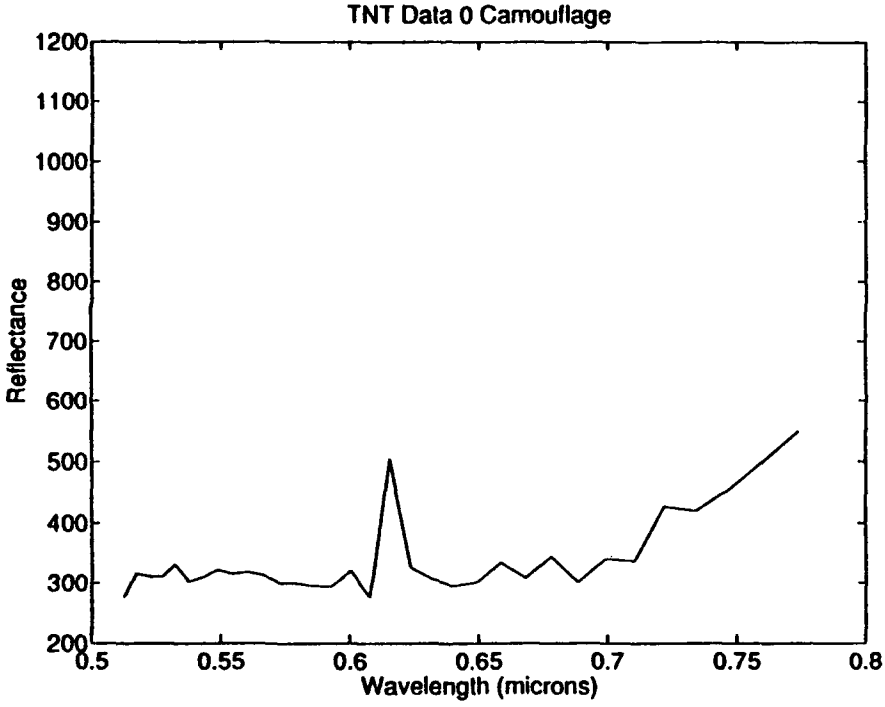
TNT Data 0 Camouflage
Reflectance
1200
1100
1000
900
800
700
600
500
400
300
200
0.5
0.55
0.6
0.65
0.7
0.75
0.8
Wavelength (microns)

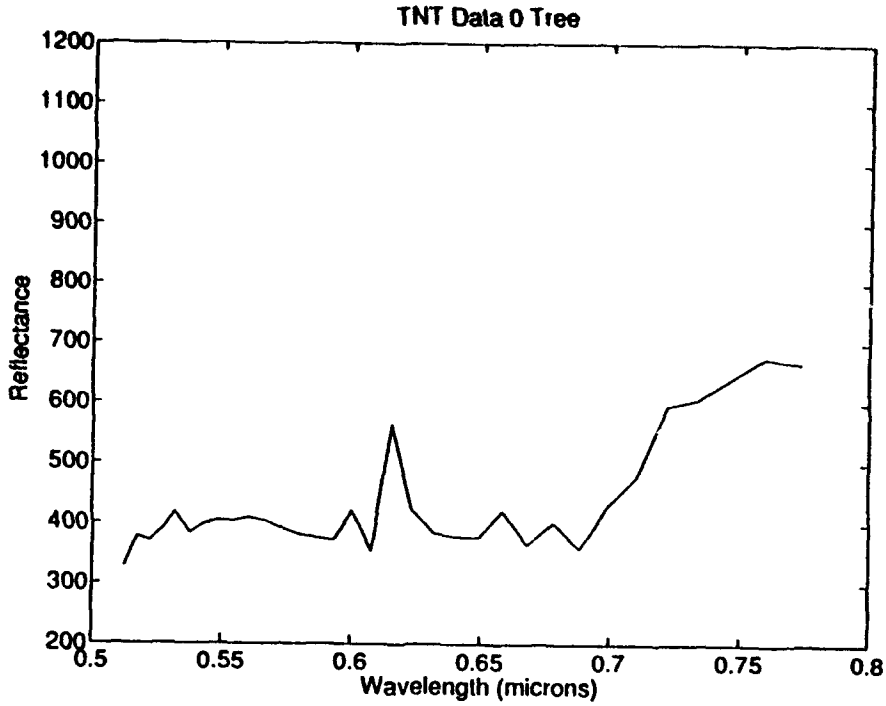
TNT Data 0 Tree
Reflectance
Wavelength (microns)
1200
1100
1000
900
800
700
600
500
400
300
200
0.5
0.55
0.6
0.65
0.7
0.75
0.8

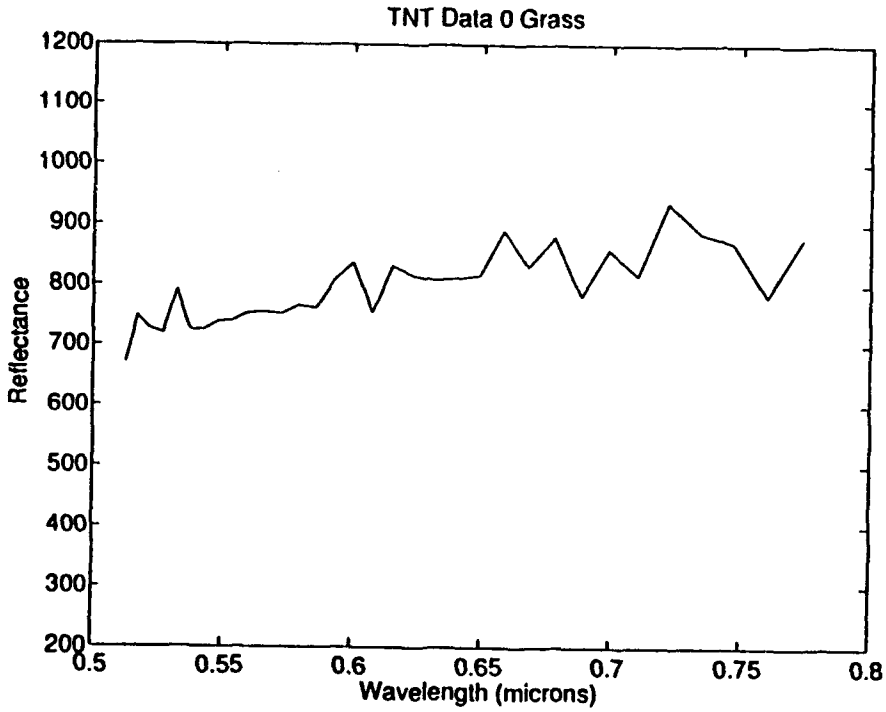
TNT Data 0 Grass
Reflectance
Wavelength (microns)
1200
1100
1000
900
800
700
600
500
400
300
200
0.5
0.55
0.6
0.65
0.7
0.75
0.8

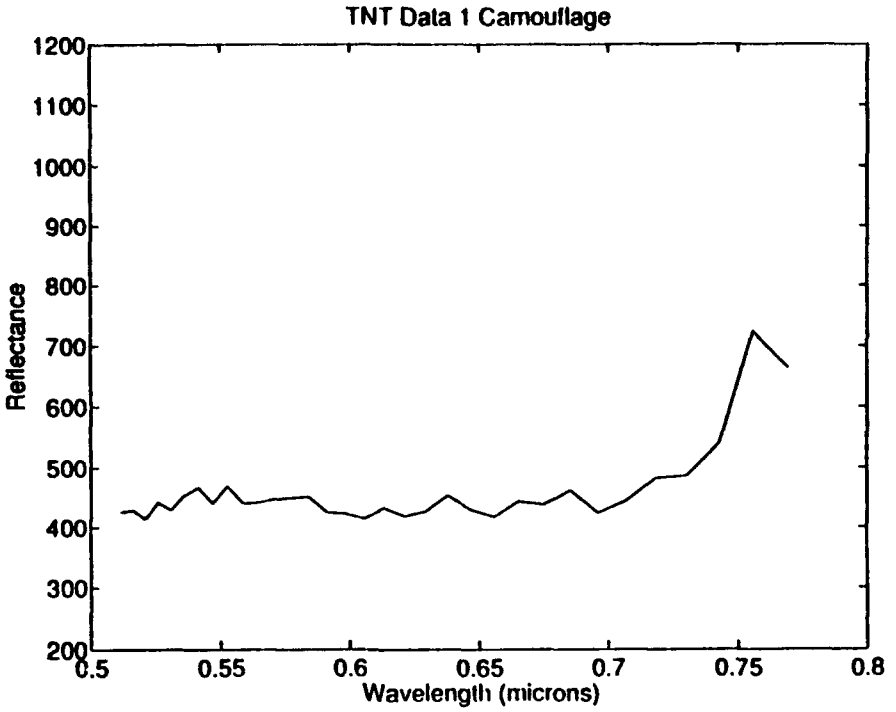
TNT Data 1 Camouflage
Reflectance
Wavelength (microns)
1200
1100
1000
900
800
700
600
500
400
300
200
0.5
0.55
0.6
0.65
0.7
0.75
0.8

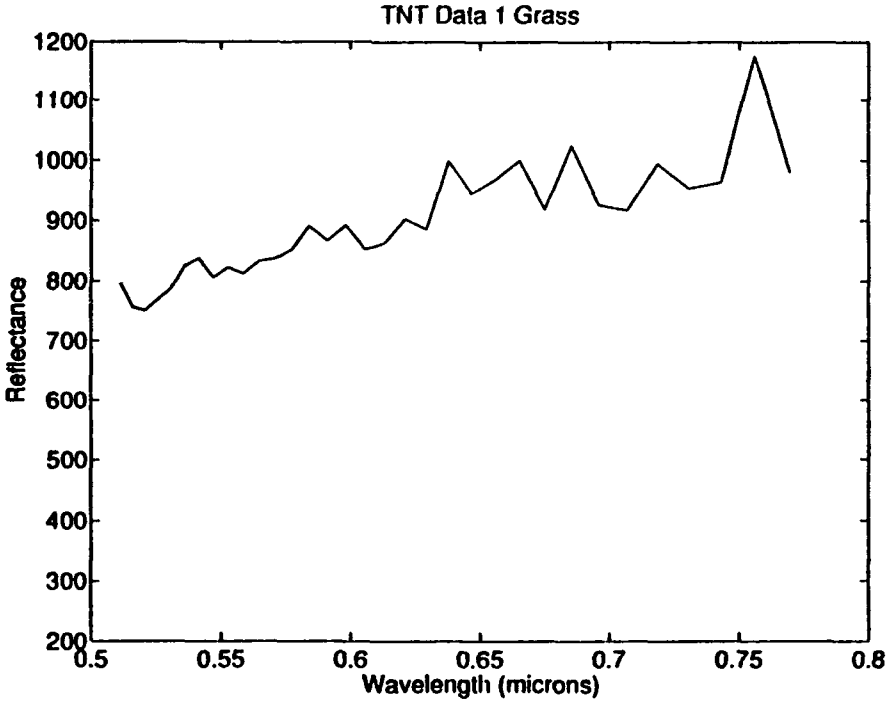
TNT Data 1 Grass
Reflectance
Wavelength (microns)
1200
1100
1000
900
800
700
600
500
400
300
200
0.5
0.55
0.6
0.65
0.7
0.75
0.8

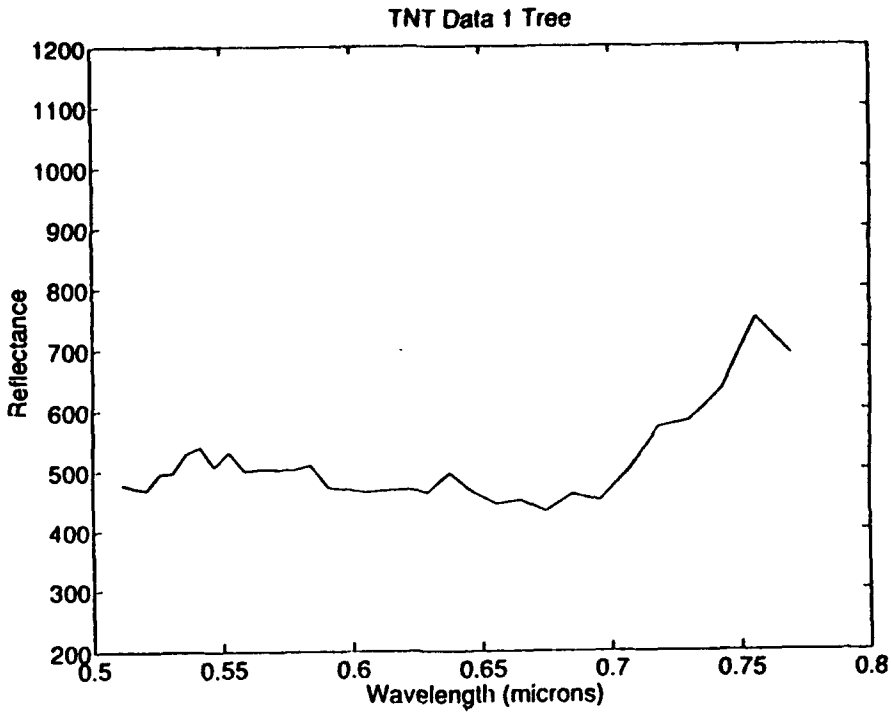
TNT Data 1 Tree
Reflectance
Wavelength (microns)
1200
1100
1000
900
800
700
600
500
400
300
200
0.5
0.55
0.6
0.65
0.7
0.75
0.8

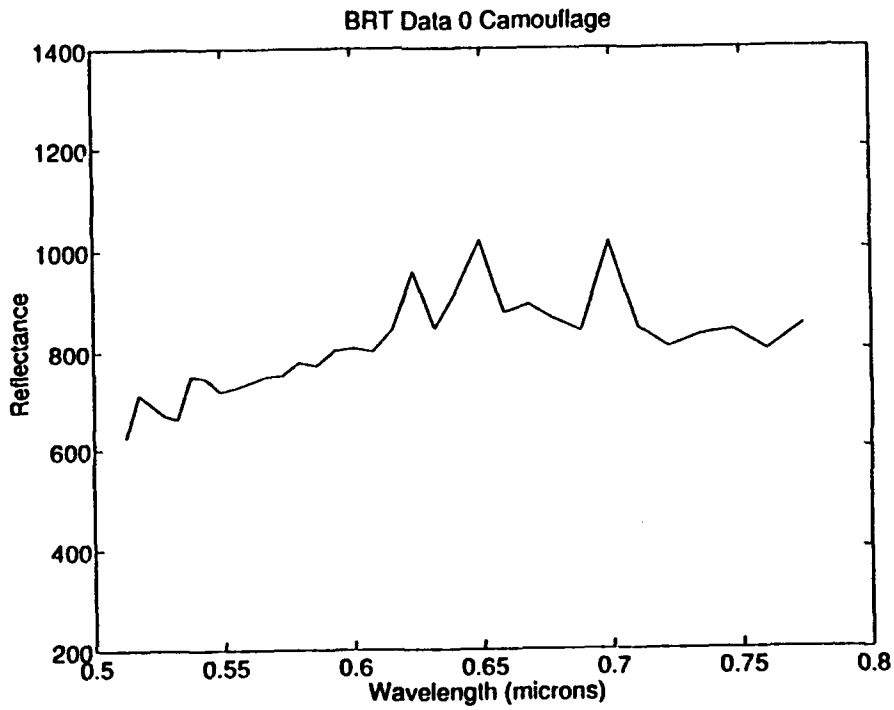
BRT Data 0 Camouflage
Reflectance
Wavelength (microns)
1400
1200
1000
800
600
400
200
0.5
0.55
0.6
0.65
0.7
0.75
0.8

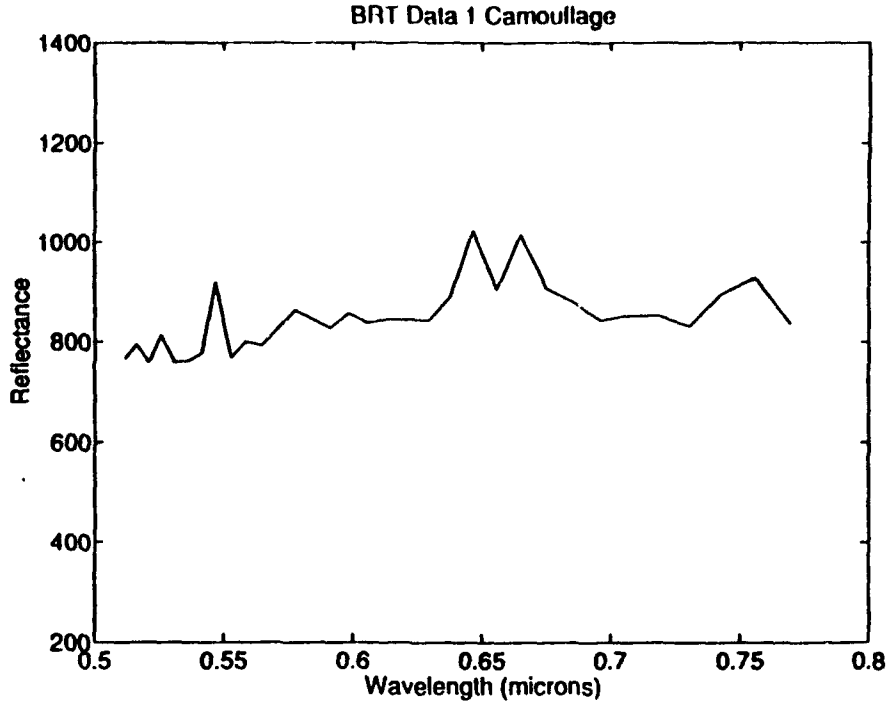
BRT Data 1 Camouflage
1400
1200
1000
800
600
400
200
Reflectance
0.5
0.55
0.6
0.65
0.7
0.75
0.8
Wavelength (microns)

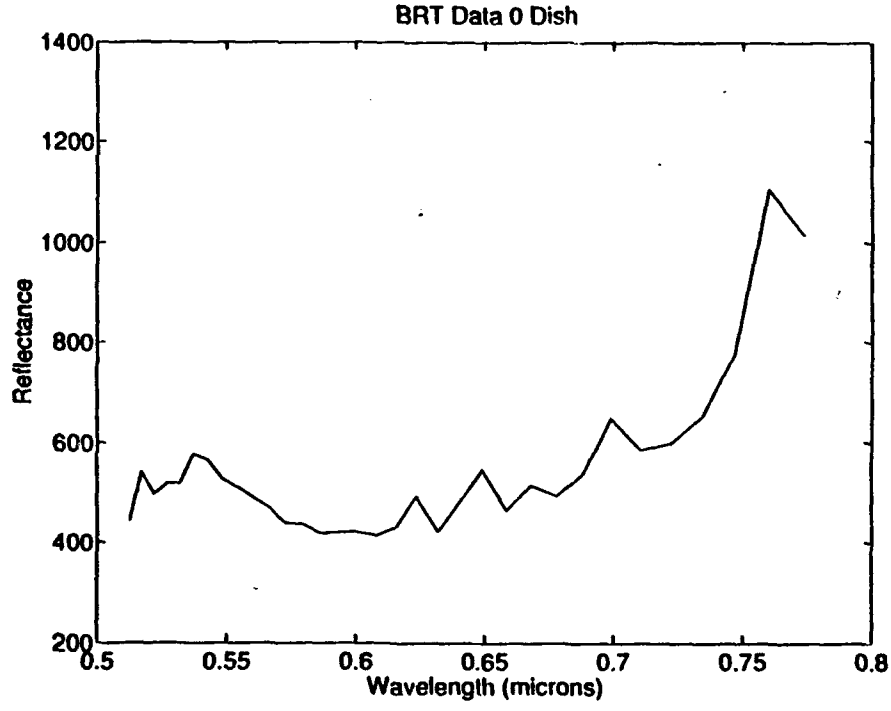
BRT Data 0 Dish
1400
1200
1000
800
600
400
200
Reflectance
0.5
0.55
0.6
0.65
0.7
0.75
0.8
Wavelength (microns)

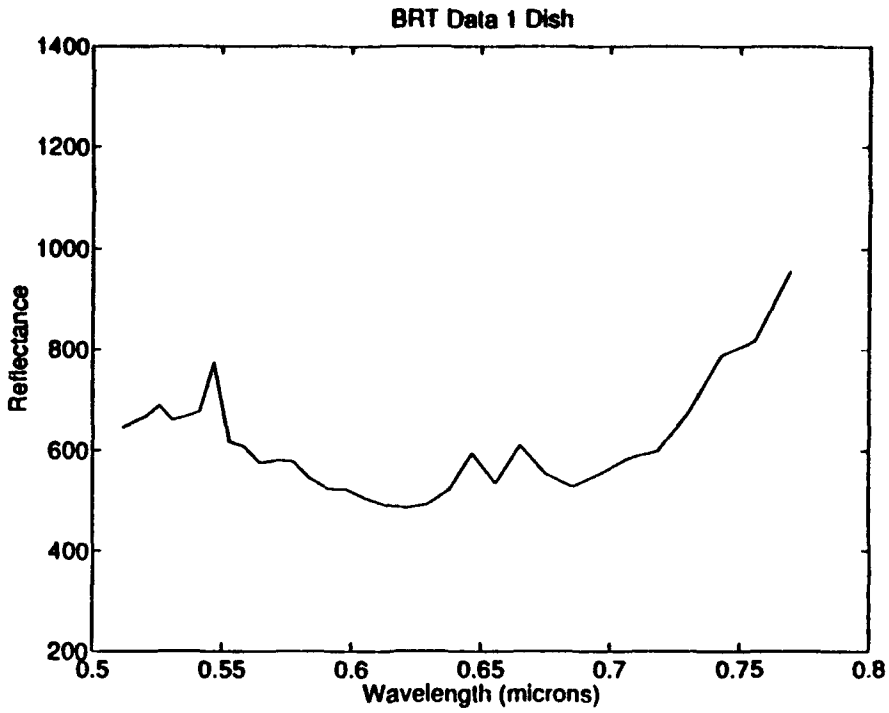
BRT Data 1 Dish
Reflectance
Wavelength (microns)
1400
1200
1000
800
600
400
200
0.5
0.55
0.6
0.65
0.7
0.75
0.8

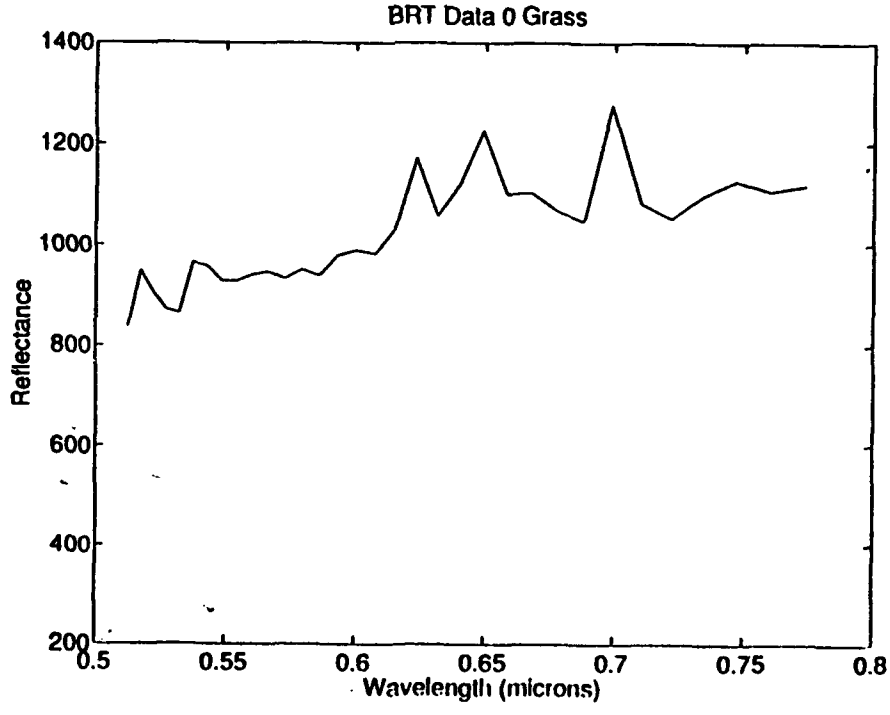
BRT Data 0 Grass
Reflectance
Wavelength (microns)
1400
1200
1000
800
600
400
200
0.5
0.55
0.6
0.65
0.7
0.75
0.8

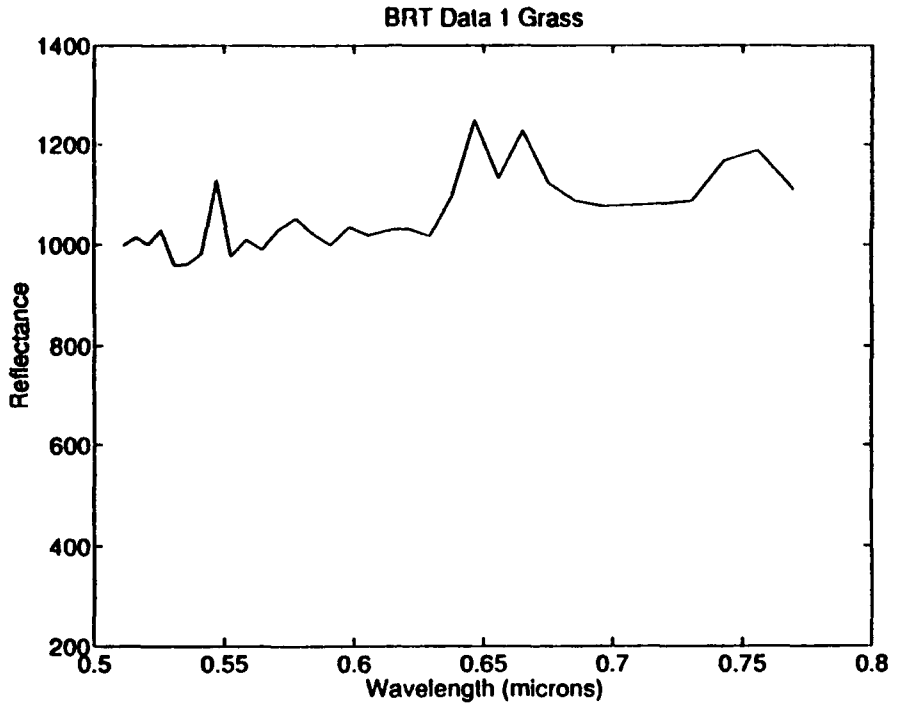
BRT Data 1 Grass
1400
1200
1000
800
600
400
200
Reflectance
0.5
0.55
0.6
0.65
0.7
0.75
0.8
Wavelength (microns)

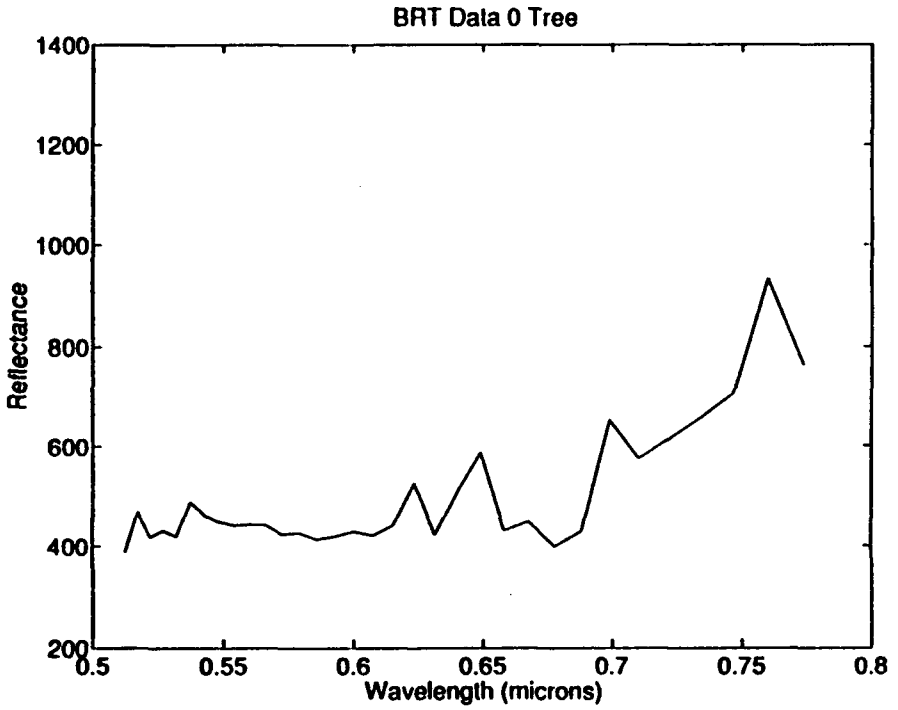
BRT Data 0 Tree
1400
1200
1000
800
600
400
200
Reflectance
0.5
0.55
0.6
0.65
0.7
0.75
0.8
Wavelength (microns)

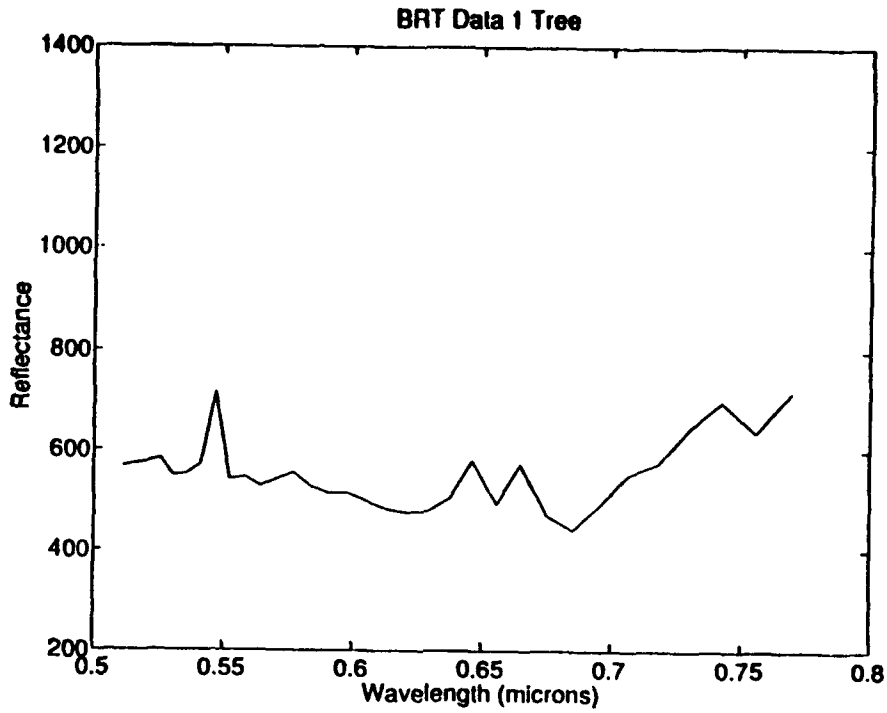
BRT Data 1 Tree
1400
1200
1000
800
600
400
200
Reflectance
0.5
0.55
0.6
0.65
0.7
0.75
0.8
Wavelength (microns)

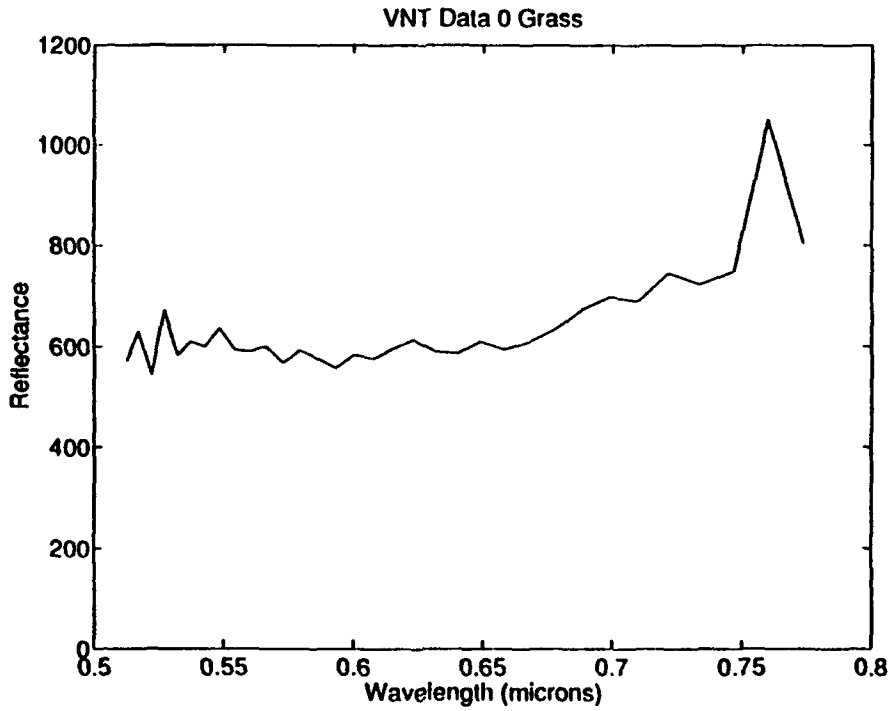
VNT Data 0 Grass
1200
1000
800
600
400
200
0
Reflectance
0.5
0.55
0.6
0.65
0.7
0.75
0.8
Wavelength (microns)

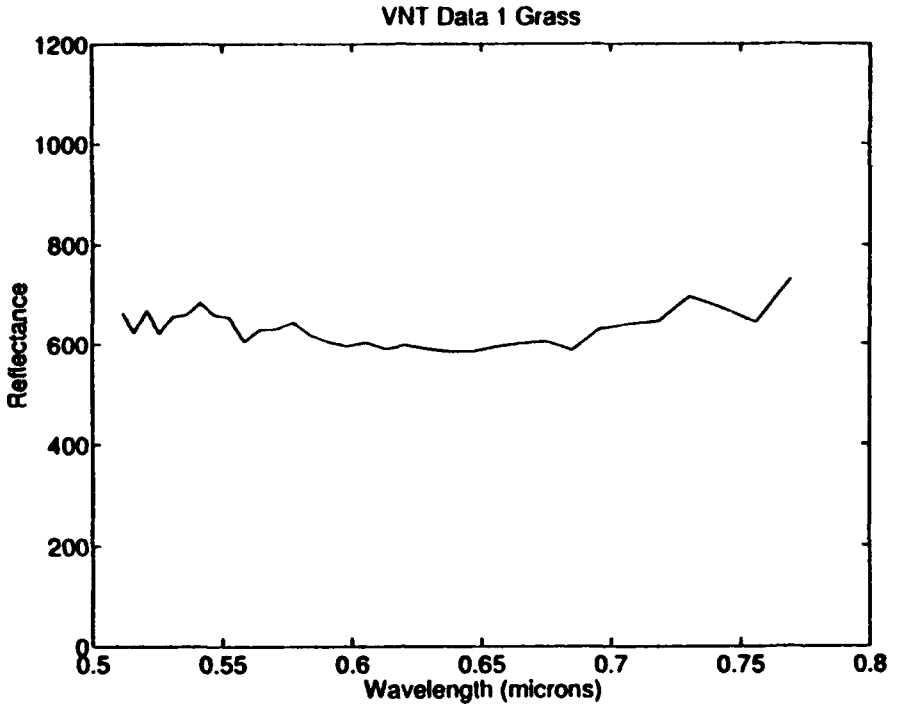
VNT Data 1 Grass
1200
1000
800
600
400
200
0
Reflectance
0.5
0.55
0.6
0.65
0.7
0.75
0.8
Wavelength (microns)

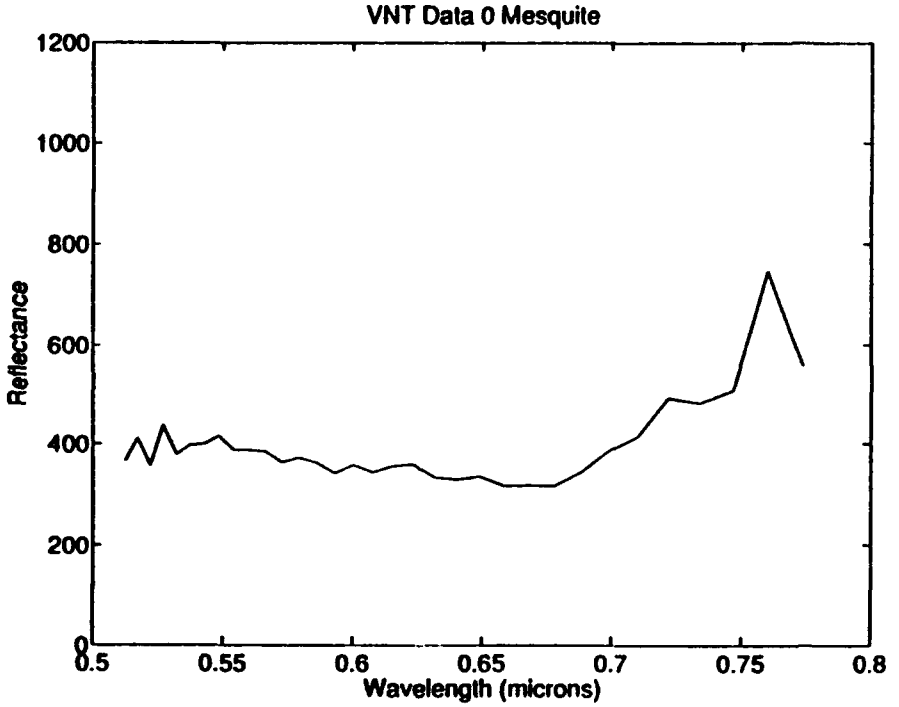
VNT Data 0 Mesquite
1200
1000
800
600
400
200
0
Reflectance
0.5
0.55
0.6
0.65
0.7
0.75
0.8
Wavelength (microns)

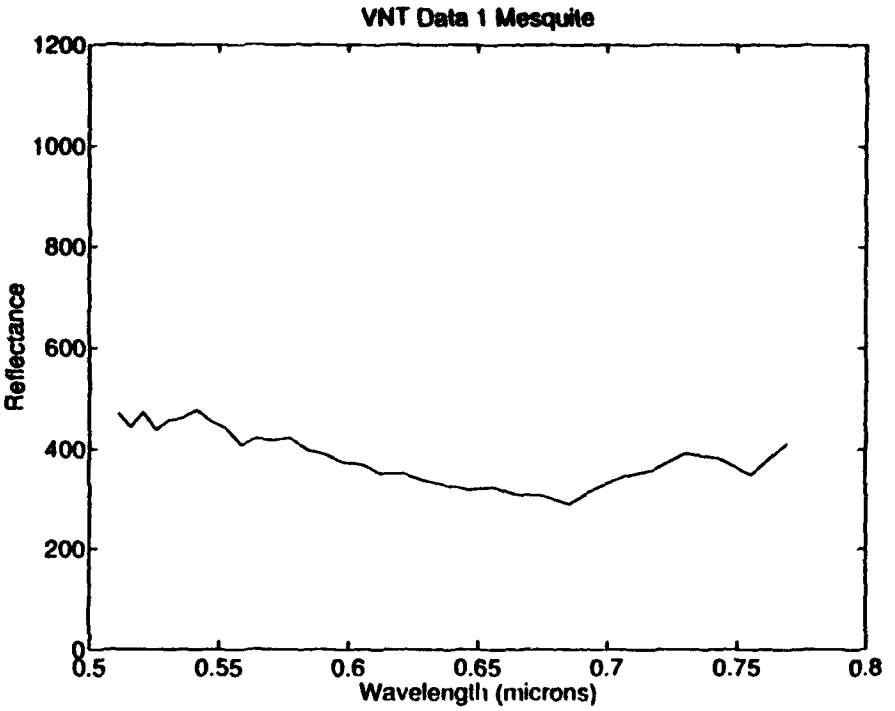
VNT Data 1 Mesquite
Reflectance
1200
1000
800
600
400
200
0
0.5
0.55
0.6
0.65
0.7
0.75
0.8
Wavelength (microns)

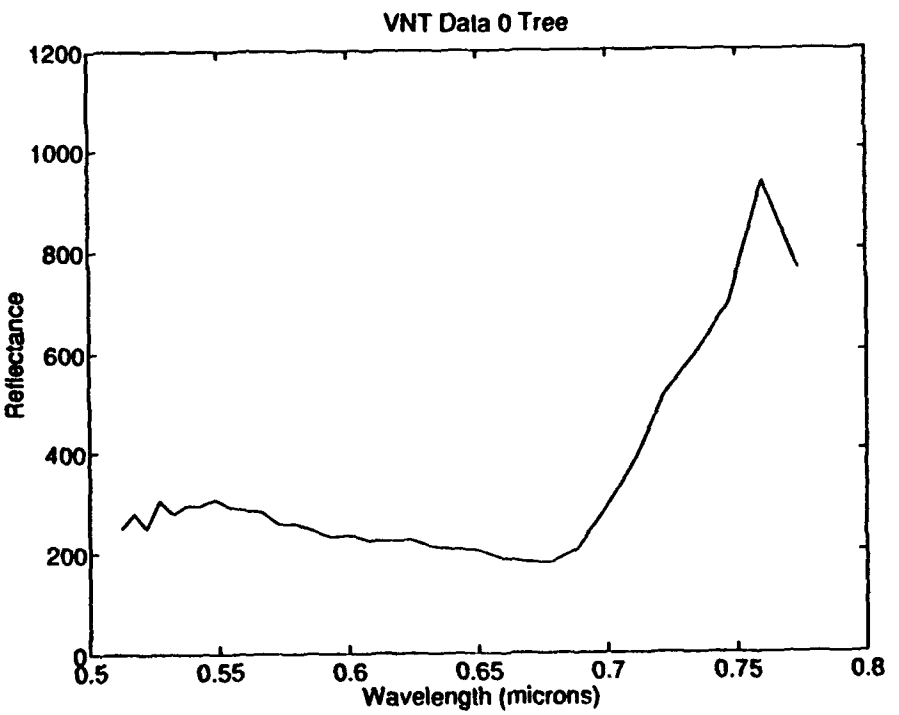
VNT Data 0 Tree
Reflectance
1200
1000
800
600
400
200
0
0.5
0.55
0.6
0.65
0.7
0.75
0.8
Wavelength (microns)

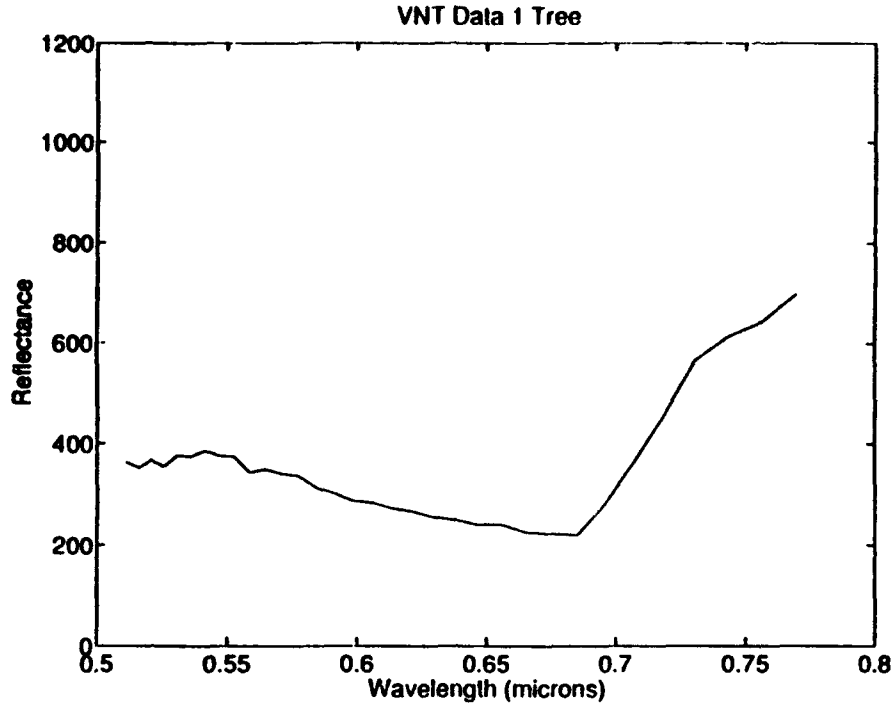
VNT Data 1 Tree
Reflectance
Wavelength (microns)
1200
1000
800
600
400
200
0
0.5
0.55
0.6
0.65
0.7
0.75
0.8

## LIST OF REFERENCES


1. Goetz, A. F., and others, "Imaging Spectrometry for Earth Remote Sensing," *Science*, v. 228, 7 June 1985.

2. Cheng, L., Chao, T., and Reyes, G., "JPL Activities on Development of Acousto-optic Tunable Filter Imaging Spectrometer," paper presented at the Third Annual JPL Airborne Geoscience Workshop, Pasadena, California, 1-5 June 1992.

3. *Manual of Remote Sensing*, 2nd ed., v. 1, American Society of Photogrammetry, 1983.

4. Halliday, D., and Resnick, R., *Fundamentals of Physics*, 3rd ed., John Wiley & Sons, Inc., 1988.

5. Egan, W. G., *Photometry and Polarization in Remote Sensing*, Elsevier Science Publishing Company, Inc., 1985.

6. Slater, P. N., *Remote Sensing Optics and Optical Systems*, Addison-Wesley Publishing Company, Inc., 1980.

7. Durkee, P. A., SS 3525 Class Notes, Naval Postgraduate School, Monterey, California, 1993.

8. Swain, P. H., and others, *Remote Sensing*, McGraw-Hill, Inc., 1978.

9. Saleh, B. E., and Teich, M. C., *Fundamentals of Photonics*, John Wiley & Sons, Inc., 1991.

10. Rider, D. M., "Acousto-optic Tunable Filter Field Spectrometer for Validation of Airborne and Spaceborne Imaging Spectrometers," paper presented at a conference on Imaging Spectroscopy of the Terrestrial Environment, Orlando, Florida, 16-17 April 1990.

11. Center for the Study of Earth from Space, Cooperative Institute for Research in Environmental Sciences, *SIPS User's Guide*, University of Colorado, Boulder, Colorado, 1992.

12. Research Systems, Inc., "Introduction to IDL," Research Systems, Inc., Boulder, Colorado, 1991.

## INITIAL DISTRIBUTION LIST

| | | No. Copies |
|---|---|---|
| 1. | Defense Technical Information Center<br>Cameron Station<br>Alexandria VA 22304-6145 | 2 |
| 2. | Library, Code 052<br>Naval Postgraduate School<br>Monterey CA 93943-5002 | 2 |
| 3. | Director, Navy Space Systems Division (N63)<br>Space and Electronic Warfare Directorate<br>Chief of Naval Operations<br>Washington D.C. 20350-2000 | 1 |
| 4. | Commander, U.S. Naval Space Command<br>Code N6/T4<br>Dahlgren VA 22448-5170 | 1 |
| 5. | Commander, U.S. Army Intelligence Center and<br>Fort Huachuca<br>ATZS-CDT-S (CW2 Hawker)<br>Fort Huachuca AZ 85613 | 1 |
| 6. | Topographic Engineering Center (TEC)<br>Attn: ASTRO (Delma Del Bosque)<br>Fort Belvoir VA 22060-5546 | 1 |
| 7. | Michael Hamilton<br>Jet Propulsion Laboratory<br>California Institute of Technology<br>Pasadena CA 91109 | 1 |
| 7. | Colin Mahoney<br>Jet Propulsion Laboratory<br>California Institute of Technology<br>Pasadena CA 91109 | 1 |
| 9. | Li-Jen Cheng<br>Jet Propulsion Laboratory<br>California Institute of Technology<br>Pasadena CA 91109 | 1 |

10. Superintendent 1
Naval Postgraduate School
Attn: Phil Durkee, Code MR/De
Monterey CA 93943-5000

11. Superintendent 2
Naval Postgraduate School
Attn: Richard C. Olsen, Code PH/Os
Monterey CA 93943-5000

12. Melissa Sturgeon 2
2651 E. Northridge St.
Sierra Vista AZ 85635